



Politecnico di Torino

FACOLTÀ DI INGEGNERIA
Corso di Laurea in Ingegneria dell'Autoveicolo

FINAL PROJECT

Drilling-Riveting Coupled Automated System

Candidato:
Alessandro Limentato

Relatore:
Prof. Luca Settineri
Prof. Giovanni Belingardi

Declaration of Originality

I hereby certify that I am the sole author of this thesis and that no part of this thesis has been published or submitted for publication.

I certify that, to the best of my knowledge, my thesis does not infringe upon anyone's copyright nor violate any proprietary rights and that any ideas, techniques, quotations, or any other material from the work of other people included in my thesis, published or otherwise, are fully acknowledged in accordance with the standard referencing practices. Furthermore, to the extent that I have included copyrighted material that surpasses the bounds of fair dealing within the meaning of the Canada Copyright Act, I certify that I have obtained a written permission from the copyright owner(s) to include such material(s) in my thesis and have included copies of such copyright clearances to my appendix.

I declare that this is a true copy of my thesis, including any final revisions, as approved by my thesis committee and the Graduate Studies office, and that this thesis has not been submitted for a higher degree to any other University or Institution.

Abstract

This thesis deals with the issue of hybrid material joints in the automotive industrial field, with a particular focus on blind riveting process optimization for composite to aluminum connections. This aspect results from the efforts of modern carmakers to integrate dissimilar materials in the same body-in-white (BIW) structure, in order to improve fuel economy and vehicle performance and meet emission regulations. The thesis first presents a general overview of joining strategies adopted as the alternatives of the conventional spot welding technique, which is not suitable for multi-material joints. The analysis then continues with the benchmark of the main Original Equipment Manufacturers (OEMs) concerning their material integration strategies and current joining technologies. Innovative riveting methods and their experimental performance assessment will be presented, with the target of improving the benchmark data for future FCA application involving lightweight and dissimilar materials.

Acknowledgements

This thesis development activity has involved many people whom I would like to thank for their help and support.

I would like to express my thankfulness starting with FCA group, Politecnico di Torino and University of Windsor for giving me the possibility to be part of the exchange project. This Dual International Master's Degree has been one of the best and most challenging experiences of my life, in terms of personal, academic and professional growth. For this reason, I would like to thank the people directly involved in this program: Prof. Giovanni Belingardi, Dott. Edoardo Rabino, Dott. Marco Mauro, Dr. Jennifer Johrendt, Mohammed Malik and Marie Mills. They helped me a lot during this year, providing me with their guidance and supporting me in solving every difficulty related to my project development.

I wish to thank my committee members, Dr. Afsaneh Edrisy, Dr. Jennifer Johrendt and Dr. Reza Riahi. They encouraged me to go in deep with several aspects of my work, guiding me in the development of new challenging research activities.

I want to thank my advisors from Politecnico, Prof. Luca Settineri and Prof. Giovanni Belingardi who, despite the long distance, have been able to support me with frequent calls and emails. Their efforts allowed me to identify and focus on the most important aspects of my research work.

I would like to express my gratitude to my advisor from University of Windsor, Dr. Reza Riahi, who provided me with his precious support during the development of this thesis and of the related experimental activity. His guidance has been fundamental for me to give the best in this research project.

I do wish express my heartfelt thanks to and all the people from the "Centro Ricerche Fiat", especially to my Italian advisors Ing. Rosanna Brun, Ing. Antonio Annicchiarico. They provided me with a continuous support sharing their experience and knowledge in their field of research. They also guided me through the information exchange process with suppliers and the experimental activity presented in this work.

I am very grateful to the Automotive Research and Development Center (ARDC) of Windsor, for guiding me during this internship year and for giving me the possibility to experience the FCA work environment.

Then, I would like to thank my advisors in Auburn Hills, Kevin Ward, head of Fastener Engineering and Narayan Menon, application engineer for FCA group. They allowed me to professionally grow up learning from their activity at the Chrysler Technical Center (CTC).

I should like to express my gratitude to all people working at University of Windsor and involved in the experimental part of my activity. In particular the head of technical support, Andrew Jenner and the technologists Matt St. Louis and Kevin Harkai. They allowed me to put in practice my ideas, turning them in the experimental activity on which this work is based.

Thanks to my family, mia sorella e mia madre. A Marcella che è sempre stata, da buona sorella maggiore, un punto di riferimento nel corso della mia vita e della mia formazione. A mia madre, alla quale va il ringraziamento più grande, per l'aver fatto di me la persona che sono oggi; sei sempre stata la mia forza, credendo in me più di chiunque altro e rendendo possibile ogni mio successo, accademico e personale.

To my father. Anche se non ti ho avuto vicino, l'idea di poterti rendere un giorno fiero di me mi ha sempre spinto a dare il massimo.

To my friends, who always believed in me not only this year but during the whole academic experience. The distance has never represented an obstacle to them demonstrating their affection.

To my trip mates, Antonio, Carlo, Salvo, Madalin and Oussama, per aver condiviso con me le esperienze di quest'anno. Grazie ad Antonio che mi ha supportato nei momenti di difficoltà, ricordandomi quotidianamente quanti giorni mancassero al rientro in Italia. A Carlo con cui ho condiviso sessioni di corsa in condizioni di neve, fango, pioggia, nebbia, buio e varie combinazioni di questi inconvenienti. A Salvo, anzi a Salvatore Marco, che ha rafforzato il mio senso di appartenenza alla cultura italiana che bandisce categoricamente l'ananas sulla pizza. Grazie a Madalin e Oussama con i quali ho condiviso tante nuove esperienze nel corso di quest'anno.

Thanks to Mike Mele, our land manager. He supported us buying real pizza, which is the secret of every happy Italian student. However, just remember that I am hearing that train horn right now, when writing the acknowledgments.

Last but not least, thanks to Valeria. Insieme abbiamo raggiunto tanti traguardi, che hanno richiesto diversi sacrifici, tra i quali il trascorrere mesi a distanza l'uno dall'altra per cinque anni, ma consapevoli che ogni sforzo fosse finalizzato al riavvicinarci in futuro. Sei ciò che mi ha spinto a non mollare mai.

Contents

Declaration of originality	iii
Abstract	iv
Acknowledgements	vi
List of Figures	x
List of Tables	xvi
List of Appendices	xvii
List of Abbreviations	xviii
Introduction	1
1 Overview of the main alternative joining techniques	4
1.1 Threaded Fasteners	4
1.2 Adhesives	5
1.3 Flow drilling screws	6
1.4 Rivets	9
1.4.1 Solid rivets	9
1.4.2 Semi-Tubular Rivets	10
1.4.3 Self-pierce rivets	11
1.4.4 Blind Rivets	13
2 Examples of multi-material vehicle body in white and joining strategy in the present market	15
2.1 BMW 7 series: an important step toward the future of multi-material vehicle body in white development	15
2.2 A benchmark manufacturer: Audi A8 multi-material BIW	19
2.3 An example of high volume North American production vehicle: Ford F-150	21
3 Literature review:	
State of the art analysis of innovative riveting methods and new suppliers identification	24
3.1 Resistance spot riveting	25

3.2	Friction Stir Riveting	27
3.3	Friction self-piercing riveting	29
3.4	Friction Stir Blind Riveting	30
3.4.1	Joint strength comparison with spot welding	31
3.4.2	Fatigue resistance comparison with spot welding	32
3.4.3	Sensitivity analysis	33
3.4.4	Thermo-mechanical effects of friction stir blind riveting	34
3.4.5	FSBR process mechanisms: failure scenarios	36
3.4.6	FSBR process mechanisms: penetration force and torque analysis	38
3.4.7	FSBR process application to CFRP-CFRP and CFRP-Al joints	39
3.4.8	Predictions of joint quality	44
3.4.9	FSBR process application to magnesium-aluminum joints	45
3.4.10	FSBR system commercialization	50
3.4.11	Additional experimental tests with FSBR technology and comparison with conventional blind riveting	51
3.4.12	FSBR performance in dynamic loading conditions	53
3.5	Robotized Riveting system	54
4	Experimental analysis of FSBR method for a specific application of industrial interest	56
4.1	First experimental campaign objectives	57
4.2	Experimental setup and dummy test	58
4.3	Test features and schedules	63
4.3.1	Study of the thickness effect	63
4.3.2	Study of the stacking sequence effect	64
4.3.3	Study of FSBR compatibility with adhesive	65
4.3.4	Study of FSBR application CFRP-CFRP samples	67
4.4	Process quality and visual inspection	68
4.4.1	Process quality issues and criticalities	71
4.5	Lap shear methodology	76
4.6	Shear tests results	77
4.6.1	Thickness factor	78
4.6.2	Riveting technology factor: comparison between FSBR and hole pre-drilling methods	80
4.6.3	Analysis of feed rate effect	85
4.6.4	Study of the stacking sequence effect	86
4.6.5	Shear tests on riv-bonded samples	88
4.7	Conclusions on the first experimental campaign	89
5	Test methodology and experimental evaluation of supplier A process feasibility and joint quality	91
5.1	Suppliers validation process	91
5.2	Methodology	92

5.2.1	Samples geometry and materials	92
5.2.2	Lap shear tests	94
5.2.3	Corrosion test	94
5.2.4	Macrographic examination	95
5.3	Supplier A process features and coupons visual inspection	96
5.4	Lap shear test results	98
5.5	Corrosion test results	99
5.6	Macrographic analysis results	100
6	Experimental evaluation of supplier B process feasibility and joint quality	102
6.1	Supplier B process features and coupons visual inspection	102
6.2	Lap shear test results	105
6.3	Corrosion test results	106
6.4	Macrographic analysis results	107
7	Technologies comparison	108
7.1	Shear test comparison discussion	108
7.2	Measured joint strength statistic reliability	112
7.3	Corrosion test results comparison	114
7.4	Installation equipment comparison	117
7.5	Macrography results comparison	119
8	Conclusions	121
8.1	Future research directions	122
	Bibliography	124
	A Structural adhesive chemical aspects overview	128
	B Extract of the epoxy resin chemical family hazard identification	130
	C Description of secondary bending in riveted samples	131
	Vita Auctoris	133

List of Figures

1	<i>Actual blind rivets installation process</i>	2
1.1	<i>Main thread fasteners classification</i>	4
1.2	<i>FDS structure</i>	6
1.3	<i>a)Friction- drilling screws in Ford F-150 body assembly (courtesy Weber Screwdriving Systems Inc.)b)Friction drilling screw section and head undercut function (source: EJOT)</i>	7
1.4	<i>Friction drilling screws installation process with a pilot hole (source: Assembly magazine)</i>	8
1.5	<i>Six-axis robot devoted to the friction-drilling fastener installation (courtesy Weber Screwdriving Systems Inc.)</i>	8
1.6	<i>Solid rivet layout after setting</i>	9
1.7	<i>Section of metal sheets joined with flush rivets [7]</i>	10
1.8	<i>Semi-tubular rivet structure and bucking procedure</i>	11
1.9	<i>Section of metal sheets joined with self-piercing rivets</i>	11
1.10	<i>Self-piercing rivets setting steps [8]</i>	12
1.11	<i>a) Blind rivet setting steps [10] b) Example of blind rivet joints in aluminum alloy door [9]</i>	13
1.12	<i>Section of Trifold rivets used to join a different number of metal plates</i> .	14
1.13	<i>Bralo drive rivet (source: Bralo)</i>	14
2.1	<i>BIW production technologies of BMW 7 Series (source: BMW)</i>	16
2.2	<i>Example of L&L Products customized epoxy film adhesive for BMW [11]</i>	16
2.3	<i>a) Roof bows, b) central tunnel, c) C pillar and d) upper cross beam carbon fiber reinforcement (source: BMW)</i>	17
2.4	<i>Fully-automated blind rivets installation between the CFRP central tunnel and the aluminum platform (source: BMW)</i>	18
2.5	<i>Tunnel production cell (source: BMW)</i>	18
2.6	<i>a) Audi A8 Space Frame morphology (source: Audi) b) New Audi A8 main joining methods (source: Audi)</i>	19
2.7	<i>a) Example of the multiple joining techniques used in the Audi A8 body assembly (source: Audi) b) Riveting adoption in the rear of the passenger cage and carbon fiber reinforced panel (source: SAE international) c)Example of FDS wide adoption in one side accessible joints (source: Audi)</i>	20

2.8	<i>F-150 line: the aluminum body is assembled by means of self-piercing rivets (Photo by Austin Weber)</i>	21
2.9	<i>F-150 line: the aluminum body is assembled by means of self-piercing rivets (Photo by Austin Weber)</i>	23
3.1	<i>Current and future joint tensile strength requirement for different materials (Photo courtesy Arconic Fastening Systems and Rings) [17]</i>	25
3.2	<i>Conventional welding gun provided with a rivet feeder for RSR (Photo courtesy Arconic Fastening Systems and Rings) [17]</i>	26
3.3	<i>Lap shear tensile strength achieved by joining different kind of aluminum-to-steel couples (Photo courtesy Arconic Fastening Systems and Rings) [17]</i>	27
3.4	<i>FSR joining steps [21]</i>	28
3.5	<i>F-SPR setting process [25]</i>	29
3.6	<i>Friction self-piercing rivet geometry [26]</i>	29
3.7	<i>FSBR process steps: a) spindle acceleration b) rivet penetration c) shank deformation d) mandrel detachment [28]</i>	30
3.8	<i>Tensile test setup [29]</i>	31
3.9	<i>Load displacement curves comparison: FSBR (red) spot welding (black) [29]</i>	31
3.10	<i>Section view of friction stir blind rivet [29]</i>	32
3.11	<i>Fatigue life comparison of joints [29]</i>	33
3.12	<i>SSPV-08-06 Avdel rivet design [30]</i>	33
3.13	<i>Load-elongation curve for FSBR joints obtained at 12mm/min feed rate and 12.000 rpm spindle speed, using 15.4 mm (red curves) and 10mm (blue curves) rivet cup diameter [29]</i>	34
3.14	<i>EBSD microstructure (step size: 3 μm) [33]</i>	35
3.15	<i>EBSD microstructure (step size: 1 μm) [33]</i>	36
3.16	<i>Micro-hardness along the hole radial direction [33]</i>	36
3.17	<i>Elements and loads involved in FSBR process [34]</i>	37
3.18	<i>FSBR setting failure modes [34]</i>	38
3.19	<i>Force and torque trends as a function of the penetration depth [34]</i>	38
3.20	<i>Penetration force and torque as a function of feed rate and spindle speed [34]</i>	39
3.21	<i>Load-displacement curve of CFRP-CFRP joint at different spindle speed and feed rate [28]</i>	42
3.22	<i>On the left, a photograph of the fractured CFRP-AA611 joint. On the right, the correspondent load displacement curve [28]</i>	43
3.23	<i>Gesipa rivet geometry [27]</i>	44
3.24	<i>Methodology flowchart [39]</i>	44
3.25	<i>Engineering-based features obtained from force and torque signals [39]</i>	45
3.26	<i>Mechanical properties comparison between magnesium, aluminum and iron [40]</i>	46

3.27	<i>Material sleeve resulting from the riveting process of aluminum (2 mm) to magnesium (2 mm) [44]</i>	49
3.28	<i>Tensile strength comparison between FSBR and pre-drilled coupons for all the tested material combinations [43]</i>	49
3.29	<i>Riveting setting steps [45]</i>	50
3.30	<i>Cross-sectional macrograph of a FSBR joint between a 1 mm magnesium and 2mm composite plates [46]</i>	52
3.31	<i>Joint strength for all the tested material combinations [46]</i>	52
3.32	<i>Load-displacement curves resulting from joints testing, with comparison between FSBR and conventional blind riveting [47]</i>	53
3.33	<i>Wohler curves for 10%, 50% and 90% survival probability [44]</i>	53
3.34	<i>Robotic module</i>	54
3.35	<i>Robotic riveting assembly mounted on a six-axis robot</i>	55
4.1	<i>Aluminum and carbon fiber samples</i>	57
4.2	<i>Samples geometry</i>	58
4.3	<i>Zinc-Plated blind rivet geometry [48]</i>	59
4.4	<i>Schematic test layout</i>	60
4.5	<i>a) Hartford LG800 CNC Machine b) Experimental layout</i>	61
4.6	<i>Dummy sample a) inlet and b) outlet sides</i>	62
4.7	<i>3M 468 MP high performance acrylic adhesive adhesion performances with respect to other products (source 3M)</i>	67
4.8	<i>Fiber orientation comparison between the two used carbon fiber composites [50]</i>	67
4.9	<i>Example of sound joint between 0.8 mm CFRP and 3.1 mm Al samples (f=150 mm/s rs=6500 rpm: a) rivet inlet side b) outlet side</i>	68
4.10	<i>Comparison of formed material sleeves on the connection blind side: a) 1.6 mm CFRP - 1 mm Al b) 0.8 mm CFRP -3.1 mm Al</i>	69
4.11	<i>Example of sound joint between 3.17 mm CFRP - 1 mm A6061 samples (f=150 mm/s rs=6500 rpm: a) inlet face b) outlet face</i>	70
4.12	<i>Rivet outlet sections with FSBR technology (left) standard pre-drilling (right): a) 1 mm A6061-3.17 mm CFRP b) 0.8 mm CFRP-3.1 mm A6061</i>	70
4.13	<i>1.3 mm CFRP - 1.7 mm CFRP sample joined by fsbr technology: a) top view b) bottom view</i>	71
4.14	<i>0.8 mm CFRP - 3.1 mm A6061 riveted sample characterized by a quality problem (f=50 mm/s, rs 6500 rpm: a) top view b) bottom view</i>	71
4.15	<i>1.6 mm CFRP - 3.1 mm A6061 riveted sample characterized by a quality problem (f=150 mm/s, rs 6500 rpm: a) top view b) bottom view</i>	72
4.16	<i>1.6 mm CFRP - 3.1 mm A6061 inlet section of the sample after the rivet removal (f=150 mm/s, rs 6500 rpm)</i>	73
4.17	<i>1.6 mm CFRP - 3.1 mm A6061 riveted sample characterized by a quality problem (f=250 mm/s, rs 6500 rpm: a) top view b) bottom view</i>	74

4.18	<i>Maximum achieved penetration depth for a 1.6 mm CFRP - 3.1 mm A6061 riveted sample characterized by a quality problem ($f=150$ mm/s, r_s 8500 rpm)</i>	75
4.19	<i>Lap shear test schematic layout</i>	76
4.20	<i>MTS Criterion model 43 tensile testing machine</i>	77
4.21	<i>Most common failure modes in riveted lap joints. (a) tensile failure in the riveted material, (b) fastener shear out, (c) cleavage, (d) rivet-shear, (e) pull-out (bearing) [51]</i>	77
4.22	<i>a) load-displacement curves b) box plot of the samples joint strength according to different thicknesses (CFRP-A6061)</i>	78
4.23	<i>Observed failure modes: a) rivet shear out in the top composite layer (1.6 mm CFRP - 3.1 mm A6061) b) secondary bending and fastener pull-out (0.8 mm CFRP - 1 mm A6061)</i>	79
4.24	<i>a) load-displacement curves b) box plot of the samples joint strength according to different thicknesses (A6061-CFRP)</i>	80
4.25	<i>a) Rivet shear out in the bottom CFRP layer (1 mm a6061 - 0.8 mm CFRP) b) Rivet shear out in the top aluminum layer (1 mm A6061 - 1.6 mm CFRP)</i>	80
4.26	<i>Force-displacement diagrams comparing FSBR and conventional riveting technology for the CFRP/Al stacking sequence: a) samples with 1 mm A6061 b) samples with 3.1 mm A6061</i>	81
4.27	<i>Comparison between failed samples joined by means of FSBR (4 and 5) and reference samples (1 and 2)</i>	82
4.28	<i>a) Composite layer shear out failure in samples joined with standard drilling (left) and FSBR (right) (0.8 mm CFRP-3.1 mm A6061) b) Composite surface damage under the rivet cap due to the fastener stir action (1.6 mm CFRP - 3.1 mm A6061)</i>	82
4.29	<i>Bar chart comparing FSBR and conventional riveting technology</i>	83
4.30	<i>Comparison between FSBR and conventional riveting for the Al/CFRP stacking sequence: a) Force-displacement diagram b) bar chart</i>	84
4.31	<i>a) Detail of the rivet-aluminum interface in the sample joined with FSBR (up) and with conventional riveting (down) b) Failure by cracks propagation at 45° with respect to the sample edge for samples riveted with FSBR (left) and conventional methods (right)</i>	85
4.32	<i>Feed rate effect on 1.6 mm composite - 0.8 mm aluminum: a) CFRP-A6061 b) A6061-CFRP</i>	86
4.33	<i>Joint strength comparison in relation to the stacking sequence: a) Force-displacement diagram b) Bar chart</i>	86
4.34	<i>Box plot representing the samples joint strength according to thickness and stacking order (0.8 mm, 1.6 mm and 3.17 mm refer to CFRP samples thicknesses. 1 mm refers to A6061 samples thickness)</i>	87

4.35	<i>Comparison between riv-bonding and riveting techniques: a) Force-displacement curves b) Bar chart</i>	88
4.36	<i>Riv-bonded sample shear out failure: a) 2.4 mm CFRP-1 mm A6061 b) 1.3 mm CFRP-1.7 mm CFRP</i>	88
5.1	<i>Geometry of the samples provided by the OEM</i>	93
5.2	<i>Schematic representation of the corrosion test chamber</i>	95
5.3	<i>2.7 mm CFRP - 1 mm A6016 FSBR joint details: a) top view b) bottom view c) sideview</i>	97
5.4	<i>2.7 mm CFRP - 2 mm A6060 FSBR joint details: a) top view b) bottom view c) sideview</i>	98
5.5	<i>Shear test curves referring to supplier A samples testing: a) 2.7 mm CFRP - 1 mm A6016 b) 2.7 mm CFRP - 2 mm A6060</i>	98
5.6	<i>Sample picture after failure and schematic representation of fastener rotation</i>	99
5.7	<i>Supplier A samples after the scab20 corrosion test</i>	100
5.8	<i>Macrography images of supplier A samples: a) 2.7 CFRP - 1 mm A6016 b) 2.7 CFRP - 2 mm A6060</i>	100
6.1	<i>Rivet shank deformation in Huck auto bulb fasteners with respect to competitors</i>	104
6.2	<i>2.7 mm CFRP - 1 mm A6016 joined with robotized system: a) top view b) bottom view c) sideview</i>	105
6.3	<i>Shear test curves referring to supplier B samples testing: a) 2.7 mm CFRP - 1 mm A6016 b) 2.7 mm CFRP - 2 mm A6060</i>	105
6.4	<i>Failure in samples riveted by supplier B: A) 2.7 mm CFRP - 1 mm A6016 b) 2.7 mm CFRP - 2 mm A6060</i>	106
6.5	<i>Supplier B samples after the scab20 corrosion test</i>	107
6.6	<i>Macrography images of supplier A samples: a) 2.7 CFRP - 1 mm A6016 b) 2.7 CFRP - 2 mm A6060</i>	107
7.1	<i>Shear test curves comparison for a) 2.7 CFRP - 1 mm A6016 and b) 2.7 mm CFRP - 2 mm A6060</i>	108
7.2	<i>Schematization of the bearing failure mode observed on the samples riveted by supplier B</i>	109
7.3	<i>Installed rivets: a) friction-based technology b) robotic installation method</i>	111
7.4	<i>Box plot representing the median and the statistic reliability interval of the joint strength measurements</i>	112
7.5	<i>FSBR process and material forming: a) penetration phase b) qualitative thermal field representation around the rivet hole (source: supplier A)</i>	113
7.6	<i>Rivet corrosion after scab20 testing: a-b) supplier A samples c-d) supplier B samples</i>	114
7.7	<i>a) Zinc plating typologies b) Rust stages for zinc coated steel [53]</i>	115

7.8	<i>Yellow zinc coating non-homogeneity for supplier B samples</i>	116
7.9	<i>Supplier A installation module</i>	117
7.10	<i>Supplier B installation module</i>	118
7.11	<i>M-900iB/700 six-axis robot used to implement the robotic riveting module along the production lines</i>	119
7.12	<i>Macrography results comparison (2.7 CFRP - 1 mm A6016): a) supplier A sample b) supplier B sample</i>	119
C.1	<i>Schematic representation of: a) regular secondary and b) nonregular secondary bending</i>	131

List of Tables

3.1	CFRP-CFRP Joining process Window [28]	41
3.2	AA611-CFRP Joining process Window [28]	41
3.3	CFRP-AA611 Joining process Window [28]	41
3.4	Tensile strength of tested joints expressed in [kN] [28]	43
3.5	AM60-AA6022 Joining process Window [43]	47
3.6	AA6022-AM60 Joining process Window [43]	47
3.7	AM60-AA6082 Joining process Window [43]	48
3.8	AA6082-AM60 Joining process Window [43]	48
4.1	Rivet characteristics	59
4.2	6061 Aluminum characteristics	60
4.3	Test schedule for the study of riv-bonding process	63
4.4	Test schedule for the study of riv-bonding process	65
4.5	Test schedule for the study of riv-bonding process	66
4.6	Test schedule for the study of riv-bonding process for CFRP-CFRP samples	68
5.1	A6061 and A6060 mechanical properties	93
5.2	Corrosion test cycle	95
5.3	Supplier A joining process features	96
6.1	Supplier B joining process features	103
6.2	ABP-R8-M3 rivet specifications	104

List of Appendices

Structural adhesive chemical aspects overview	128
Extract of the epoxy resin chemical family hazard identification	130
Description of secondary bending in riveted samples	131

List of Abbreviations

BIW	Body in white
CFRP	Carbon fiber reinforced polymer
CNC	Computer numerical control
CTE	Coefficient of thermal expansion
EBSD	Electron-backscattered diffraction
F-SPR	Friction self piercing riveting
FCA	Fiat Chrysler Automobiles
FDR	Flow drilling rivet
FDS	Flow drilling screws
FSBR	Friction stir blind riveting
FSR	Friction stir riveting
HAB	High angle boundary
HSS	High strength steel
IMC	Intermetallic compound
LASSO	Least absolute shrinkage and selection operator
MMA	Methyl methacrylate
NVH	Noise Vibration Harshness
OEM	Original equipment manufacturer
PCA	Principal component analysis
RSR	Resistance spot riveting
RSW	Resistance spot welding
SBR	Spin blind riveting

SMC Sheet molding compound

SPR Self piercing rivets

SZ Stir Zone

TMAZ Thermomechanical affected zone

Introduction

One of the thesis main targets is to improve the efficiency and effectiveness of blind rivet joining technology. In order to understand the importance of this process optimization, it is necessary to explore the current technology scenarios in the field of mechanical joints for automotive applications. The need of more and more advanced techniques is not just the result of production output optimization, but also the consequence of stringent requirements in terms of vehicle performances, weight, fuel consumption and emissions.

The automotive industry has been characterized by significant changes in the basic design concepts which, nowadays, are more and more oriented toward environmentally sustainable vehicles. This is not just matter of moral responsibility, but to the necessity for modern manufacturers to deal with very stringent requirements in terms of pollutant emissions. These, which are among the factors necessary to guarantee the new vehicle homologation, can be only in part satisfied through more efficient pollutant after treatment systems. Indeed, a more direct way to deal with the problem of emission is the reduction of fuel consumption which, in turns, can be achieved by reducing the vehicle weight. This is the reason why light alloys and composites are taking the lead in the automotive industry, promoting the multi-material body in white approach. For instance, the aluminum usage for automotive applications is expected to double by 2025. In particular, in Europe, it is expected to reach nearly 200 kg per vehicle [1]. Different aluminum alloys are used to manufacture bumper beams and crash boxes for lightweight and crashworthiness. Also, high strength steels (HSS) are more and more employed for longitudinal beams, in order to provide the vehicle structure with the proper stiffness level. Moreover, carbon fiber reinforced materials can be used for panels or as reinforcement in order to increase the body stiffness by reducing its weight [2]. In addition, magnesium components are becoming more and more common in modern vehicle body structures.

One of the major implications of this multi-material approach, is the deep change in the production process it requires, particularly for the body in white assembly. This is especially the case of joining techniques, among which welding has lead the scene from the very beginning of vehicle industrial production. Indeed, the thermal properties, such as the coefficient of thermal expansion (CTE) or the melting point of aluminum, steel, magnesium and composites, are significantly different between them. This implies that conventional welding technologies would be not effective in performing multi-material connections. Consequently, the progressive replacement of steel with light alloys is

deeply related to the more and more significant utilization of alternative joining techniques.

In the just described scenario, the aim of the thesis is to optimize one of the most adopted mechanical joining method, namely the riveting one. The increase of the joining efficiency and the reduction of the required cycle time is of paramount importance for the feasibility of dissimilar material body in white production.

As it will be discussed in the following, riveting is among the most common joining technique for connecting dissimilar materials, such as aluminum to steel and aluminum to carbon fiber. The latter combination, is often joined by means of blind rivets. The installation of this kind of fastener presents several practical criticalities (schematized in figure 1), whose solution is the main target of the present research. In particular, blind rivet setting requires that the material sheets to be joined present a pre-drilled hole.

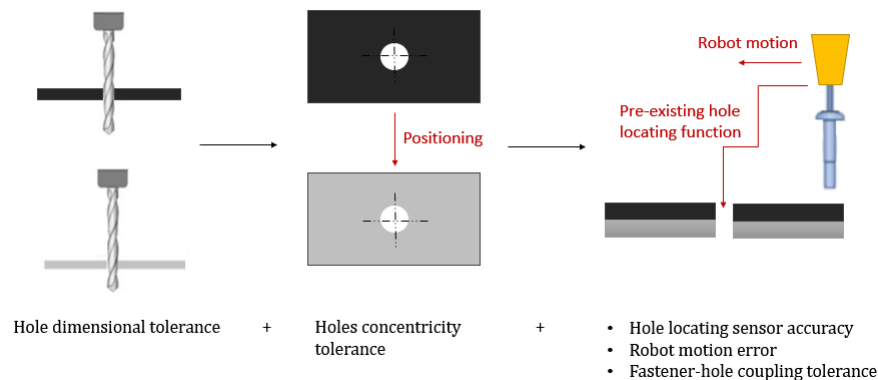


Figure 1: *Actual blind rivets installation process*

Nevertheless, in actual automotive production processes, the drilling and rivet setting operations are decoupled between each other. Indeed, the body panels are drilled separately in specific workstations and, only subsequently, riveted together on the assembly line. This process workflow introduces some criticalities that make difficult the implementation of an automated blind rivet installation equipment. These difficulties are mainly related to the accumulation of processes errors and tolerances in the various step of the joint manufacturing. Indeed, the hole drilling dimensional tolerance must be taken into account, as well as the components holes coaxiality tolerance before the rivet insertion. This situation leads to two alternatives that are the manual rivet installation, performed by an operator with semi-automatic riveters, or the over-dimensioning of the drilled holes, which allows to deal with the previously mentioned tolerances and with the robot additional motion error. In order to make the process more efficient, the drilling operation should take place almost together with the rivet setting, when the components are already in their designed position in the vehicle body assembly. By performing the drilling and riveting operation in a single step (or in two strictly sequential ones), it is possible to get rid of all the previous manufacturing issues and to make the process fully automated. In general, automation means higher efficiency and lower cycle time, providing a relevant improvement for the whole assembly line management.

Entering in the industrial details of this thesis, the application of new blind riveting

process has been requested by FCA for a well-defined application, in order to enrich the benchmark data useful for future projects. This application involves the hybrid connection of carbon fiber and aluminum layers by means of blind rivets plus structural adhesive. As it will be presented in some examples of other car manufacturers, this material combination can be considered quite widespread. For instance, Audi and BMW adopt carbon fiber structural and reinforcement elements assembled on the aluminum body in white. This kind of solution combines the lightweight and stiffness for those applications in which manufacturers look for a trade-off between low weight and costs. Indeed, a vehicle body entirely made of carbon fiber is very expensive and adopted just for very high-end cars. Much more common and realistic applications for many carmakers, including FCA, is that of connect stiff and lightweight composites with more conventional aluminum or steel body frame component. This multi-material connection by means of an innovative blind riveting technology represents the driving force of the present work.

Besides the identification of an innovative and more efficient blind riveting technology, the present work is based on the cooperation with specific suppliers to verify first of all the feasibility of given process with a well-defined carbon fiber reinforced plastic (CFRP)-aluminum combination. The process effectiveness will be then verified by means of some preliminary mechanical analysis

Chapter 1

Overview of the main alternative joining techniques

In order to discuss the main practical issues related to the most employed joining techniques for automotive applications, it is worth to briefly revise their most relevant features. The choice of the joining strategy must be compliant with each design specification and requirement, which are not just including the fastening technical features, but all the economic and practical concerns related to the process implementation. A mechanical fastener is a device employed in order to mechanically join two or more components together. A quite common fasteners classification is that between permanent and non-permanent ones, in which it is possible to identify respectively rivets and threaded fasteners.

1.1 Threaded Fasteners

A threaded fastener consists in devices, like bolts, nuts, screw, and stud, featured by an internal or external screw thread, which allows connecting two or more components together.

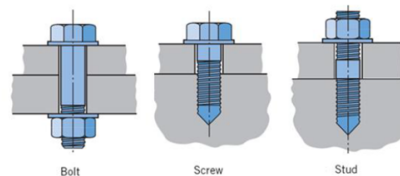


Figure 1.1: *Main thread fasteners classification*

Figure 1.1 shows the three main categories of fasteners, which are bolts, screws and studs. The former present a head on one extremity and a threaded segment on the other one, where a nut is used to secure the joint. A wide variety of automotive bolts are available in the market such as wheel bolts, hub bolts, and U-bolts.

Screws are used to secure a blind connection, namely just one of the two components possesses a through hole while the second part has a blind threaded hole. The advantage

with respect to the bolt is the accessibility of the parts couple, which is required just on one side. Moreover, the absence of the nut ensures a weight reduction, but additional machining operations are required in order to internally thread the part.

Studs are in between the previous two solutions, being characterized by a thread in both extremities, one of which is tightened in the second piece, while the other is used to create the fastener head by means of a nut.

Automotive fasteners can be produced using different metals according to the specific application. Typical choices are stainless steel, iron, brass, aluminum or nickel.

It is not necessary to enter into the details of threaded fasteners' working features, since they are quite standardized and well-known. What is worth noticing is that, in the industrial and automotive field whenever this kind of mechanical connection is employed, especially for critical bolted joints, it is necessary to control both input torque and angle of turn to achieve the desired result of proper preload of the bolted assembly. The key parameter to understand the relationship between torque, angle, and tension is the friction generated in the fastener under-head and in the threaded contact area.

The importance of threaded fasteners in the automotive field is demonstrated by the fact that the worldwide automotive industry is regarded as one of the single largest consumers of fasteners. It can be quantified considering that, in average terms, the automotive industry creates a demand of about 26 billion fasteners per year.

1.2 Adhesives

The previously discussed fastening drawback, related mainly to costs and weight, can be potentially mitigated by the structural adhesives adoption. The general adhesives definition is that of chemical substances, of different nature, applied on one or both surfaces of two distinct components, binding them together and resist their separation. An adhesive is "structural" if it has sufficient strength to transfer or share loads between highly stressed components, like in a car body structure. Indeed, in the field of structural adhesives, it is required a minimum load of 6.9 MPa to separate the bonded components. They can be used to bond coated metals like steel to aluminum, carbon fiber panels to steel or aluminum, sheet molding compound (SMC) to aluminum and more.

Apart from the weight saving, structural adhesives do not require any pre-hole, which contribute to make the assembly process more expensive and complex. The elimination of drilling operations could potentially decrease the manufacturing cycle time, which in turns is responsible of the overall cost decrease even if the adhesive costs were higher than traditional fasteners. Nevertheless, it is worth to consider that a certain surface preparation and treatment is still required in order to maximize adherence, like surface cleaning (prior to adhesive application), fixturing and cure. These can determine a prolonged processing time and cost with respect to the adhesive application in itself.

However, the absence of holes is responsible for a much better system fatigue resistance. The boost in adhesive technology is mainly given by its efficient application in several industrial fields like marine, architecture and automotive ones. The importance

of this joining technology is emphasized by its economic impact. Structural adhesives market is now around US\$ 4.5 billion, but with large growth margins according to the Freedonia Group (leading international business research company), which foresees a further growth to US\$6-\$7 billion by 2020 [4]. An overview of the chemical aspects and adhesives preparation for industrial application is presented in Appendix A.

1.3 Flow drilling screws

Another joining technology, which is becoming more and more widespread in the automotive field, is the flow drilling screw (FDS). It is part of those solutions specifically designed in order to join lighter alloys and mixed material vehicle body components. The original design was developed by EJOT GmbH & Co, which is also the main supplier for modern carmakers. One of the most remarkable reasons why this kind of fastener is going to be increasingly employed in automotive industry is its single-sided fastening solution, suitable for the assembly of extruded profiles in difficult-to-reach BIW zones. Nevertheless, as it will be seen, a certain room in the blind side of the assembly is still required for the accommodation of the created boss and the fastener protruding tip.

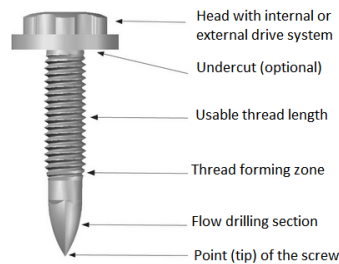


Figure 1.2: *FDS structure*

An example of this technology application, is its significant usage in the Ford F-150 (figure 1.3.a) and Chevrolet Corvette, both of which are largely made from aluminum. There are also other vehicles featuring FDS, like Cadillac CT6, Acura NSX, Mercedes-Benz SLS, Audi TT, A4, A6 and A8, Porsche 911 and Boxster, Lotus Evora, Jaguar XK, Ferrari California, and Lamborghini Gallardo. These applications include not only the car body, but also the coolant pipe assembly.

The flow drilling screw structure is featured by a flat and wide head and a thick stem. The former can be shaped in different ways, depending on the drive system, and the bottom of its surface can present an undercut. The latter has the function of accommodating the material flowing upward, toward the screw head during the boss formation (figure 1.3.b).

Nevertheless, sometimes this cavity is not enough, especially when many material layers are joined, or when they are quite thick, or also when one of the material layer is not so suitable to the process features. In these cases, the so-called clearance hole is pre-drilled in the upper layer, in order to provide a place for the material to flow. The mentioned case is showed in figure 1.4. The stem is divided into three segments,



Figure 1.3: *a) Friction- drilling screws in Ford F-150 body assembly (courtesy Weber Screwdriving Systems Inc.) b) Friction drilling screw section and head undercut function (source: EJOT)*

which are the unthreaded drilling tip, the lower and upper threaded sections, needed respectively for thread forming and to apply the clamping load. The fasteners are made of neutral or hardened carbon steel. The former is used just for aluminum-only applications, while a zinc-aluminum coating is almost always used for corrosion protection and to minimize the assembly torque. Concerning its working principle, flow drilling screws, or friction drill screws, can be regarded as self-piercing fasteners for metal sheet layers. They combine the process of friction drilling with that of thread forming.

As shown in figure 1.4, the screw penetrates the layers, extrudes a short protrusion, forms its own threads, and applies clamping force between the sheets. The installation process presents a cycle time of about three seconds and follows six steps, which are heating, penetration, extrusion, thread forming, screw driving and tightening.

The heating phase, which is due to the screw high speed rotation and downforce (from 1.5 to 2.5 kN), cause the material surface to reach a temperature in between 150 to 250°C, depending on the material itself. Clearly, all the involved parameters are strictly dependent of the material properties, as hardness and thermal conduction coefficient. For instance, the driver speed must switch from 4000 to 6000 rpm if aluminum must be joined, instead of steel. This is due to the aluminum tendency to faster dissipate heat compared to steel. During the penetration, the downforce reduces and the fastener conical shape allows for the extrusion of a short boss on the blind side of the material stack. It follows the thread creation, occurring at a lower screw driver speed (around 2000 rpm), and the screwing at about 200 rpm to not damage the thread. Finally, the tightening occurs in full control of torque and speed.

Compared to all the previously joining technologies, friction drilling screws provide also a stronger joint, with greater peel strength than spot welding, clinching and self-piercing rivets. Moreover, beside the advantage of one side accessibility requirements, the fact that the hole is drilled by the fastener itself, makes not necessary to align the pre-drilled holes prior the assembly. In addition to that, FDS are suitable for dismounting and replacing, since they are a kind of reversible join. This is a key feature considering how much fasteners removability is nowadays important from the recyclability requirements viewpoint. No tolerance issues must be faced for the coupling between male and

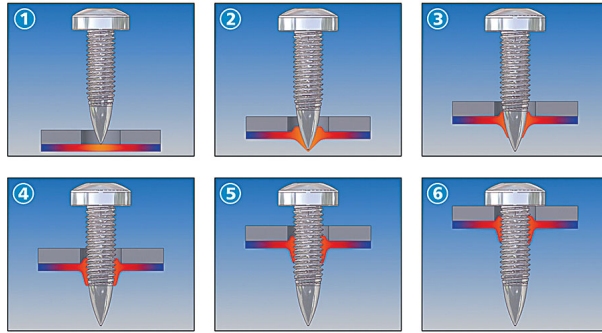


Figure 1.4: *Friction drilling screws installation process with a pilot hole (source: Assembly magazine)*

female thread, since the former creates the latter (which is metric, generally M4, M5 or M6) and matches with it. Furthermore, they have been proved to present a high loosening torque and vibration resistance, with no requirements for additional safety elements. Finally, no chips are generated during the installation and, consequently, they not create any waste, like in the case of thread-cutting screws or drilling and tapping operations [5].

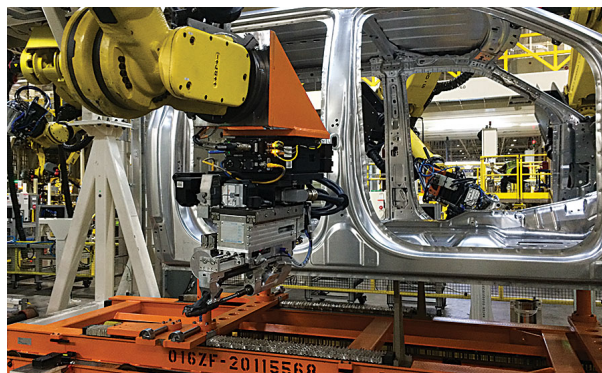


Figure 1.5: *Six-axis robot devoted to the friction-drilling fastener installation (courtesy Weber Screwdriving Systems Inc.)*

A possible disadvantage from the production process viewpoint, could be the higher equipment complexity, since the larger number of parameters to be controlled makes standard screwdrivers not so suitable for friction-drilling screws setting. Beyond torque and angle, the screwdriver must check, during all the previously described installation phases, the rotation speed, axial force and fastener depth. All of these factors must be properly set depending on the specific application, namely number and thickness of the metal sheets, material properties, surface treatments and overall joint requirements. Because of this level of complexity, these drivers are generally mounted on fully automated systems such as six-axis robot, which must be clearly suitable to deal with the involved loads (in order to ensure the proper fastener downforce).

1.4 Rivets

Riveting is another type of mechanical joining method. It is one of the most corroborated solution to substitute spot and laser welding in innovative light alloy vehicle bodies, because of its high strength, mechanical reliability and relatively short cycle time. The latter actually depends on the riveting technology and its minimization is one of the target of the present study.

Rivets are a particular kind of permanent mechanical fastener, which are deformed during the setting process. Before it, the rivet appears similar to a traditional fastener, with a head and a smooth cylindrical shaft, whose extremity is called tail. Concerning the most traditional rivet version, this type of fastener requires a pre-drilled hole in which the rivet is then inserted and fixed by means of different kind of plastic deformation mechanisms. This is responsible of creating another sort of head on the tail side, flattening the shaft extremity. At the end, the rivet has two heads, the original one and that obtained during the setting process, which are called factory and shop head respectively. After the setting procedure, the rivet tail is said to be upset or bucked.

This fastening layout allows the rivet to act as a clamp that keeps in place more components together, resisting axial loads, which would tend to separate them. However, even if a properly installed rivet will resist tension to a certain extent, its main purpose is to transmit loads along the piece direction, and not at a major angle away from it.

Before exploring the main applications in automotive field, it is worth to briefly describe the main riveting techniques and rivet designs, whose differentiation is aimed to deal with several cost, strength and accessibility requirements.

1.4.1 Solid rivets

Solid rivets are the oldest (the first evidences of their employment date back to the Bronze Age) and probably the conceptually simplest kind of rivets. Nevertheless, they are also one of the most reliable type of fastener and, because of that, they are largely employed in applications where safety is the main concern, such as in aircrafts structural elements.

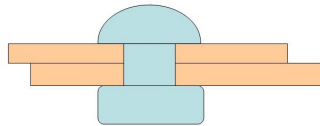


Figure 1.6: *Solid rivet layout after setting*

Almost hundreds of thousands of solid rivets are employed in the assembly of modern aircrafts and, for this application, different materials can be used such as aluminum alloys, titanium and nickel-based alloys. Steel rivets can be instead used in static structures such as bridges and building frames. Nevertheless, steel structural rivets have been gradually replaced by bolts. The reason is essentially related to the complexity of bucking procedure, which requires the double of workers with respect to those needed for

obtaining a mechanical joint through bolts. Moreover, the procedure in itself is requiring for much more skilled workers, because it includes a warming of the rivet in the furnace, bringing the hot rivet to the joint place and induce the plastic deformation. Besides the disadvantages related to the process complexity, this kind of solid rivets are no more used because hot rivet cannot be properly heat treated in order to increase strength and hardness. This caused poor performances in case of excitations, like seismic ones, on structures using this kind of technique, like bridges.

From a structural viewpoint, solid rivets are featured by a head and a shaft which, during the setting procedure, is plastically deformed by means of a hammer or a rivet gun. This can be hydraulically, electromagnetically or pneumatically driven.

A very common type of solid rivet is that of flush rivets, also known as countersunk rivets. One of their peculiar features is related to the good appearance of the riveted surface after the setting process. The usage of flush rivets allows having a smooth surface, which represents a key factor especially in the aeronautic field, where the aerodynamic drag reduction is an absolute priority. For this reason, also after the rivet installation, some machining operations can be performed in order to minimize the air flow resistance. As the majority of rivets, they require a pre-drilled hole, but an additional machining operation is required to get the hole copying the cone shaped head of the flush rivet. The countersinking operation is that responsible of the flush rivets high cost in a production process which, in the past, caused constructors to limit the adoption of this solution to as few components as possible [6].



Figure 1.7: *Section of metal sheets joined with flush rivets [7]*

However, one of the solid rivets disadvantages is in general related to the need of having access to both side of the structure during the setting procedure, unlike blind rivets. Because of all the mentioned reasons, solid rivets are not employed in automotive field.

1.4.2 Semi-Tubular Rivets

Tubular, or semi-tubular, rivets are conceptually and structurally similar to solid rivets apart from the presence of a blind hole in correspondence of its tail. Its function is that of reducing the amount of force needed to set the rivet by causing the tail deformation. Indeed, this force is 1/4 of that needed for the correspondent solid rivet. The setting process is so versatile that many different tools can be employed from the simplest manual squeezer to impact riveter and completely automated PLC-controlled robotics (Programmable Logic Controllers). Tubular rivets have several applications in

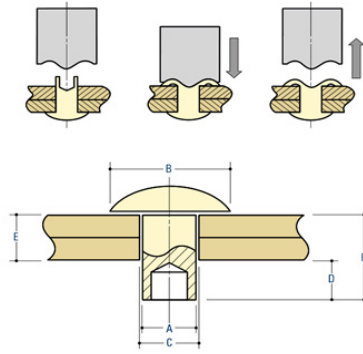


Figure 1.8: *Semi-tubular rivet structure and bucking procedure*

mechanical and electronic fields thanks to the variety of employed materials such as steel, brass, copper and aluminum. As seen presenting solid rivets, also in this case the setting procedure requires the assembly accessibility on both sides.

1.4.3 Self-pierce rivets

Self-pierce rivets (SPR) are aimed to provide conceptually the same joining action of blind and solid rivets, mechanically connecting two or more dissimilar materials, such as aluminum, steel, plastic or composite, even if they are pre-coated or pre-painted. The significant difference is, as suggested by their name, these rivets do not require the pre-hole drilling, simplifying the joining process.



Figure 1.9: *Section of metal sheets joined with self-piercing rivets*

The rivet structure is similar to semi-tubular ones, presenting a blind hole in the rivet stem (opposite to the head), but an additional chamfering allows the piercing of materials to be joined. Different rivet length and diameters are employed depending on the specific application, as well as the rivet head, which can be a pan or countersunk one.

Concerning the setup process, showed in Figure 1.10, it is a single-step technique in which a hydraulic or electric setter driver is used to guide the rivet into the materials. Its deformation is controlled by the die on the opposite side of the metal sheets (i.e. the die provides a cavity in which the bottom metal sheet can flow during the deformation). The rivet setter choice affects the joining cycle time, which can be around one second.

The rivet deformation is so that its tail interlocks into the lowest material layer creating a small button. The setter makes the rivet piercing the top layer(s) of material, while the lowest one is just deformed but not pierced at the end of the process. This aspect is what ensures the joint sealing from water or gas.

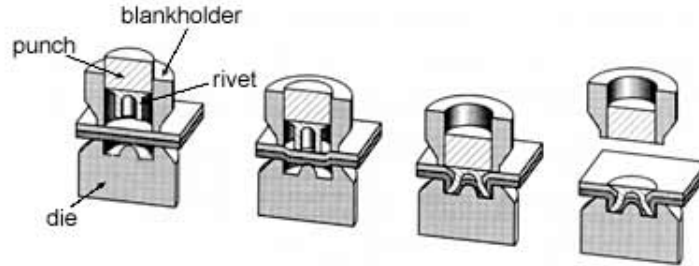


Figure 1.10: *Self-piercing rivets setting steps [8]*

It is quite evident that, in order to pierce the metal sheets, the rivet must be harder with respect to them. Consequently, depending on the material to be joined, the rivet undergoes different levels of hardening heat treatments. Indeed, it is fundamental to find the proper matching between the rivet hardness and that of the materials to be joined. If a rivet is too soft for a material stack, the rivet will buckle or be compressed during the riveting process. If, instead, the rivet is too hard with respect to the metal sheets, the rivet will exhibit too little deformation after setting. This would imply an insufficient interlocking between the different material sheets and, consequently, a low joint strength.

From the productive viewpoint, self-piercing rivets benefits are summarized by:

- Low energy demand, no heat, fumes or sparks production
- High and repeatable quality.
- High strength
- Suitable to visual inspection
- Single step process (no pre-drilling required)
- Possibility to join metallic and non-metallic materials
- Flexibility to join different material strength and thickness

The riveting system can be manual or automatic, so suitable both for low and high-volume productions. In the latter case, one of the key issues is the continuous feeding of rivets to the automated systems along the line. This is generally achieved by means of tape and come in cassette or spool form. One of the possible disadvantages, which is overcome by flow-drilling screws, is the both sides accessibility requirement during the rivet setting. This can be a problem in such areas of the vehicle BIW, which can be difficult to be reached during the assembly process.

1.4.4 Blind Rivets

In the industrial context, it is not always easy to ensure to the worker or the robot the accessibility on both sides of the panels or components to be riveted, especially along the line of a large volume production process. For this reason, blind rivets, also known as POP rivets, became more and more common in modern production environments.

From the structural viewpoint, the rivet presents a mandrel, which is used for the setting of the rivet itself. As all the other discussed rivets, this system still requires a pre-drilled hole passing through the two components to be mechanically coupled. The rivet is inserted through this hole and it is set by means of a specific tool, which is aimed to pull the mandrel causing a plastic deformation of the rivet blind end, determining the creation of the so-called shop head. The setting process ends when the head of the mandrel reaches the face of the blind side material, the pulling force is resisted, and this causes the local fracture of the mandrel in a well specified position, where the mandrel stem separates in two parts, leaving the head of the mandrel encapsulated at the blind side. Anyway, missing a non-locking mandrel, vibrations or other dynamic excitations can cause the mandrel to fall out. In this case, the joint would rely only on a hollow rivet, characterized by a much lower load bearing capability if compared to solid rivets. In other terms, the state of art in terms of blind riveting technology requires the pre-drilling of the material to be joined and is characterized by an extra cost and weight due to the presence of the rivet itself. However, the main advantage of this joining method is the required access to the material from one side only, the little material damage and the joint strength which is comparable or higher than spot welding. The latter consideration is especially valid in the joint between steel and aluminum, since blind riveting, unlike spot welding, does not produce any brittle intermetallic compound (IMC) [9]. An example of blind riveting application in the automotive field is reported in Figure 1.11.b, showing blind rivets usage for fixing the steel door impact beam in the Mazda RX-8.

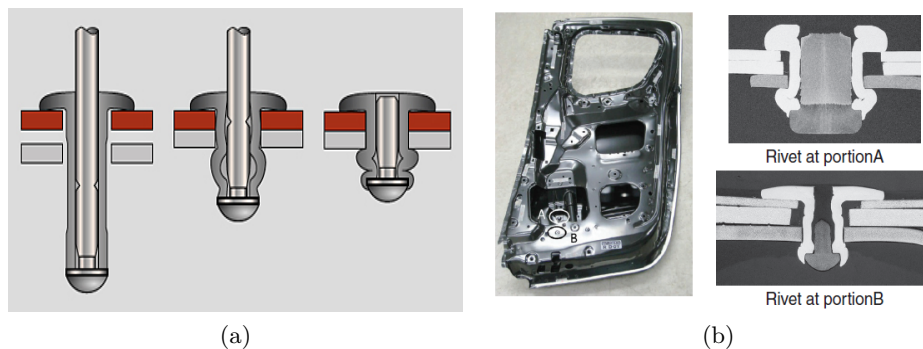


Figure 1.11: a) Blind rivet setting steps [10] b) Example of blind rivet joints in aluminum alloy door [9]

There are different head shapes and available material such as aluminum alloy, steel, copper and Monel (a group of nickel alloys). It is also possible to find different variants of pop rivets, depending on the application. The main typologies are:

Trifold rivets

This kind of rivet is generally made up of aluminum and designed for the assembly of soft, brittle or thin materials. It is so called because of the formation of three equal leaves during the setting process, which allows having a wider footprint on the blind surface, reducing the risk of cracking the material and compensating for possible oversized holes.



Figure 1.12: Section of Trifold rivets used to join a different number of metal plates

Drive rivets

It is also called drive screw and represents a kind of blind rivet not requiring a through hole. It is used to join plastic, metal or wood panels, sheets and profiles in the construction sector, since it leaves an aesthetically pleasant appearance. As shown in Figure 1.13, the drive rivet mandrel is protruding from the thread before the rivet setting. This process does not require any special setting tool, but just a hammer, which is used to drive the mandrel within the rivet body (generally in aluminum). In this way, the rivet body opens in three different blades fixing it with the hole internal walls.

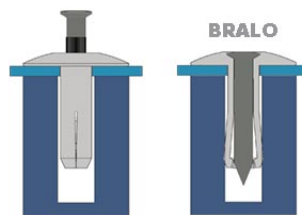


Figure 1.13: Bralo drive rivet (source: Bralo)

However, because of its structure, the clamping force is clearly lower with respect to previously discussed riveting systems. The main advantages of drive rivets are related to:

- The possibility of riveting components with blind drills
- Good resistance (without loosening) to vibrations
- Good resistance to corrosion
- Speed and low complexity

Chapter 2

Examples of multi-material vehicle body in white and joining strategy in the present market

As aforementioned and discussed, the growing tendency of car manufacturers to reduce the vehicle weight, which is a key factor for the minimization of fuel consumption and emissions, is resulting in the progressive substitution of steel with lighter alloys. By combining the properties of low density materials, such as aluminum, magnesium, plastic, composites, and high strength steels the weight of a vehicle can be reduced, thus increasing the energy efficiency. Clearly, this requires to use the proper bonding and riveting strategy. This section is aimed at discussing the blind rivet installation techniques in the most important carmakers competitors, starting from the European market. The target is to understand if any of the fully-automated systems previously described is actually employed on the existing production lines. The considered models are those featured by a high variety of light alloys and composite materials, since in this case the employment of mechanical joining technologies is more significant.

2.1 BMW 7 series: an important step toward the future of multi-material vehicle body in white development

A significant effort, oriented toward the progressive development of multi-material vehicle body, is that of BMW. This is particularly the case of the new 7 Series, whose production process determined a significant investment of more than half billion euros. The latter allowed improving and increasing the automation of aluminum die casting, carbon fiber-reinforced plastic production and the efficiency of the overall body in white assembly process. The development of the new production process required not only the mentioned economic investment, but also a three-years study and tuning of the process itself. This increase of complexity is even more impressive if considering that BMW Dingolfing plant is already the largest manufacturing site in Europe, in which 15 different models are produced, from 3 to 12 cylinders, plug-in hybrids, bodies for Rolls-Royce

and from 3 to 7 Series.

The main result achieved with the 7 Series is a lightening of 130 kg with respect to its direct competitor, the S-class Mercedes. A weight saving of 40 kg has been achieved introducing just 3% of CFRP parts in the vehicle BIW, characterized by an overall weight of 13 kg.

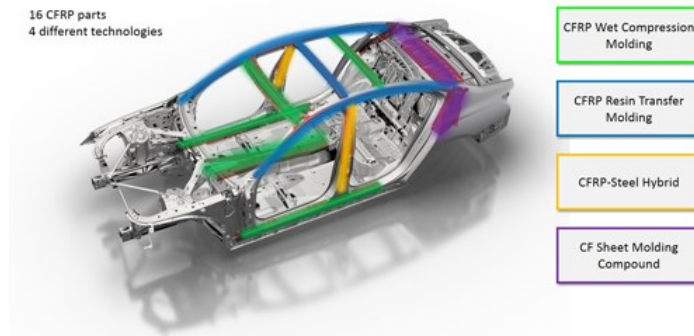


Figure 2.1: *BIW production technologies of BMW 7 Series (source: BMW)*

The innovation of carbon reinforced elements can be observed in 16 different components, which have been produced following four different technologies, listed in figure 2.1. These elements allow getting a reinforcement and, at the same time, a lightening of the passenger compartment, which is referred as “carbon core”. Concerning some examples of the joining methods adopted in this innovative vehicle, the B-pillar structure is constituted by a formed steel part and a carbon fiber prepreg, joined together by epoxy adhesives (supplied by L&L Products).



Figure 2.2: *Example of L&L Products customized epoxy film adhesive for BMW [11]*

Other components like the tunnel, sills and roof bows are reinforced with carbon fiber by using wet compression molding. L&L adhesive have been mainly employed in the BMW 7-Series B-pillar assembly. In this application, which is illustrated in figure 2.2, the epoxy film adhesive is employed to bond the metal with an internal carbon fiber stiffener for the central pillar, providing also the function of galvanic isolation.

The curing temperature is around 190°C and it lasts about 2 minutes for this specific application, and no surface preparation is required for both surfaces. A particular feature is the addition of a glass layer allowing to separate the steel surface from the carbon prepreg. This is done in order to avoid galvanic effects.

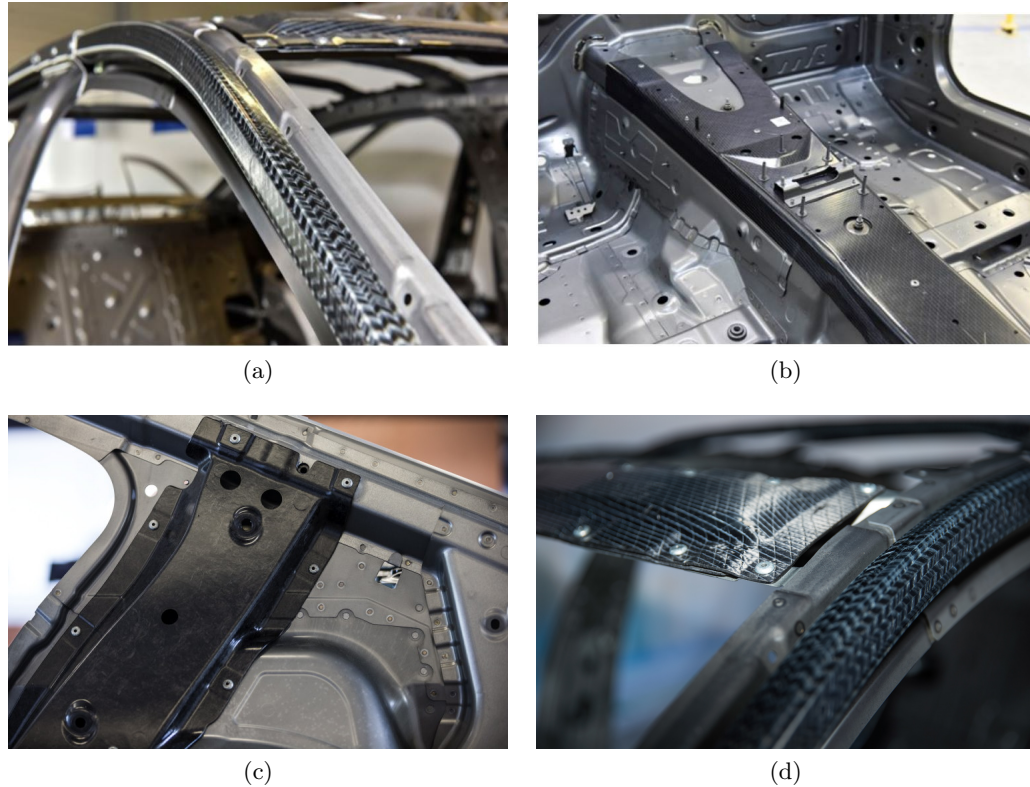


Figure 2.3: a) Roof bows, b) central tunnel, c) C pillar and d) upper cross beam carbon fiber reinforcement (source: BMW)

The body shop is, clearly, highly automated. The shop section of the 7 Series alone is characterized by 460 robotic arms, which are overseen by 130 technicians per shift. The different components, after washing and drying, are sent to the 20 automated production cells to join the CFRP parts to the metal ones. If, on one hand, all the employed joining methods had been already adopted in the automotive industry, on the other hand, BMW had to adapt them to the new materials and production cycle. In addition, another challenge is that of qualify personnel for the maintenance and management of the required equipment for joining multiple material. To provide some examples, roof rail and sills reinforcement are assembled by means of adhesives and rivets. Blind rivets are used together with adhesive in order to achieve an hybrid joining technology called riv-bonding. On one hand, this allows to keep in position the carbon fiber components during the epoxy adhesive curing. On the other hand, they significantly improve the joint strength and reliability. Blind rivets represent a sort of backup joining method that play an crucial role in case of accident, when the peel resistance of adhesive cannot ensure enough crashworthiness. Multiple examples of riv-bonding adoption are shown in figure 2.3

An important achievement of the benchmark analysis has been to demonstrate that

blind rivets are installed in a fully-automated way. This process is presented in figure 2.4. Evidences prove that composite tunnel and the metal frame are joined by means of a riveting module mounted on a six axis robot. However, both the tunnel and the body floor are pre-drilled before being positioned one on top of the other. This means that the automated riveting equipment still requires the hole-locating function, which takes about 2 seconds per spot in order to ensure the riveting tool proper positioning before the fastener installation.



Figure 2.4: *Fully-automated blind rivets installation between the CFRP central tunnel and the aluminum platform (source: BMW)*

BMW uses also the innovative technology of flow-drill-screws. They are characterized by a very fast installation, during which the screw heats up the material, enhancing the fastener penetration. The joining is still reversible and the fastener can be unscrewed and re-screwed as long as the thread is not damaged. In that case a common maintenance solution is to replace it with a blind rivet. Around 150 flow drill screws are used for each 7 Series BIW. Nevertheless, the tendency is that of gradually eliminate fasteners with lighter adhesives, like in the tunnel assembly cell, where the CFRP tunnel rotates under a dispense nozzle, distributing the adhesives.



Figure 2.5: *Tunnel production cell (source: BMW)*

After that, some quality checks are performed in order to assess the width of the adhesive bead and the absence of interruptions. The new BMW 7 Series uses about 150 m of adhesives. One of the main adhesive supplier for this model is the chemical company Sika AG, a swiss provider manufacturing and distributing products for bonding, sealing, damping and reinforcing for the building sector and the motor vehicle industry. These

products are already used in more than 50% of the vehicles manufactured worldwide. As mentioned, the composite tunnel is mated with the metal part by using rivets, which fix the components in position during curing and hardening. The discussed tunnel production cell has a throughput of 17 units per hour [11].

2.2 A benchmark manufacturer: Audi A8 multi-material BIW

Audi is one of the most active car manufacturer company in terms of light material employment for the vehicle structure, and joining techniques. This tendency seems to become more and more significant with time and, as a proof of this, the Audi A8 has been presented as one of the most revolutionary cars in the field of material choices and production process. The structural solutions introduced by Audi engineers allowed for BIW weight reduction from 282 to 231 kilograms.

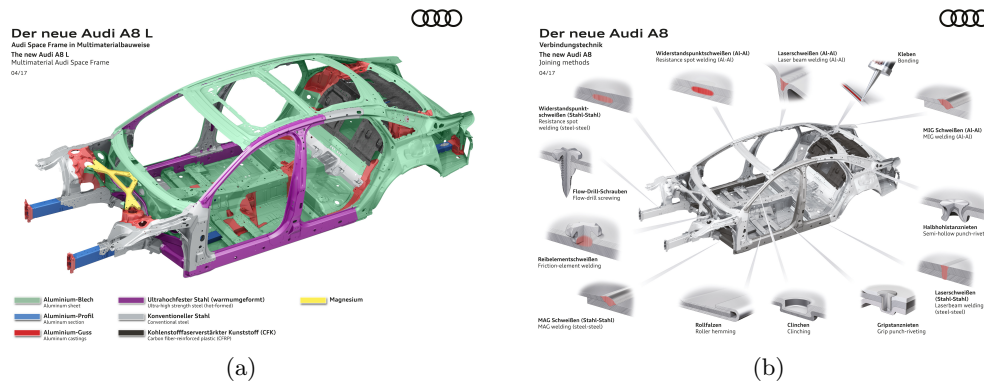


Figure 2.6: a) Audi A8 Space Frame morphology (source: Audi) b) New Audi A8 main joining methods (source: Audi)

As it can be observed in figure 2.6.a, the new A8 structure is constituted by 58% of aluminum, magnesium front strut tower and ultra-high strength steel (UHSS). Concerning aluminum, the company states to have developed a new heat-treated cast alloy, which is supposed to be stronger than before, improving the crash tests performance. The magnesium front strut is attached to the chassis by means of aluminum bolts. This results in a 28% lighter but stiffer body structure. Indeed, despite the overall vehicle lightening, it has been achieved a higher torsional stiffness, which is considered by Audi as "the critical parameter for precise handling and pleasing acoustics". The introduction of a carbon-fiber panel in the rear of the passenger cage is one of the main innovations allowing to provide 33% of the overall vehicle torsional rigidity, increasing its value of 25% with respect to the previous A8 model [12]. This high variety at material level is reflected in the process complexity, especially for what concerns the joining methods, which are 14 in total. For instance, cold roller hammering is used to connect the aluminum side-wall frame to the ultra-high strength steel in the B-pillar, sills and roof rail.

Figure 2.7.a provides a detailed view of multiple joining methods employed in this

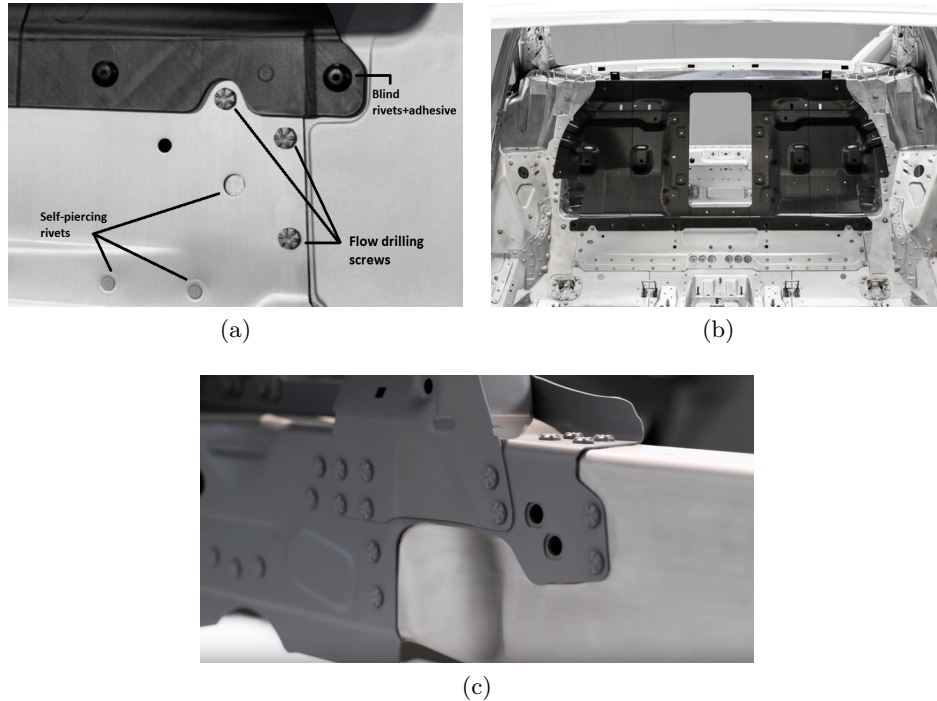


Figure 2.7: a) Example of the multiple joining techniques used in the Audi A8 body assembly (source: Audi) b) Riveting adoption in the rear of the passenger cage and carbon fiber reinforced panel (source: SAE international) c) Example of FDS wide adoption in one side accessible joints (source: Audi)

vehicle model. It is possible to recognize the utilization of flow drilling screws, self-piercing and blind rivets. In particular the CFRP rear panel is installed in the car by means of a two-component structural adhesive, for preventing contact corrosion, in combination with manually installed rivets to join the rear panel to the metal components (riv-bonding). Indeed, Neckarsulm plant, is characterized by a robot population of more than 500 machines, but consisting in 90 adhesive systems, 60 machines for self-tapping screws, 270 punch riveting systems and 90 resistance spot welding tongs. Nevertheless, according to what declared by the manufacturer, blind rivet application takes place without fully automated equipment. In addition, FDS are preferred when single access metal-to-metal mechanical connections are needed (figure 2.7.c). However, as general tendency, self-piercing riveting is the most adopted technology to join metallic sheets when a two-side access to the material stack is available. This is proven by the dedicated 320 systems used in Bratislava plant for the Q7 model assembly. The main supplier for Audi is the Bollhoff group, according to which Audi is heavily investing on SPR, in order to increase the number of riveting systems to 450 units along the Q7 production lines.

What turns out from the significant efforts made by Audi to develop these extensive production technologies, is that the same philosophy and technical contents analyzed in the A8 (which sold “only” 4149 units in 2016) can be applied on other Audi, Volkswagen or Porsche models [13]. It is true that Audi is not the only manufacturer having as a target the weight reduction, but it is probably the one closer to that objective, thanks to its innovative approach both in material choices and joining techniques. As a proof of

what said, the new A8 presents a higher aluminum and magnesium content with respect to the direct rivals, as the BMW 7 series and, especially, the Mercedes S-class, which uses a largely conventional construction [14]. Nevertheless, concerning the integration of composites and the related joining processes, BMW has done a much more intensive effort. This is also demonstrated by the automation level adopted in the riv-bonding joining operations which, unlike in Audi assembly process, are featured by an automated rivet installation system

2.3 An example of high volume North American production vehicle: Ford F-150

The Ford F-Series pick-up, because of its selling numbers, has been presented as a sea change in attitudes toward aluminum vehicle construction. Indeed the 2015 version of the F-150 model, which sold 760,000 units in its previous release (2013), was entirely made of aluminum. This choice represented a gamble for Ford, because the F-150 is not just a truck, but the most sold vehicle in its category in North America for decades, being the Ford's top moneymaker. In particular, it represents the 70% of the F-series total revenues [15].



Figure 2.8: *F-150 line: the aluminum body is assembled by means of self-piercing rivets (Photo by Austin Weber)*

The utilization of aluminum for the 13th generation of this truck represented the revolutionary step after less deep interventions, like the aluminum hood, introduced in the 12th generation. The main aluminum alloys which have been employed are the 5000 and 6000 series. The former provides the advantage of easiness in stamping process, allowing to get complex shapes for the body panels, while the 6000 series has been employed for outer body panels and cargo areas due to its higher yield strength to resist damage and dents. This radical departure from conventional design allowed to get a vehicle more than 300 kg lighter than its predecessor. The frame still presents some parts in steel, in order to provide torsional stiffness and durability, with weight saving of almost 25 kg.

Because of passive safety reasons, also some body components as the bottom edge of the tailgate and anti-intrusion door beams are made of steel. As underlined many times, the most significant challenge of aluminum or multi-material usage in industrial production is the massive retooling. In the case of Ford, the step forward undertaken had implied the biggest retooling effort since the switch between Model T to Model A production. This includes a massive replacement of spot welding robots with 500, smaller, more compact and less energy consuming six-axis robots mounted on overhead rails. Many partners and suppliers supported Ford in this deep production line variations, such as:

- **Comau Inc.**, for system integration
- **FANUC America Corp.**, for six-axis robots
- **Henkel Corp.**, for structural adhesives and pre-treatment processes
- **Henrob Corp.**, for self-piercing rivets and related equipment
- **Percepton Inc.**, for inspection systems
- **Semplex Corp.**, for flow-drill screws
- **Tox-Pressotechnik** , for clinching tools
- **Weber Screwdriving System Inc.**

Concerning the assembly innovations technologies, self-piercing rivets represented the leading technique for the BIW assembly, with all the implicit advantages compared with spot welding. The F-150 is built in Dearborn Truck Plant, where several robot mounted equipment are installed along the line. They include rivet setter and die assembled on a C frame which, in order to get the joint, requires a double-side access to the stack. The process is quieter without heat release, simpler and can be better monitored with respect to spot welding, thanks to integrated systems. A visual inspection device allows to automatically validate 80 joining point of each body. However, rivets are not the only joining technique exploited in the F-150 BIW, indeed steel flow-drill screws are used when the access on one side of the sheets is not there or is limited. This applies for about the 15% of the vehicle joints, for instance in the underbody, framing, body side and the cargo box. One of the main supplier of FDS is the Weber Group, providing installation modules to be integrated in fully-automated equipment (figure 2.9).

Another really significant joining technique is clinching: there are about 150 to 200 TOX joints per truck, with the advantage of not requiring any consumable feeder, reducing weight (initial target) and cost.

As pioneer in the massive usage of innovative joining techniques, the F-150 uses also three times as much adhesives as previous models, that is more than one hundred meters of structural adhesives to confer higher stiffness to the structure, but also to reduce noise transmission and avoid moisture formation. To summarize, the 2015 F-150 version has been built with 2000 rivets against the 5000 spot welds in the 2014 version. Laser welding is finally used for the roof assembly.



Figure 2.9: *F-150 line: the aluminum body is assembled by means of self-piercing rivets (Photo by Austin Weber)*

From these considerations and from the information available in literature, no blind rivets are used for this vehicle model. The reason is essentially related to the lack of composite or other brittle materials which cannot be joined by means of SPR, clinching or FDS. Indeed, all of these joining methodologies involve plastic deformation processes, which would not be feasible with carbon fiber. However, as it will be discussed later on, composite utilization is becoming more and more significant in the automotive industry, so that riv-bonding (discussed in the previous two benchmark examples) and similar technologies need to be better understood and optimized for larger production volumes.

This chapter concerning the main manufacturers benchmark can be concluded underlining that blind riveting is a quite common fastening technology which premium manufacturers use mainly in combination with adhesive, getting the so called riv-bonding technique. However, this joining technique is still mainly performed manually. With the exception of BMW, the rivet is installed by operators provided with riveting guns. No evidences of drilling-riveting coupled automated system have been found during the benchmark analysis.

Chapter 3

Literature review:

State of the art analysis of innovative riveting methods and new suppliers identification

The content of the following chapter represents the starting point for the research aim of this thesis. As stated in the previous sections, the introduction of lighter alloys for automotive industry has spawned a significant interest in mechanical joining technologies, compatible with aluminum, composite and high strength steels. Other requirements are those related to practical aspects such as cycle time, joint setting procedure accessibility, and the leading parameters determining the joint effectiveness. The target is not only to get a highly resistant joint, but also to design a fast and reproducible procedure, which can be adopted in the medium-high volumes automotive industrial context. Indeed, this analysis focuses both on current studies related to joining techniques and on their economic impact on the industrial activity. The present chapter describes in the following the main innovative riveting techniques that are still in a development stage. Some of those joining methods have been already summarized by work [16], which reviews the newest techniques aimed at satisfy the previously mentioned industrial needs. Additional issues, including retooling, consumable, and joining process management, are investigated here, since they represent non-negligible aspects when dealing with such level of industrial scale.

The basic method, on which the study is focused, is the riveting one, which has been already presented, in its conventional configurations, such as blind and self-piercing riveting. Advantages and criticalities are pointed out, in order to select the most suitable method to be automated and introduced in the industrial context.

3.1 Resistance spot riveting

Some of the joining methods previously discussed as flow-drilling screws and self-piercing riveting, have been proposed in the automotive field with the target of effectively assembling light aluminum alloys and high strength steels. Nevertheless, the most challenging aspect is mainly related to the industrial complexity and cost of the retooling process, consisting in a massive replacement of welding equipment with innovative joining machines. This problem can be solved by adopting resistance spot riveting (RSR) technique. The name of this riveting method recalls the well-known welding technology, since RSR is actually a combination of resistance spot welding with riveting itself. This sheet-metal joining technology has been developed by Arconic Fastening Systems, and is proposed by the company as an effective solution for joining dissimilar materials. The process cycle time is comparable with that of spot welding (3 to 5 seconds) and, above all, it exploits the same conventional equipment, like welding guns. Consequently, it is not necessary that the OEMs completely change their assembly line, but they can convert in a reversible way their equipment to switch from traditional steel-to-steel welding to mixed material assembly. The manufacturer declares this technology would be suitable for different assembly stages in the vehicle BIW processes, such as frames, roofs and intrusion beams assembly. Moreover, the supplier presents RSR as the joining method which will replace self-piercing riveting. This could be more likely to happen with the progressive development of Ultra High Strength Steel and High Strength Aluminum, which requires much higher joint strength. From a practical view point, RSR is an extension of spot welding, since it can be achieved just by adding a feeding system, which supplies rivets to the conventional welding gun. Concerning the rivet itself, it has a quite simple geometry, recalling that of a mushroom fastener, characterized by a circular head and a cylindrical stem [17].

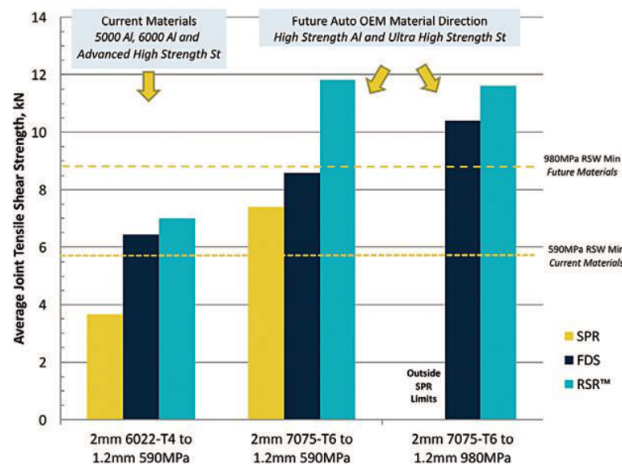


Figure 3.1: Current and future joint tensile strength requirement for different materials (Photo courtesy Arconic Fastening Systems and Rings) [17]

The typical material choice for the rivet is aluminum or low carbon steel with zinc corrosion protection. This kind of design choice is strictly dependent on the bottom sheet

material, so that a steel-to-steel or aluminum-to-aluminum joint is performed. Arconic Fastening systems provides four different rivets geometries, in order to be compatible with almost all possible applications in automotive industry. As declared by Graham Musgrove, project engineer at Arconic Fastening Systems, the target for the development of RSR was to reach at least the joint strength of conventional steel-to-steel or aluminum-to-aluminum welding joint strength. Nevertheless, the better nugget diameter generally ensures to RSR joints an even higher strength, not only with respect to resistance spot welding, but also if compared with self-piercing riveting (figure 3.1) [17].

The joining procedure starts with the positioning of sheets to be joined in between the electrodes of a standard spot welding gun. It is important to notice that all the material sheets, but the bottom one, are pre-machined with a through hole, in which a rivet is inserted by the already mentioned feed unit. This is then retracted once the weld cycle is initiated, while the rivet is pressed in between the electrodes delivering the required welding current [17].

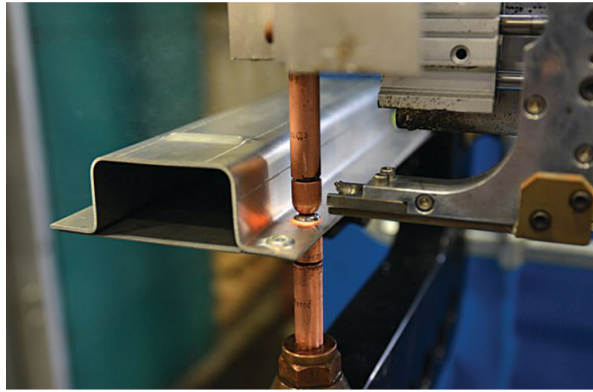


Figure 3.2: *Conventional welding gun provided with a rivet feeder for RSR (Photo courtesy Arconic Fastening Systems and Rings) [17]*

The welding itself occurs between the rivet and the bottom sheet, while the upper ones are not involved from an electrical stand point, but just mechanically clamped by the fastener. This is one of the key advantages of RSR, since the joining effectiveness is not dependent on the top sheets material, which can be whatever alloy or composite, and can present any possible surface treatment. The welding properties are dependant just on the bottom sheet, whose thickness must be over a certain value, depending on the top plates geometrical properties and number [17].

The shape of the rivet head allows to use conventional welding guns, specifically designed to match the welder electrodes geometry. This is typically radiused on the top one and flat on the lower one in order to confer good flatness and aesthetic properties to the joint. Similarly to RSW, the process control parameters are the clamping force exerted by electrodes and the applied current, without any particular requirement or increase of these quantities with respect to the conventional welding process. Conversely, Arconic Fastening Systems and Rings declares a lower current requirement (especially in the aluminum-to-aluminum joint) with respect to the correspondent welding process, providing also an energy saving advantage for the company. This is mainly due to the

fastener presence, which concentrate the current in the actual welding point. Similarities between RSW and RSR also include the design rules for spot spacing and edge distances. All these analogies promote RWR technology as a relatively low economic impact investment for those OEMs gradually increasing the content of composite and light alloys in their vehicles BIW, without abandoning traditional spot welding techniques. Indeed, if a normal spot weld is needed, the same equipment and design rules can be adopted. The only variation would be the interruption of the rivet feeder operation [17].

It has been said that the top material sheets must be provided with the fastener hole, but this is not necessarily the case if an aluminum to steel joint has to be set. In this case, the steel rivet is capable to extrude its way through the first aluminum sheet, before being welded with the second sheet. This presents a drawback with respect to the pre-hole method, that is the doubling of cycle time [17].

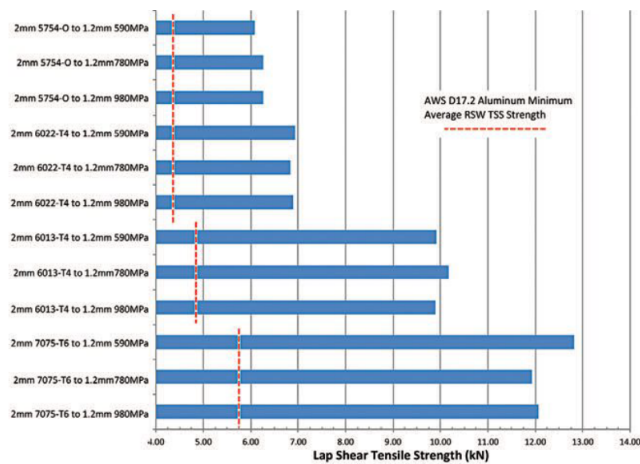


Figure 3.3: *Lap shear tensile strength achieved by joining different kind of aluminum-to-steel couples (Photo courtesy Arconic Fastening Systems and Rings) [17]*

Another advantage of RSR is the possibility to join more than two metal plates, such as an aluminum plate with two steel bottom sheets, of which just the last one is welded with the fastener.

From an industrial viewpoint, Arconic Fastening Systems is working with several OEMs to integrate RSR in current production lines. According to the company, this technology will be fully mature within 2019, while a second generation is in development stage, with the target of furtherly increase compactness and adaptability, reducing costs. However, RSR is a joining methodology born to satisfy emerging automotive industry needs, but now pretty oriented toward other fields, including aerospace and heavy trucks sectors [17].

3.2 Friction Stir Riveting

Friction stir riveting represents the reference method from which all the other friction-based joining process were developed. It can be considered as in between self-piercing riveting and friction stir welding [18], providing a fast and valid alternative to conventional riveting or adhesive bonding. Indeed, FSR combines the advantages of both

techniques, such as no pre-drilled holes, no filling materials or detrimental metallurgical alterations of conventional welding [19].

FSR has been invented by researchers at Helmholtz-Zentrum, Geesthacht in Germany [20]. It was called FricRiveting and is mainly employed for joining combinations of thermoplastic components. Their use has increased significantly in transportation industry during the recent years, thanks to the thermoplastic and fiber-reinforced polymers advantages [21]. Indeed, thermoplastic composites offer higher fracture toughness, stress corrosion resistance and recyclability with respect to metals. Thus, because of the increasing applications of plastics and plastic composites, their joining process is becoming more and more important, especially in multi material assemblies [22]. FSR has been proposed as one of the most effective joining method for this application.

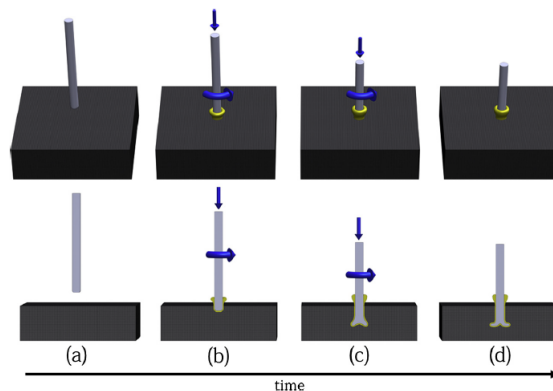


Figure 3.4: *FSR joining steps* [21]

The working principle of FSR (shown in figure 3.4) is based on the interaction between the plastic component surface and the rotating round profiled rivet. The rivet rotation is typically characterized by a speed of 21,000 rpm [23]. Moreover, the fastener is subjected to an axial load, pushing it toward the part. Both linear and rotating rivet motion, by generating frictional heat, cause a softening of the workpiece and the consequent rivet penetration. The rivet tip itself is heated through friction and, after the rivet full penetration, the spindle is stopped so that the reaction of the colder and harder material below it is exploited to get the fastener tip deformation. In this phase, just an axial forging force is applied, in such a way to avoid friction and heat generation. It results a rivet diameter increase (almost twice the initial size, determining the parts anchoring after cooling and consolidation). The average cycle time for the process is around 3 seconds, and the minimal surface preparation helps to make this joining technique efficient and environmentally friendly [23].

Additional studies have been carried out by [24], in order to subdivide and classify the altered zones around the rivet. These are Base Material (BM), Heat Affected Zone (HAZ) and Thermomechanical affected zone (TMAZ). The difference between HAZ and TMAZ is the mechanical deformation undergone by the grains in the second region. The conclusion of this analysis was the derivation of the material microhardness in the investigated zones. A hardness reduction has been observed in both HAZ and TMAZ of the aluminum layer (ranging from 5 to 15%), while a 10% hardening was noticed in

the HAZ of the polymer.

3.3 Friction self-piercing riveting

As its name suggests, friction self-piercing riveting (F-SPR) is a joining process quite similar to traditional self-piercing riveting, but assisted by the material softening due to rivet rotation and friction generation. The setting process consists in the rotating rivet penetration into the top material layer and subsequent interlock formation with the bottom material. The last step is enhanced by the softening of both material and rivet itself. Before the joining process completion, the rivet penetration is stopped, but it is let rotating into the parts in order to generate additional heat and interlocking between the fastener and the part materials. The process steps are shown in figure 3.5, referring to work [25] in which F-SPR is used to join aluminum with magnesium alloys.

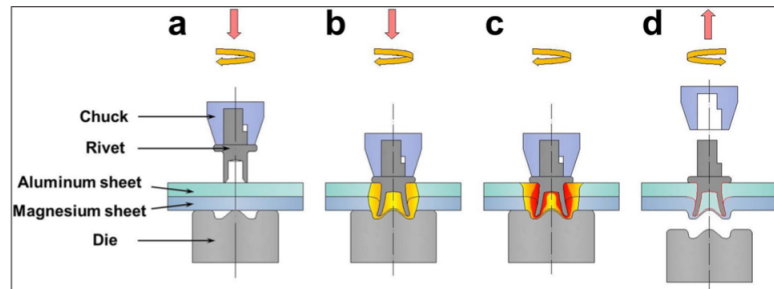


Figure 3.5: *F-SPR setting process* [25]

According to this reference, F-SPR overcomes the problem of conventional SPR in joining low ductility materials, such as magnesium. In more brittle materials, indeed, traditional SPR encourages the crack initiation close to the riveted junction. The research results proved how the magnesium joining process window can be widened by F-SPR with respect to traditional SPR, determining also a higher joint strength.

Another study, carried out by [26], still focuses on aluminum-to-magnesium joint, but evaluating the effect of rivet hardness and geometry on the joint quality.

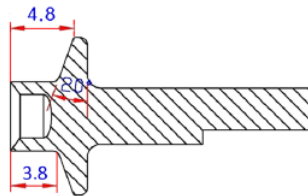


Figure 3.6: *Friction self-piercing rivet geometry* [26]

This study demonstrates the importance of the angle under the rivet shoulder (figure 3.6) in the material flowing around the rivet shank. An optimal value of 10 degrees is what ensures the best joint strength avoiding cracks in the top sheet. Finally, because of frictional heat and material softening, the rivet requirements in terms of hardness are lower in F-SPR with respect to traditional SPR.

3.4 Friction Stir Blind Riveting

The innovative riveting methodologies discussed in the previous sections demonstrate how one of the most relevant priority, in mechanical joining process optimization, is that of coupling the hole drilling and rivet setting process. The most efficient way to achieve this target is that of integrating the drilling operation in the rivet installation process, namely making the rivet itself the drilling tool. In the field of blind riveting, this way of thinking has been used for the development of Friction Stir Blind Riveting (FSBR) method.

FSBR, also called Spin Blind Riveting (SBR), is a recently developed joining procedure which comes from the contribution of two fastening methods previously described, namely friction stir and blind riveting. It is aimed to perform a riveted joint between dissimilar material sheets without need of pre-machined holes. FSBR uses a modified blind rivet as tool and joining element at the same time [27].

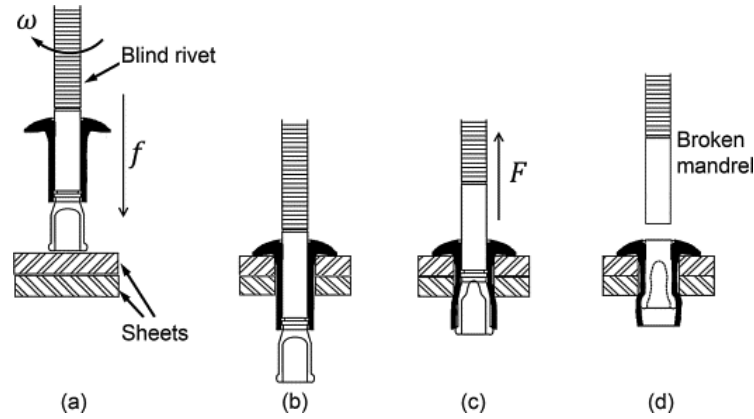


Figure 3.7: *FSBR process steps: a) spindle acceleration b) rivet penetration c) shank deformation d) mandrel detachment [28]*

The process is graphically shown in figure 3.7. The fastener, which can be taken as a standard blind rivet, is put in rotation at a speed ranging from 6000 to 12000 rpm, and brought into contact with the workpiece. The concept of stir riveting consist in exploiting friction in order to get a material softening to an extent sufficient to allow the rivet penetration. It follows the traditional setting process of blind rivets, by means of the internal mandrel. The most relevant advantages of this procedure are the consistent strength under tensile loads and the robustness of the process results. This joining method is characterized by the formation of a material sleeve on the blind side of the joint, which is caused by the material displacement during the process. This factor is considered as one of the causes why Spin Blind riveted joints provides a significantly higher shear load resistance than conventional riveting methods [27].

Thanks to the experimental analysis carried out in work [29], it can be demonstrated that FSBR results, in terms of joint strength, is almost insensitive to changes in operating parameters. This makes the process easily implementable in various types of productions, from the rapid prototyping to the high volume one, also thanks to the good cycle time of about 2-3 seconds. Moreover, the same study shows how FSBR joints

provide a significantly higher fatigue resistance than conventional spot welding, which would make possible to reduce the number of necessary joints for a given structure [29].

As mentioned, the first testing of this riveting technique, has been done using 3 mm thick aluminum 5052-H32 coupons, whose dimensions were 30 x 125 mm. The employed rivet was a standard one (SD66SPRLF.255-steel mandrel and shank, 7.76 diameter), but modified creating a flat tip, so that to avoid lateral material displacement during the rivet penetration and misalignment between the mandrel tapered tip and its axis.

3.4.1 Joint strength comparison with spot welding

One of the target of experimental studies carried out on the FSBR system, is to quantify its joint strength compared with spot welding. In order to do that, the adopted test layout is shown in figure 3.8.

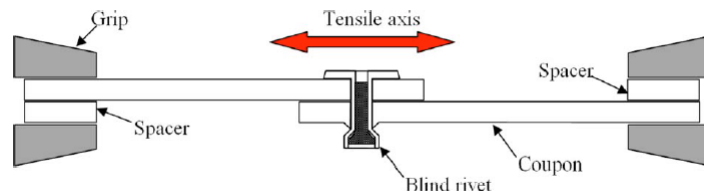


Figure 3.8: *Tensile test setup [29]*

It is worth to notice that the test results are provided in terms of joint strength at parity of involved area. This means that the static strength analysis has been carried out on a spot weld whose nugget diameter is the same of the rivet shank one, which stands at 4.7625 mm. The test results are shown in figure 3.9. The load-displacement curves show initially the same behavior, but FSBR presents a 45% higher maximum recorded load with respect to spot welded samples (3902 N with respect to 2693 N).

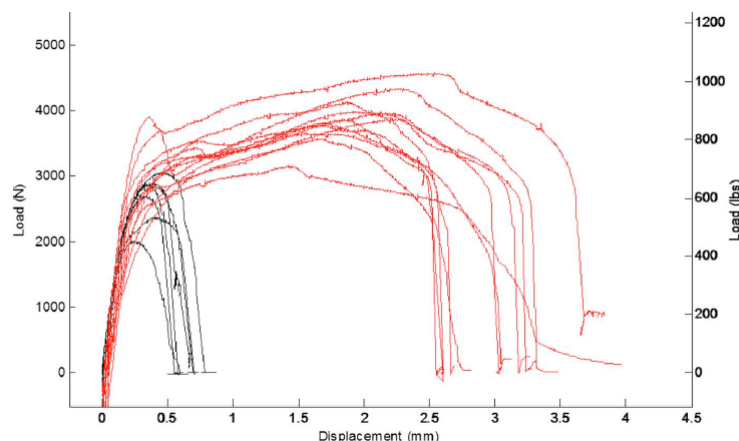


Figure 3.9: *Load displacement curves comparison: FSBR (red) spot welding (black) [29]*

Other important aspects to be emphasized are also the sample elongation at fracture and the amount energy absorbed by the joint prior to it. The latter is 6.5 larger in riveted than in welded joints.

An interesting point of this analysis is that, despite the stir riveted joint performances being much better than welded ones, there are evidences of further potential improvement in the joining method. The commercialized rivet used in the tests (not the ones optimized for FSBR applications) presented their mandrel rupture point below the joint line (figure 3.10). This cause the shear load to be resisted by the shank only, and not by the residual part of the mandrel. Supposing to use a rivet specifically designed for friction stir applications, the mandrel would break much closer to the rivet head, increasing the tensile strength of the joint.

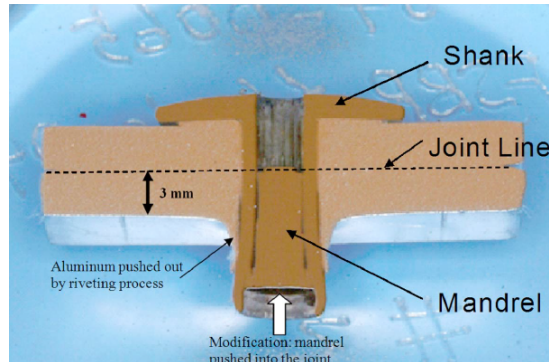


Figure 3.10: *Section view of friction stir blind rivet [29]*

In the previously mentioned research, this was simulated by pushing up the mandrel into the joint. It resulted in an increase of tensile strength up to 7660 N, stressing the significant improvement margins achievable through a specific process optimization. Actually, specific rivet design for this application has been now defined so that, provided no failures occur during the setting process, the mandrel always breaks in correspondence of the shank head. Nevertheless, the study these considerations are referred to, is useful to get an idea of how much stronger FSBR joint can be with respect to traditional spot welding [29].

3.4.2 Fatigue resistance comparison with spot welding

Larger welding currents (7.5 mm weld nugget) were applied for fatigue testing, so the rivet diameter in this case is lower than the weld nugget. FSBR technology has been tested both with no modification and with mandrel retaining (discussed above), and compared with traditional blind riveting and spot welding. Results are shown in figure 3.11.

Also from the fatigue viewpoint, FSBR results to be more effective than resistance spot welding and, when the mandrel is retained, also than standard blind riveting. The performance advantage is more evident in high cycle fatigue testing, meaning in long tests at low load (lower than the yielding limit). It is possible to conclude that FSBR, with a correct mandrel positioning after setting, presents a fatigue life one to two orders of magnitude higher than those of resistance spot welding [29].

An important remark must be made concerning the results of work [29], since the employed rivet was not the one actually identified as the most suitable for FSBR appli-

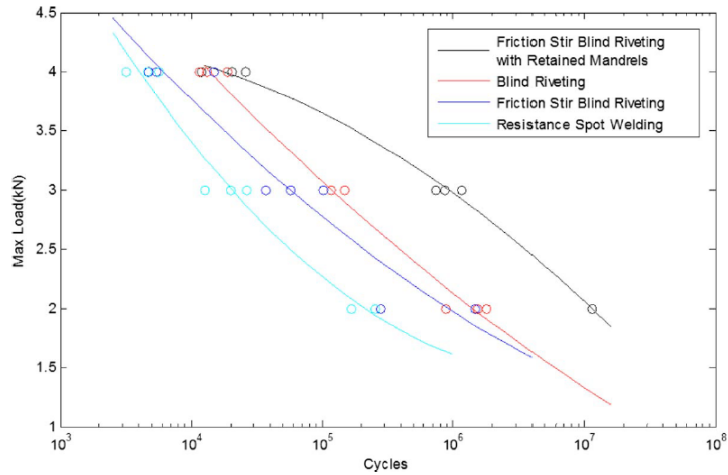


Figure 3.11: *Fatigue life comparison of joints [29]*

cations. Indeed, a significant number of FSBR experiments, featured by several different designs of blind rivets, allowed to understand that hollow mandrel head geometry (shown in figure 3.12) requires significantly lower penetration force with respect to rivets with solid mandrel heads [31]. This furtherly emphasizes the performance improvement that can be achieved with FSBR with respect to traditional riveting and spot welding. Moreover, said rivet model, which is the one used for all the experiments reported in the more recent references, allows to reduce the cycle time, making the process even more suitable for industrial applications.

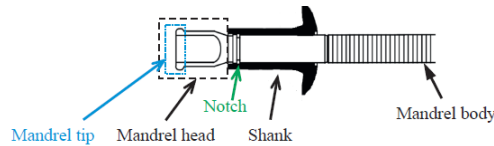


Figure 3.12: *SSPV-08-06 Avdel rivet design [30]*

3.4.3 Sensitivity analysis

As mentioned during the description of friction stir blind riveting, the process sensitivity to working parameters results to be fairly negligible. The parameters investigated by [29] are:

- Spindle speed effect
- Feed rate effect
- Off-axis angle effect
- Rivet cup diameter effect

None of these operating variables result in a relevant variation, making the process robust. In order to provide an example, figure 3.13 shows the load-displacement curve comparison with two different rivet cup diameters.

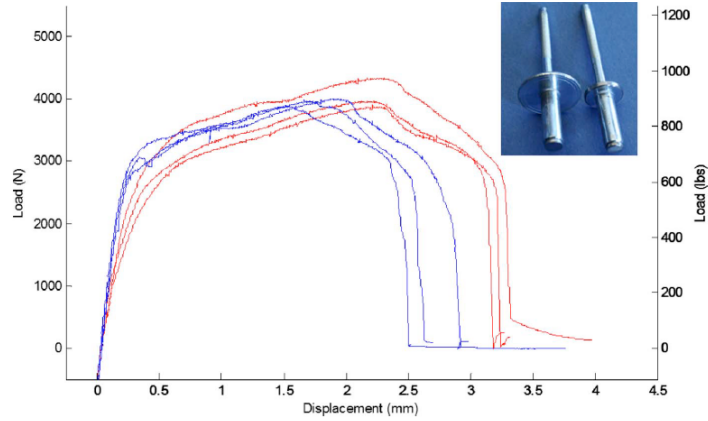


Figure 3.13: Load-elongation curve for FSBR joints obtained at 12mm/min feed rate and 12.000 rpm spindle speed, using 15.4 mm (red curves) and 10mm (blue curves) rivet cup diameter [29]

Despite the results of this analysis being quite positive for what concerns the applicability of FSBR in automotive field, the full characterization of the joining process should be provided. This is what has been attempted to do in some researches which analyze new and relatively inexpensive, portable FSBR machine aimed at providing in situ X-ray imaging of the FSBR process. This should allow specialists to understand and improve the FSBR process [32].

3.4.4 Thermo-mechanical effects of friction stir blind riveting

According to reference [30], one of the factors determining the higher tensile load and better fatigue resistance of FSBR with respect to spot welding, is the absence of porosity in the metal due to material fusion. Indeed, porosities are commonly associated to likely crack nucleation sites.

This aspect has been investigated also by reference [33], in which thermal and thermo-mechanical affected zones nearby the riveted joint are identified and distinguished by the authors. Concerning the experimental details of this analysis, two 0.9 mm thickness AA6111-T4 sheets were joined using SSPV-08-06 rivets (manufactured by Avdel and identified as the optimal rivet geometry for friction stir riveting applications), with a shank diameter of 6.4 mm. The operating parameters, used for the joining process, consisted in a spindle speed of 6000 rpm and 780 mm/min as feed rate. Once completed, the joint has been sectioned in order to investigate the material microstructure.

The rivet setting is responsible of heat generation, due to the frictional penetration of the fastener. The heat is then conducted from the hole surface to the surrounding workpiece material in a radial direction, affecting each region in a different way. The electron-backscattered diffraction (EBSD) technique was used to observe and distinguish among five main thermal and thermo mechanical affected zones close to the riveted joint. These zones are shown in figure 3.14 and 3.15. The region 773 μm away from the hole edge was defined as zone X. It represents the area in which the riveting process did not cause any micro-structure or average grain size variation with respect to the base

material.

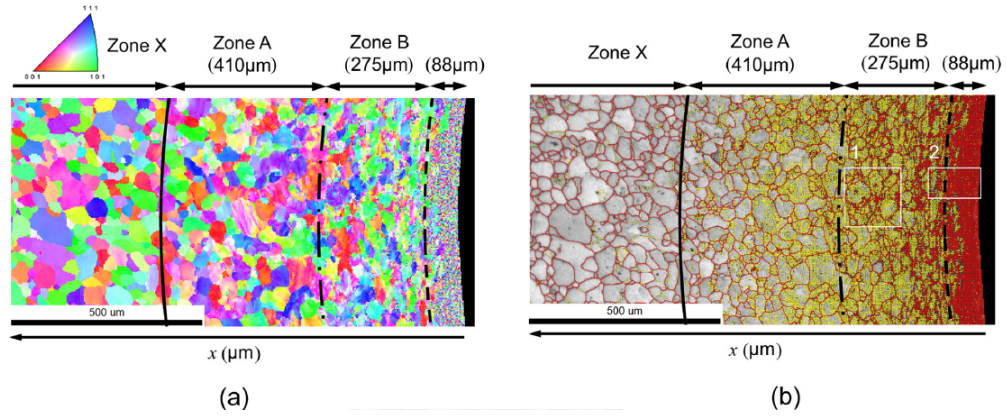


Figure 3.14: EBSD microstructure (step size: 3 μm) [33]

Moving to zone A ($363\mu\text{m} < x < 773\mu\text{m}$), the average grain size results to be still comparable with that of the base metal. This means that this zone is not thermally, but just mechanically affected by the riveting process. Indeed, the ratio of high angle boundary (HAB) was observed to be much lower than the base metal value. This quantity is commonly employed to quantify the mechanical deformation undergone by the analyzed material. Zone B, defined in the radial distance range $88\mu\text{m} < x < 363\mu\text{m}$, presented essentially the same features of zone A, but with evidences (HABs observation) of a larger grain deformation.

The zone closer to the hole ($x < 88\mu\text{m}$) is shown in figure 3.15, since a new rescanning with step $1\mu\text{m}$ was required in order to catch the investigated aspects. The region at a distance $26\mu\text{m} < x < 88\mu\text{m}$ has been defined as zone C. What results from its observation is a significant decrease of the grain size, due to the thermal effect of friction stir process and the consequent material recrystallization. In particular, the grain size was noticed to be the smaller the closer it was with respect to the rivet hole. Just in zone C, it decreased from 6 to $2\mu\text{m}$. Regions A, B and C represent the so-called thermo mechanical affected zones (TMAZs), characterized by an increasing grain shear deformation, due to the local temperature increase. Indeed, the shear deformation is clearly dependent on the local value of yield shear stress which, in its turn, depends on temperature.

Concerning the grain size reduction tendency, this was even more evident in zone D, namely the closest to the riveted junction, characterized by the finest grain (around $1\mu\text{m}$). Region D was designated by the authors as the stir zone (SZ) in the frictional penetration process, namely the one in which the highest temperature and, consequently, the most relevant recrystallization phenomenon was observed.

The discussed changes in the material microstructure close to the rivet hole, determine also a microhardness alteration in the affected zone. Figure 3.16 shows the microhardness trend in radial direction, considering x the distance from the hole internal surface. This property varied in the different material regions according to two main mechanisms. These are the softening due to the heat effect and the hardening due to

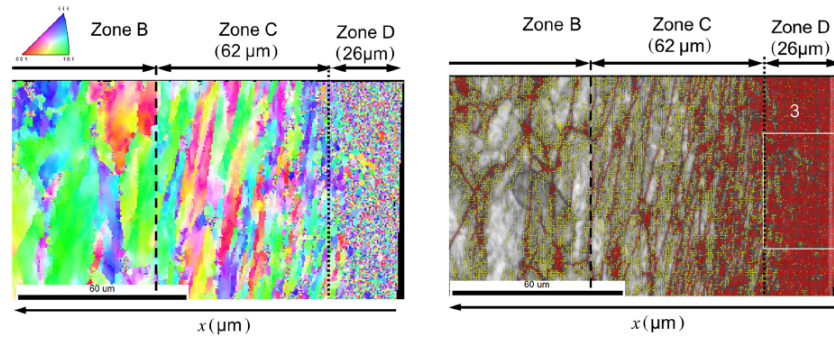


Figure 3.15: EBSD microstructure (step size: 1 μm)[33]

the shear deformation. As it can be noticed, in the heat altered zone, the measured hardness was even lower than the base material one. This local softening, which has been observed also on friction stir welded joints, is presented by the author as due to the decomposition of aluminum precipitates, which were a source of strengthening in the base material. However, what is worth to notice, is that all references agree on the hardening occurring on the internal hole surface. This aspect can be relevant from the fracture mechanics view point since, as most anti fatigue treatments demonstrate, the material hardening close to likely crack nucleation sites helps to face fatigue failure. This is the case, for instance, of shot peening or nitriding process, which are aimed to create an hard case around the material core.

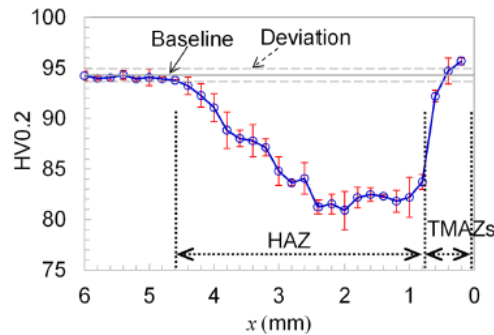


Figure 3.16: Micro-hardness along the hole radial direction [33]

Furthermore, the decrease of the average grain dimension close to the rivet hole, can potentially lead to an increase of the joint endurance limit and fatigue performances. However, being FSBR a quite new joining technology, more specific fatigue tests need to be carried out. Nevertheless, reference [29] proved FSBR joints to provide better fatigue resistance than other riveting or welding techniques. It can be stated that this result is also due to the positive effect of material recrystallization and hardening close to a stress concentration site, like the rivet hole.

3.4.5 FSBR process mechanisms: failure scenarios

Friction stir blind riveting is still a quite new joining technique, having been invented by Wang and Stevenson in 2007. This means that, for an effective implementation

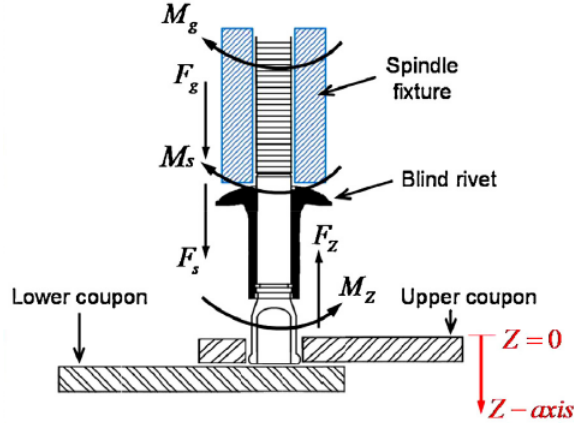


Figure 3.17: *Elements and loads involved in FSBR process [34]*

in the production context, it is useful to analyze possible failure causes. These can compromise the riveted joint quality, thus negatively impacting on the overall process efficiency and cycle time. Reference [34] presents three main failure modes detected by performing FSBR joints on a CNC machine equipped with a load cell used to record the penetration force (hereon defined as F_z) and the reactive torque (M_z) during drilling operations. In the reference study, most of the failure scenarios resulted to be caused by the occurrence of a relative motion between the mandrel body and the spindle fixture.

This motion occurs either in translational and rotational direction when a certain threshold value, of penetration force or torque respectively, is exceeded. The thresholds correspond to the maximum force and torque which can be transmitted by friction from the spindle fixture to the mandrel. These two cases are deeply coupled, since both of them generally occur when a friction reduction takes place between the said components. Nevertheless, they have well distinguished effects.

If a sliding in translational direction takes place, the spindle fixture would be eventually put in contact with the shank head, pressing it and causing the mandrel head to penetrate in the shank, expanding it and the workpiece hole. This would lead to an ineffective and loose joint (figure 3.18.a). In order to avoid this phenomenon, the force difference between the load applied by the spindle fixture and that actually transferred to the mandrel should be lower than a certain threshold, proper of the rivet, over which the shank would be intruded by the mandrel head.

When, instead, a rotational relative motion occurs, the rivet angular speed is lower than the spindle one, or even null. This would cause an insufficient friction and softening of the material sheet, so that the feeding motion will determine the rivet failure (buckling) instead of penetration (figure 3.18.c).

A third possible failure mode is related to the rivet mandrel notch, constituting the weakened point used for the mandrel detachment after the setting process. It is also true that the notch lowers the torsional resistance of the mandrel, so that if the reaction torque it experiences during penetration is higher than a threshold, the mandrel will break before the penetration itself (figure 3.18.b). As already mentioned, all these failure

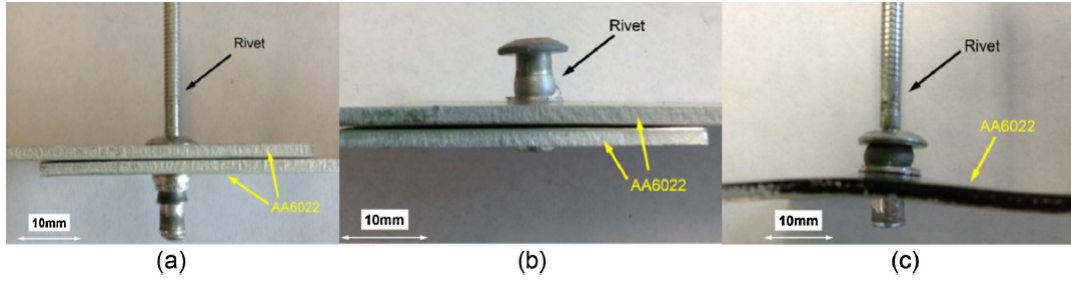


Figure 3.18: FSBR setting failure modes [34]

modes are not independent among each other. For instance, if the penetration force is excessive and the mandrel head intrudes the shank, expanding the workpiece hole, also the reaction torque on the rivet will increase, because of the increased contact area. This could cause the mandrel rupture even if the torque transmitted by the spindle is below the critical threshold. In conclusion, some countermeasures can be taken in order to avoid these failure modes. First of all, it is advisable to maximize the friction between the mandrel and the spindle fixture, so that to avoid any relative motion. It is also important, as experimentally observed, to employ a spindle speed higher than 6000 rpm, in order to increase the friction and softening effect on the workpiece, minimizing the penetration linear and rotational resistance. Finally, the rivet design must be so that to maximize the intruding force (at which the mandrel head enters in the shank during the sheet penetration) and properly defining the rated torque causing the mandrel breaking in the notched region [34].

3.4.6 FSBR process mechanisms: penetration force and torque analysis

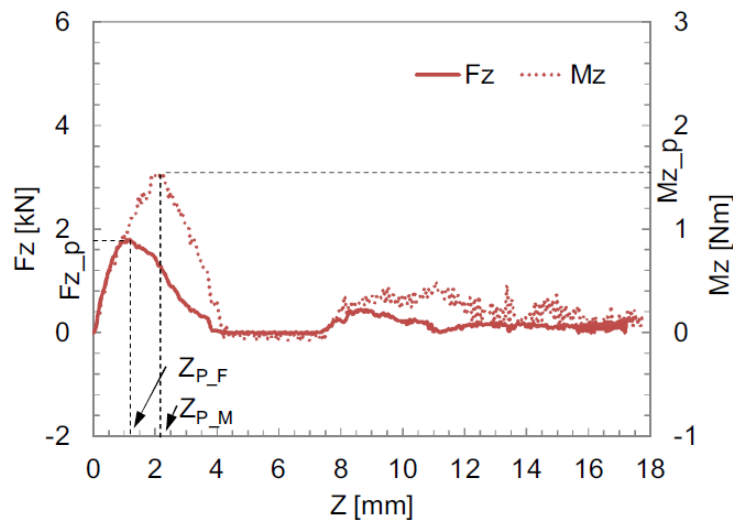


Figure 3.19: Force and torque trends as a function of the penetration depth [34]

Figure 3.19, from reference [34], provides the reaction force and torque versus the rivet penetration in the workpiece. They refer to a measurement carried out on two

0.9 mm AA6111 coupons with spindle and feeding speed respectively equal to 3000 rpm and 420 mm/min. Both force and torque sharply increase as soon as the mandrel enters in contact with the part. The vertical load grows due to the increase of the material removal rate of the mandrel tip, while the moment goes up because of the increase of the contact area between the mandrel tip and the workpiece.

Due to the material softening, which reduces the penetration resistance, both F_Z and M_Z decrease during the hole creation process. They remain null for a certain penetration depth, where the mandrel body diameter becomes smaller than that of its head. After that, the resistances grow again due to the shank penetration into the workpiece. Nevertheless, the second peak is lower than the first one, since the shank diameter is almost the same of the mandrel tip. Figure 3.20 shows, instead, the effect of feed rate and spindle speed on the reaction force and torque peak. These reactions grow up with the increase of the feed rate and decrease with the increase of the spindle speed. The former tendency is justified by the shorter time available for the mandrel to soften the aluminum, resulting in a higher penetration resistance. Conversely, the increase of the spindle speed increase also frictions and workpiece temperature, so the material become softer and more ductile.

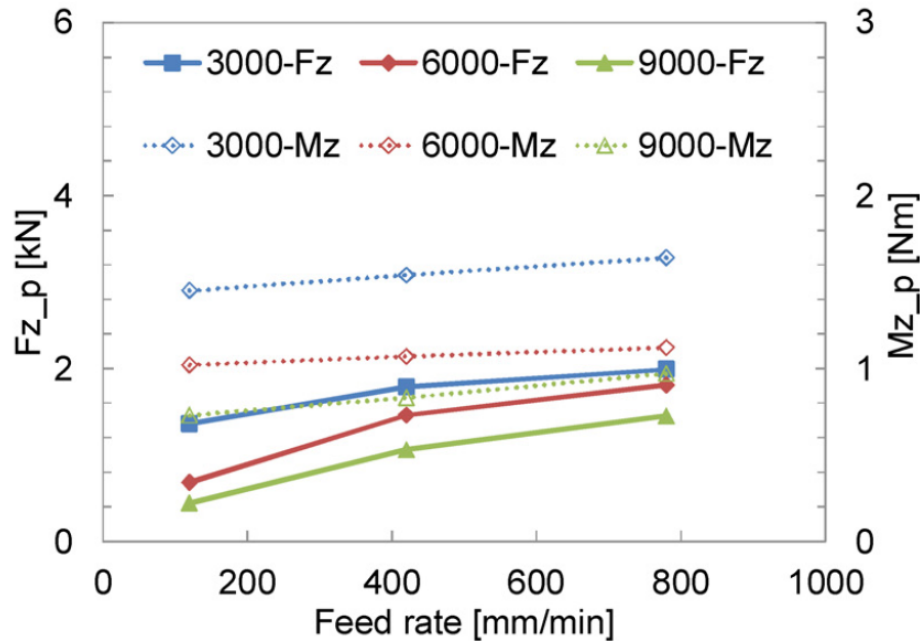


Figure 3.20: Penetration force and torque as a function of feed rate and spindle speed [34]

3.4.7 FSBR process application to CFRP-CFRP and CFRP-Al joints

One of the main innovations adopted in the automotive field, in order to achieve the weight reduction and high-performance targets, is that of using more and more composite materials in the vehicle BIW. The main driving factor for the development of composites in the automotive industry is weight saving. This is strictly related to fuel consumption and can be achieved thanks to the high specific strength and stiffness of automotive composites with respect to aluminum and steel.

Composite materials can be considered the best solution when a combination of properties is required, such as stiffness and light weighting. Indeed, by dispersing fibers or particles of one substance in a matrix, it is possible to get properties that neither of the constituting materials shows on its own. Moreover, the final composite features are not depending just on the constituents of matrix and fibers, but mainly on their interface and capability to transmit loads. These factors can strengthen or toughen the final composite, increasing the amount of required work to fracture it [35].

The increasing utilization of composites, such as carbon fiber reinforced polymers, does not involve just high-end carmakers. If, on one side, composites are employed for high-profile sport cars to improve performance, on the other side, startup automakers use the same composites in hybrid and electric vehicles to reduce mass and increase the driving range. However, almost all carmakers are starting using composites materials on conventional vehicles, in order to meet the more and more stringent emissions standard.

This tendency does not just introduce the issue about how to join between each other sheets of composite, but, above all, how to integrate them with an aluminum vehicle structure. Indeed, composites and particularly CFRP, still present high cost, so that, with the exception of very high-performance cars, a mix of metals and CFRP constitute the vehicle structure. In order to perform the joint between these two material categories, several strategies are being currently used by OEMs, mainly involving adhesives (see chapter 1). These present both advantages and disadvantages if compared with mechanical fastening methods. On one hand, adhesives application avoids the presence of stress concentrations, distributing the loads on the entire bonded surface and providing a certain compliance to the joint. On the other hand, structural adhesives require quite often a curing process. This has a negative impact both on the production cycle time and, potentially, on the CFRP parts, since the adhesive curing temperature can cause distortion of the composite itself. Because of these reasons, mechanical fastening is gaining more and more credit for this application. In particular, all the advantages presented for FSB technique can be exploited in the joining of CFRP-to-CFRP or aluminum-to-CFRP sheets, as proved by reference [28]. In this work three material stack-ups are tested, namely CFRP-to-CFRP, aluminum-to-CFRP and CFRP-to-aluminum. AA611 is the selected metal for the multi-material joint, while the CFRP is obtained by molding composite plaques at 320°C, using pellets of BASF Ultramid®T KR 4370 C6 PA6/6T-CF30 with 30 wt% random short carbon fiber. The tested aluminum and composite layers thickness were 0.9 and 3 mm respectively. The rivet, supplied by Avdel, is a Monobolt®SSPV-06-04 mild steel, characterized by a shank diameter of 4.8 mm.

The rivet penetration procedure is performed on a CNC machine, while fastener setting is achieved by pulling the mandrel with a handheld gun. It is clear that, in industrial production applications, all these operations should be carried out by a single equipment, most likely completely automated.

It is worth to underline how the mechanical joint of CFRP presents some intrinsic criticalities. Indeed, as discussed in reference [36], the main process challenge is the hole machining in the composite layer, avoiding the quite common exit delamination.

This phenomenon has been studied in different researches, such as [37] and [38], which agree on the idea that the delamination occurrence is strictly related to the tool feed force. These considerations are referred to the study of conventional drilling operations, namely not involving the friction stir process. However, as it will be presented in the following section, CFRP delamination occurred also in FSBR process, where the same constrain on the feed rate has been observed. Nevertheless, the effect of material softening, due to friction, can be considered beneficial for the delamination avoidance, with respect to traditional drilling operations. Consequently, as it will result from the following analysis, FSBR process is suitable to provide an effective mechanical fastening of composite materials.

3.4.7.1 Process feasibility and quality issues

The first step of the mentioned work is the definition of the joint feasibility and process window, shown in table 3.1, 3.2 and 3.3.

Spindle speed [rpm]	Feed rate [mm/min]				
	60	120	270	420	600
3000	QI	QI	-	-	-
6000	√	QI	QI	-	-
9000	√	√	QI	QI	-

√sound joint, QI quality issue, - not tested

Table 3.1: CFRP-CFRP Joining process Window [28]

Spindle speed [rpm]	Feed rate [mm/min]				
	60	120	270	420	600
3000	√	QI	QI	-	-
6000	√	√	QI	QI	-
9000	√	√	QI	QI	-

√sound joint, QI quality issue, - not tested

Table 3.2: AA611-CFRP Joining process Window [28]

Spindle speed [rpm]	Feed rate [mm/min]				
	60	120	270	420	600
3000	√	√	QI	QI	-
6000	√	√	√	QI	QI
9000	√	√	√	√	QI

√sound joint, QI quality issue, - not tested

Table 3.3: CFRP-AA611 Joining process Window [28]

The parameters influencing them are the material stack up sequence, the spindle speed and feed rate. A minimum threshold of spindle speed and a maximum feed rate limitation are present for all the tested combinations, since the first ensure the sufficient material frictional softening, while the second significantly affects the penetration resistance. When these requirements were not matched, quality issues arose, consisting in the brittle delamination of the CFRP bottom surface. This is not occurring on aluminum sheets due to its higher ductility and thermal conductivity. Consequently, the CFRP brittleness turns out to be the deterministic factor limiting the process window size. Nevertheless, as it will be discussed in the following part, these quality issues do not cause the joint failure but just a relatively acceptable tensile strength reduction of the joint itself. The brittle delamination is mainly occurring in the CFRP-to-CFRP sheets joint. Indeed, when aluminum is the top sheet, (so the first in contact with the rivet) it generates higher friction and heat, which soften also the bottom CFRP sheet and the mandrel tip.

3.4.7.2 Tensile tests results

Concerning the first discussed joint (CFRP-CFRP), the following load-displacement curves show the joint tensile strength in different spindle and feed rate conditions (figure 3.21).

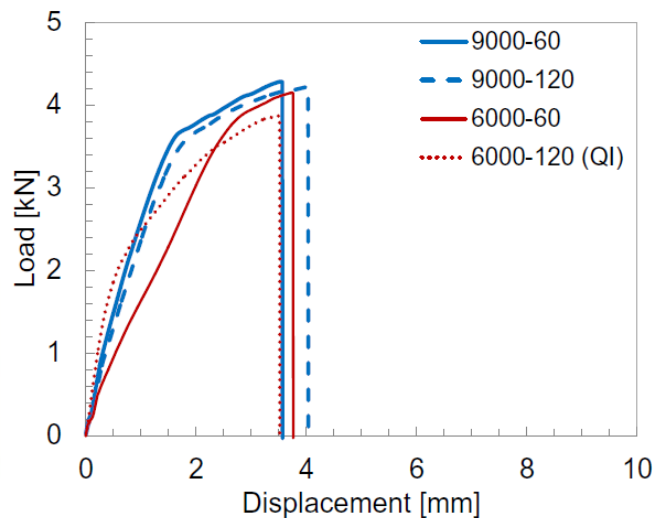


Figure 3.21: Load-displacement curve of CFRP-CFRP joint at different spindle speed and feed rate [28]

All the tested coupons showed the fracture in the bottom sheet, due to the higher stress concentration. Indeed, the larger rivet head can better distribute the load with respect to the shank tail after rivet setting. As previously reported for tensile tests on aluminum samples, the joining parameters does not affect significantly the joint strength in none of the test setup. This first material coupling showed the highest tensile strength (4.2 kN), as shown in table 3.4. It has been observed how the presence of a quality issue decreases the joint maximum resistance to 3.8 kN, so 10% less than the nominal case.

Concerning the second tested condition, the joint between AA611-CFRP showed a

lower resistance, due to the bending moment which arose during tensile loading, mainly due to the material sheet difference in thickness. The bending moment caused a local stress concentration at the hole edge of the CFRP bottom sheet, causing the joint failure at 3.4 kN for the nominal joint and at 3.1 kN when a quality issue was present.

The third test layout (CFRP-AA611) resulted to be the weakest one, presenting a joint strength of 3.1 kN, without being significantly affected by the presence of quality issues.

Material combination	No quality issue	Quality issue
CFRP-CFRP	4.2	3.8
AA611-CFRP	3.4	3.1
CFRP-AA611	3.1	3.1

Table 3.4: Tensile strength of tested joints expressed in [kN] [28]

The failure mode is shown in figure 3.22, and it consists in the rivet slabbing out in the bottom aluminum layer, showing higher tearing and bending effects with respect to the AA611-CFRP joint. However, since the failure occurred in the aluminum sheet, the quality issue of CFRP plate delamination turned out to be not influencing the results.

What can be concluded after these tests is that the only influencing parameter is the material stack-up sequence, while the presence of slight composite delamination causes just a joint strength reduction of 10%. The main conclusion is that it is possible to produce a joint between carbon fiber-reinforced polymers and aluminum by means of FSBR, with high level of effectiveness and robustness.

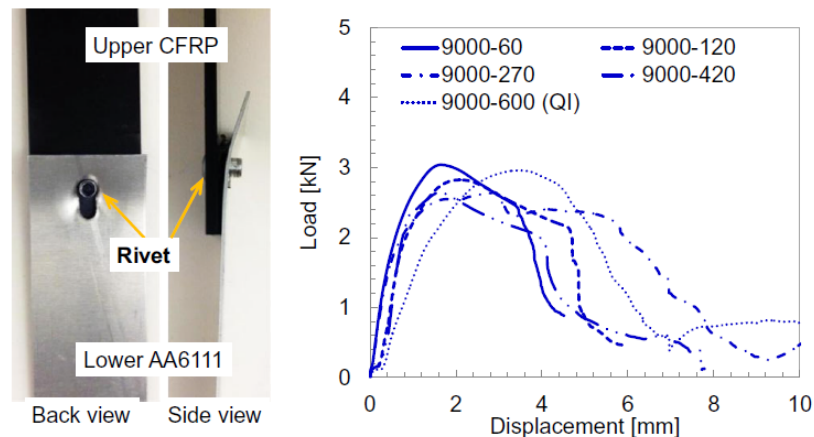


Figure 3.22: On the left, a photograph of the fractured CFRP-AA611 joint. On the right, the correspondent load displacement curve [28]

Reference [27] performed the same kind of test, joining CFRP with aluminum sheets. It concluded that FSBR causes less damage to the composite material fibers, since the CFRP layer is often heated up above the matrix glass transition temperature. This allows to displace fibers instead of destroying them like it often happen in drilling operations. A different kind of rivet model has been employed in this case, manufactured by the German supplier Gesipa and shown in figure 3.23. Unlike the Avdel rivet, the

Gesipa fastener has a steel mandrel head with a conical shape. Concerning the tensile test results, they were comparable with reference [28], with a joint shear strength around 3.1 kN.

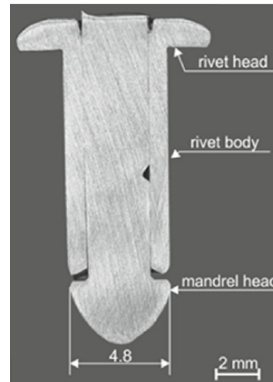


Figure 3.23: *Gesipa rivet geometry* [27]

3.4.8 Predictions of joint quality

Concerning the aluminum to CFRP joints, it is worth to briefly mention an interesting study carried out by reference [39], aimed at developing a joint process monitoring and quality prediction method. The target of this research is to acquire the process data and model them to predict the joint quality. In particular, collected data were force and torque signals, recorded as discrete variables with a sampling period of 0.001 s. The recorded signals needed to be processed in order to get rid of the irrelevant data points in the raw signals, which are clearly complex and nonlinear. The model has been developed by analyzing the just discussed FSBR process fabricated joints, namely those between CFRP and AA611, using various spindle speed and feed rate.

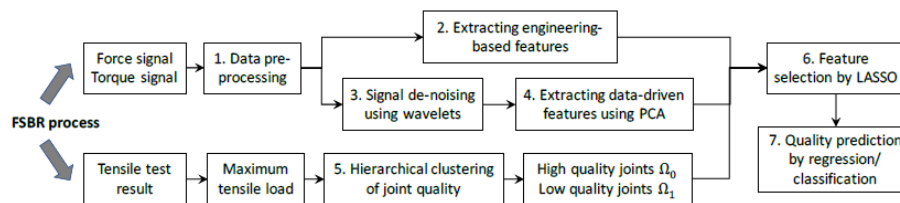


Figure 3.24: *Methodology flowchart* [39]

The adopted methodology was quite complex and based on statistical analysis. The logic schematization is provided in figure 3.24, and basically consists in force and torque signals de-noising and elaboration by means of regression analysis and orthogonal transformation methods, such as LASSO (least absolute shrinkage and selection operator) and PCA (Principal component analysis) respectively. Engineering based features coming from the torque and force trend are integrated and compared with the tensile test results, in order to get a correlation between process data and joint quality. For the purposes of this work, the most relevant aspect is the attempt to find a correlation between some physical quantities, measured during the process, and the joint quality.

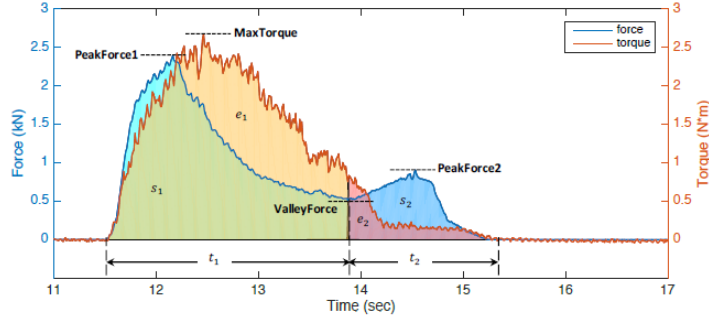


Figure 3.25: *Engineering-based features obtained from force and torque signals [39]*

Figure 3.25 shows the engineering-based features, used to estimate the joint process effectiveness. Among these, there are the first and second force peak, torque peak, valley force, time duration of top and bottom sheet penetration and area under the signals curves during the two rivet penetration stages.

Being FSBR a new developed technology, the reliability of the discussed model still needs to be verified on a larger number of samples. Moreover, according to the author, the model can be potentially improved by exploiting other signals, in addition to force and torque, such as temperature and infrared images. The important remark, from an engineering standpoint, is the possibility to have a process monitoring algorithm, allowing to detect quality issues in a large-scale production.

3.4.9 FSBR process application to magnesium-aluminum joints

An important requirement for new joining methods is their compatibility with emerging material types, which are becoming more and more common in the automotive field. An example of that is magnesium which, thanks to its properties, has been increasingly adopted by carmakers during the last 10 years. One of the driving factors, in the magnesium wide utilization, is its low density (1.74 g/cm^3), which makes it the lightest engineering material, being 35% lighter than aluminum [40]. Moreover, it is characterized by very good castability and better noise and vibration performance with respect to aluminum [41]. As shown in figure 3.26, the specific stiffness of magnesium is slightly less, but comparable to that of aluminum and iron, while the specific strength is 14% and 67% higher than the said metals respectively. Furthermore, magnesium is the eighth most abundant element on the earth, which should decrease its cost as raw material. For these reasons, due to the lightening tendencies in automotive field, magnesium is going to gradually replace denser materials not only for single components manufacturing, but also for BIW elements. For instance, Volkswagen-Audi were the first to use, in 1996, magnesium for the B80 gearbox housing, achieving a weight saving of about 20-25% with respect to the aluminum version [42]. However, the most relevant indicator in magnesium growing in automotive sector is the increase of the used amount in between 2005 and 2015, that is from 3 to 50 kg per vehicle [40].

As with any other innovative material introduced in the automotive production en-

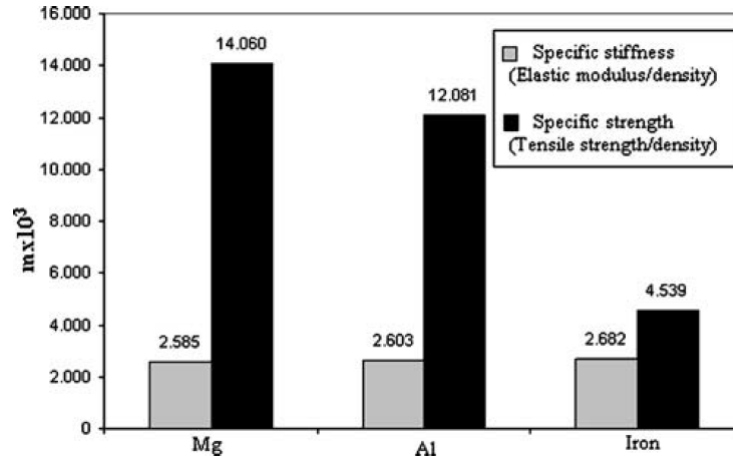


Figure 3.26: *Mechanical properties comparison between magnesium, aluminum and iron [40]*

environment, magnesium involves some issues related to the joining possibility, with other magnesium components and, especially, with other materials. Typically, the selected joining method for magnesium is inert welding, either Arch plasma, friction stir, ultrasonic spot and stir spot welding. However, not only do welding processes introduce several issues (like high shrinkage, large heat affected zone and residual stresses), but they are also not that effective when different materials have to be joined. This is the reason why mechanical fasteners seem to be the best choice for joining magnesium and, in particular, hybrid structures. Among all the mechanical fastening techniques, FSBR can provide all the advantages already discussed in the previous sections.

One of the most limiting factors in the feasibility of the mechanical joint, is the reduced room temperature formability of magnesium in comparison to aluminum alloys [42]. Indeed, unlike most of metallic materials, which are characterized by a cubic crystal structure, magnesium crystals present the hexagonal structure. From the basic crystallography notions, it results in a higher resistance to dislocation motion, since only three slip systems are present, and a lower ductility. This is essentially the reason why FSBR, thanks to its heating and softening action on the material to be joined, has been proposed as one of the most efficient joining techniques for magnesium.

Reference [43], carried out several tests on aluminum-to-magnesium specimens joined by means of FSBR, in order to identify the factors affecting the process window and the final joint strength. Concerning the experiments details, 3.05 mm Mg AM60 sheets have been joined with 1.5 mm AA6022 and with 3.15 mm AA6082, using the already seen SSPV-08-06 Avdel rivet. A reference coupon was also joined using a pre-drilled hole, in order to better identify the effects of friction stir process. Once the joints were completed, they have been sectioned along their center axis in order to perform some hardness measurement.

3.4.9.1 Process window discussion

The first part of the experimental analysis performed by [43] is focused on the process window. It resulted to be strictly related to the position of Mg and Al sheets with

respect to the rivet penetration direction, and limited by three quality issues:

- **Quality issue I** The mandrel head intruded into the shank, enlarging the drilled hole. So, the existing gap between rivet and hole made the joint ineffective.
- **Quality issue II** Semi brittle fracture occurred in the outlet side of the rivet hole, when magnesium was placed as second layer in the sheets stack. Indeed, with high feed rate and low spindle speed the magnesium softening was not enough to overcome the reduced material ductility.
- **Quality issue III** Shank overheating due to high spindle speed and low feed rate. Especially when the material layer is thick, the prolonged friction generation excessively increases the rivet temperature.

Table 3.5: AM60-AA6022 Joining process Window [43]

Spindle speed [rpm]	Feed rate [mm/min]				
	120	270	420	600	780
3000	√	√	X'	X'	-
6000	√	√	√	√	√
9000	√	√	√	√	√

√sound joint, X' quality issue I, - not tested

Table 3.6: AA6022-AM60 Joining process Window [43]

Spindle speed [rpm]	Feed rate [mm/min]				
	120	270	420	600	780
3000	X''	X''	-	-	-
6000	√	X''	X''	-	-
9000	√	√	X''	X''	-

√sound joint, X'' quality issue II, - not tested

The process window for the four tested combinations are shown in tables 3.5 to 3.8. It can be noticed that quality issue II is predominant when the bottom sheet is the magnesium one, while in almost all the other cases (except one occurrence of rivet shank overheating) the process is affected by a quality issue of type I, especially when high feed rates and low spindle speeds are used. It is interesting to underline two considerations. The first is that, when magnesium was placed on top of the stack, the thicker AA6082 provided a narrower process window with respect to the correspondent joint performed on the thinner AA6022. The difference is not related to the aluminum type, but on the different thickness, since the thicker is the layer, the higher is the friction that must be generated in order to allow a rivet penetration without any quality issue. Conversely, reverting the stacking order, the joint performed with the thicker aluminum layer at

feed rate and spindle speed of 120 mm/min and 3000 rpm respectively, did not present any quality issue, unlike in the case with the thinner AA6022. This is due to the higher heat generation occurring during the thicker aluminum layer penetration, which softens the magnesium sheet to an extent sufficient to increase its ductility and avoid a quality issue of type II.

Table 3.7: AM60-AA6082 Joining process Window [43]

Spindle speed [rpm]	Feed rate [mm/min]				
	120	270	420	600	780
3000	X'	X'	-	-	-
6000	√	X'	X'	-	-
9000	X'''	√	√	X'	X'

√sound joint, X', X''' QI I and III, - not tested

Table 3.8: AA6082-AM60 Joining process Window [43]

Spindle speed [rpm]	Feed rate [mm/min]				
	120	270	420	600	780
3000	√	X''	-	-	-
6000	√	X''	X''	-	-
9000	√	√	√	X''	X''

√sound joint, X'' quality issue II, - not tested

3.4.9.2 Tensile tests results discussion

The tensile test results turned out to be strictly dependent on the material strength close to the rivet shank, namely where the crack initiates. This aspect, in its turn, is deeply affected both by the rivet frictional penetration and tail forming. This is characterized by the mandrel head intrusion into the shank, which expands the hole in the bottom sheet, causing the material hardening. This is proved by the experimental evidences, since the reference pre-drilled joint showed a hardening, due to tail forming, from 64 to 76 HV0.2. On the other hand, frictional penetration process determines a further strengthening of the material around the hole, due to multiple reasons. First, the thermal effect of friction induces the grain refinement in the material, which opposes the crack propagation and fracture. Moreover, a certain deformation of the material causes a strain hardening close to the rivet hole. Finally, the stir action causes precipitate hardening in the aluminum layer, as a further hardening mechanism. This means that the frictional penetration process results in an additional hardness increase up to around 83 HV0.2.

Another difference between conventional blind riveting and FSBR is that, in the second case, a material sleeve is formed on the blind side of the joint (figure 3.27),

which increases the resulting strength of the connection.



Figure 3.27: *Material sleeve resulting from the riveting process of aluminum (2 mm) to magnesium (2 mm) [44]*

As mentioned, almost all the tested joints failed in the bottom layer, where a higher stress concentration is present. Indeed, on the top sheet, the rivet head better redistributes the load on a wider surface, avoiding the point loading.

The first tested combination was the AM60-AA6022 joint, in which the FSBR presented better results, in terms of maximum tensile load, with respect to the pre-drilled joint, thanks to the frictional penetration hardening mechanisms. All joints failed in the aluminum layer.

When the position of metal sheets was reversed (AA6022-AM60), the fracture always occurred in the magnesium layer. The tensile strength achieved with FSBR was just slightly above the reference pre-drilled coupon (0.25 kN more). A possible explanation is the lack of the precipitate hardening in aluminum close to the joint outlet face, but especially the smaller material sleeve formed on the tail side of the rivet. The latter is related to the ductility of the bottom material layer so, in the case of magnesium, the lower formability leads to a lower protrusion of metal in the joint blind side.

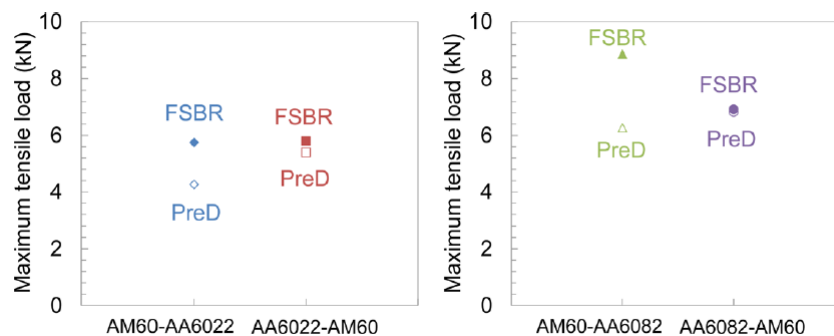


Figure 3.28: *Tensile strength comparison between FSBR and pre-drilled coupons for all the tested material combinations [43]*

When magnesium was joined with the thicker AA6082 (3.15 mm), the failure occurred always in the AM60 layer, regardless from the stack order. In the AM60-AA6082 samples, those joined by means of FSBR present higher resistance values with respect to the reference case. In AA6082-AM60 joints, similar results have been obtained in FSBR

and pre-drilled joints, basically for the same reasons of AA6022-AM60 case. However, as it can be observed in figure 3.28, summarizing all the obtained results, when a thicker aluminum layer is employed, the joint tensile strength increases.

In conclusion, FSBR resulted to be effective in the joining of magnesium and aluminum alloys. The process window is significantly affected by the sheets layout and resulted to be wider when aluminum was placed on the bottom.

3.4.10 FSBR system commercialization

In November 2017, the first practical application of FSBR joining solution has been proposed on the market by a European supplier, which is one of the leading international companies in the blind rivet sector. Because of confidentiality reasons, this supplier will be referred from now on as supplier A.

FSBR system has the target to simplify and quicker the mechanical joining of hybrid structures, avoiding the requirement of pre-drilled holes, positioning tolerances and complex drill hole locating systems, typical of standard blind riveting. This patented solution is presented as a fully automated process, which is shown in figure 3.29. Flow Drilling Riveting exploits the same working principle discussed in FSBR description.

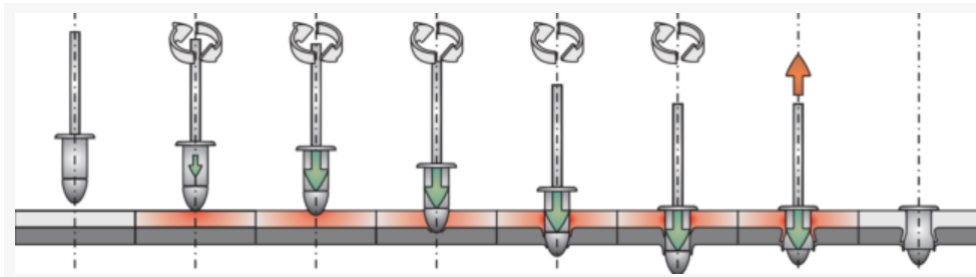


Figure 3.29: *Riveting setting steps* [45]

With the possibility to perform material drilling and rivet setting in one step only, the process time can be reduced to less than 3 seconds for aluminum sheets of 2 mm thickness. Another important aspect of this technology is the avoidance of dirt or dust resulting from traditional joining methods. Indeed, FSBR is a forming and not a cutting process, that means no chips are produced and a clean working environment is ensured, which is especially important when joining closed profiles. Moreover, the material protrusion created on the rivet exit face can significantly increase the joint load bearing capability with respect to conventional blind riveting [45].

The system has been addressed especially to high volume productions, being conceived to be used on industrial robots along automated production lines. It satisfies also the requirements in terms of process monitoring, which is now almost mandatory in every large scale productive environment. The setting tool, used for this riveting system, is endowed with sensors capable to map the entire riveting process, detecting and reporting possible deviations from the ideal one. This allows to perform constant product quality assessment, in order to reduce errors and costs.

According to supplier A, the rivet design, in terms of adopted material, geometry

and surface coating is flexible and depends on the specific application [45].

Before starting the actual collaboration between FCA and this fastening system company, a benchmark of the supplier has been done. It resulted in the discovery of previous collaboration between supplier A and other automotive companies aimed at the development and integration of friction-based blind riveting methods in several industrial projects. One of them was concerning the use of FSBR technology in the assembly process of battery housings for electrical vehicles. Another more detailed project was carried out with Brose Fahrzeugteile, a renowned German automotive industry supplier producing seats, electric motors and mechatronic systems for doors. This application involved the connection of a window lift rail to a door module, involving dissimilar materials like aluminum and fiber-reinforced plastic for which conventional blind rivets were used. Due to the complex geometry of the installation space, an automated process for standard rivet installation was not possible, until supplier A developed its technology. This cooperation between the two different companies accompanied the development of the new friction-based riveting method, pointing out potential application fields and making the process more and more oriented toward the automotive sector. Currently, more studies are being conducted with new partners in the automotive scenario in order to develop a reliable joining process for a wide variety of material combinations. With these findings, future developers and planners can be provided with boundary conditions and economic as well as technical parameters for design and production planning.

3.4.11 Additional experimental tests with FSBR technology and comparison with conventional blind riveting

FSBR has been recently tested in many researches, due to its large potential in the hybrid fastening context. Reference [46] used the rivet provided by supplier A to join different combinations of aluminum (EN AW-5754), magnesium (AZ31) and composite (Tepex@dynamite 102) with thickness varying between 1 and 2 mm. The optimal set of parameters, in terms of feed rate and spindle speed, had been previously defined and used to get the maximum joint performances for each sheets combination. Moreover, the cross-sectional macrograph of each FSBR joint was analyzed in order to assess the sheets interlocking and the material sleeve formation.

Due to its lower ductility, magnesium formability around the rivet resulted to be lower than what achieved with aluminum, which represents one of the reasons why a lower joint strength is achieved in former case. However, all the coupons failed in the composite layer, which was always placed on the bottom of the stack. The failure mode was the bearing one, with the rivet pulled through the plastic sheet in a gradual way, so that no catastrophic failures were observed. One of the most interesting aspects of these tests was the comparison of FSBR joints with the correspondent conventionally riveted ones, in order to assess the advantages of this joining technology. As shown in figure 3.31, FSBR provides a joint resistance improvement up to 68% if compared with traditional blind riveting. As it could be expected, the larger is the plates thickness, the higher is the joint strength, since more material is available to create a sleeve. The

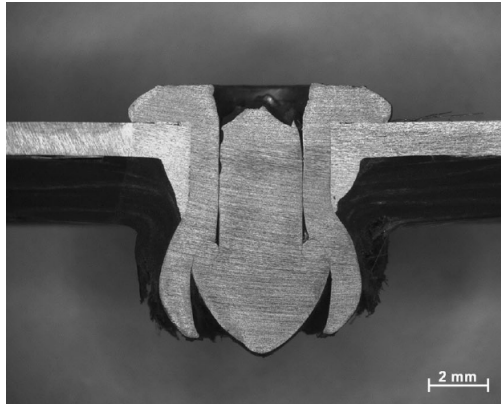


Figure 3.30: *Cross-sectional macrograph of a FSBR joint between a 1 mm magnesium and 2 mm composite plates [46]*

overall conclusions of this experiment are the good mechanical properties and process robustness of FSBR, which make this method attractive for high volume and high reliable production processes.

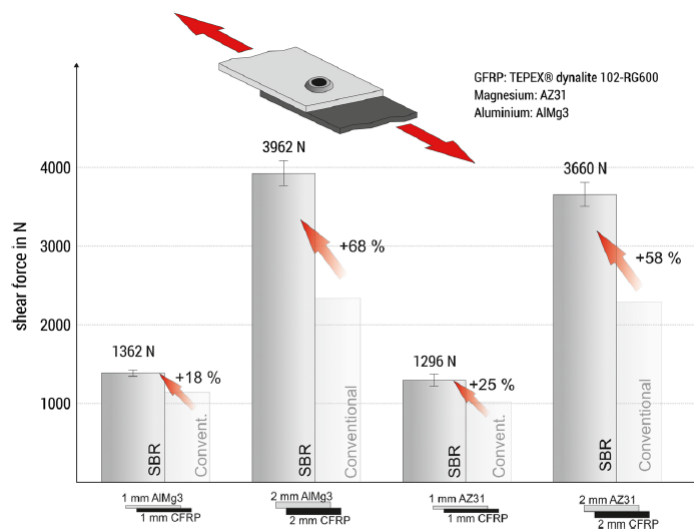


Figure 3.31: *Joint strength for all the tested material combinations [46]*

Another example of FSBR mechanical properties, in the field of hybrid joints is provided by reference [47]. In this work, Magnesium (ASTM AZ31B), Aluminum (EN AW-5754, namely AlMg3), CFRP (Tepex®dynalite 201-C200) and GFRP (Tepex®dynalite 102-RG600) are joined using spinning blind rivets and comparing the joint strength results with conventionally blind riveted coupons. All the tested material plates were characterized by a thickness of 2 mm.

Concerning the testing procedure, the rivet specifically designed by supplier A was used, while 4200 rpm and 3000 N were the spindle speed and penetration force respectively. The obtained results are graphically presented in figure 3.32, from which it can be noticed the significant improvement provided by SBR with respect to conventional blind riveting. It is worth to notice that this joint strength difference results to be more marked than what evidenced by other experimental campaigns, like that presented by

reference [43]. One of the differences may be the geometry of the rivet which, according to the available data, has been optimized by supplier A. Indeed, a possible explanation is that the conical shape of the rivets provides a more significant material flow in the riveting direction, with a consequent larger sleeve formation with respect to the hollow mandrel tip of the SSPV-08-06 Avdel rivet. This aspect, together with the preservation of the composite fibers, represents the main difference between Spin and conventional blind riveting.

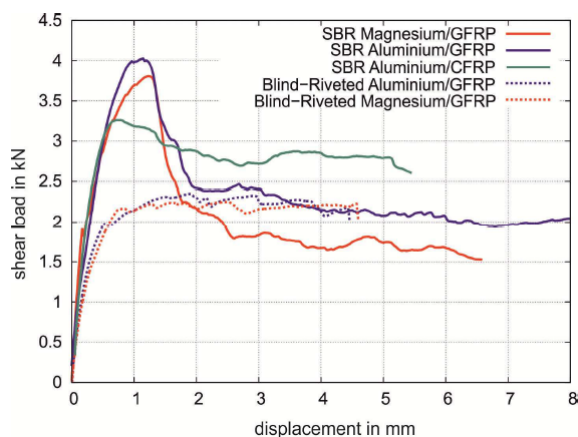


Figure 3.32: Load-displacement curves resulting from joints testing, with comparison between FSBR and conventional blind riveting [47]

3.4.12 FSBR performance in dynamic loading conditions

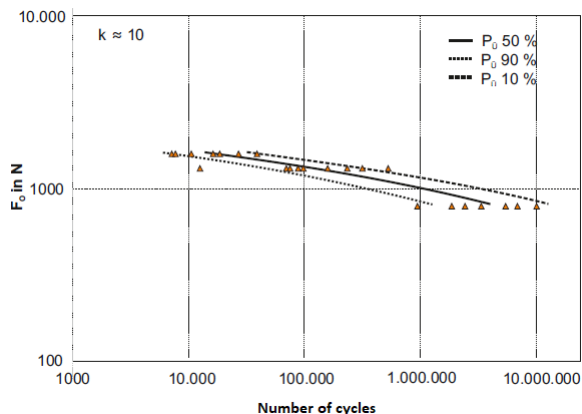


Figure 3.33: Wohler curves for 10%, 50% and 90% survival probability [44]

The performances of Flow Drilling Riveting technology have been largely investigated by work [44], in which it is also provided a fatigue behavior analysis of these riveted joint types. The tested sample is a riveted coupling of 2 mm aluminum with 2 mm glass reinforced polymer, which has been subjected to several load amplitudes, recording each time the percentage of survived components, so that three Wohler curves have been plotted for different percentages of survival probability (10%, 50% and 90%), as shown in figure 3.33. For the three obtained curves, it resulted a fatigue exponent equal to 10.

Two different failure modes have been observed in low and high cycle fatigue. In the first case, when the highest load values were applied, the failure was observed to take place in the plastic layer. Conversely, in low load testing, the failure was localized in the aluminum layer, where the highly deformed region of the metal sheet played as a notch, whose stress concentration effects are more pronounced in high cycle fatigue conditions.

3.5 Robotized Riveting system

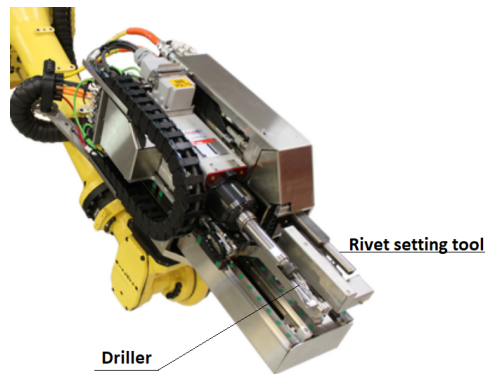


Figure 3.34: *Robotic module*

The previous sections presented some innovative riveting methodologies which are supposed to improve the efficiency of automotive rivet fastening. However, the improvement of said process can be achieved not only by modifying the working principles of the riveting technique (substituting the conventional drilling step with the rivet penetration by the rotating action), but also changing the process layout and operations sequence of the rivet installation process. In other terms, the increasing relevance of blind riveting technique has not just determined a deep study of the joining method in itself, but also the development of installing equipment. An example of what just said is provided by the Robotic riveting system.

It is an automated solution for blind rivet installation, developed by a company operating in the US market and defined here as supplier B. The innovative module, which can be easily mounted on a six-axis robot, integrates in a single assembly the drilling and riveting tools. The system is specifically designed for high volume production like in automotive and transportation fields, where reliability, robustness and low cycle time are among the main priorities. The same assembly can be used to install several kinds of rivet geometries, since up to three feeders can be mounted on the system, with the possibility to feed them in sequence.

The working operation consists in the robot positioning the module on the joint location. Then the robot stops while the riveting module extend the spindle up to the part, where the drilling occurs. The spindle maximum rotation is about 24.000 rpm and there is the possibility to cool the drill and collect the material chip. The six-axis robot is not directly used for the riveting operation, since their precision in the linear motion is not really high.

The robotic riveting module moves the riveting gun in the hole position, inserts the fastener and sets it. The typical process cycle time is of 5 seconds, during which several operating parameters are measured and acquired, like the torque, spindle speed, contact force and setting force. Some instantaneous controls are provided, such as the chip and spent mandrel collection verification. Moreover, each rivet exiting from the feeder is inspected by a vision system, in order to ensure the final joint quality level.

Despite this system performs the drilling and rivet setting processes in two different steps, these are coupled and sequentially carried out. It means that instead of having a specific workstation devoted the drilling operations, this step is directly performed on the assembly line and, immediately after, the fastener can be inserted. This provides several advantages, such as the reduction of workstations required for the assembly process and the simplification of the assembly procedure. Moreover, since the pre-drilling operation is performed when the material sheets are already overlapped in the designed position, a single drilling operation can substitute the multiple ones which are conventionally done for each sheet of the stack. This determines a further process optimization and decrease of the cycle time.

Another very important advantage of this system is that, machining the holes on all the material layers at the same time, no concentricity tolerance issues can arise, with a consequent simplification of the tolerance chain management process.

It is true that, compared to some of the other fastening technologies, blind rivets can carry a slightly higher consumable cost. However, the robotic riveting system offsets the higher cost by improving the cycle time through automation of the fastening process. This increases the throughput of the production line while decreasing the overall manufacturing cost. So, a faster ROI can be achieved if compared to the use manual tools and associated operator overhead

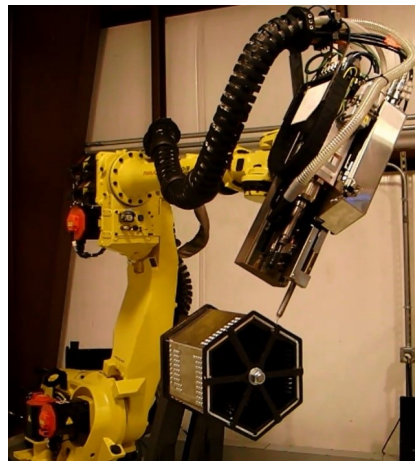


Figure 3.35: *Robotic riveting assembly mounted on a six-axis robot*

Chapter 4

Experimental analysis of FSBR method for a specific application of industrial interest

The previous chapters are aimed at providing the reader with an overview of the joinability problem in the industrial and automotive field, pointing out the most common technological alternatives and how they are actually implemented by some carmakers. Starting from the knowledge of this scenario, the focus has been moved to a specific joining method, namely blind riveting, which is of much interest in the field of dissimilar materials joints, whether it involves or not adhesive usage. Unlike other riveting methodologies, blind rivets allow combining the single side accessibility feature of SPR, with higher joint resistance, installation process robustness and lower fastener weight (if compared with FDS).

Starting from this chapter, the thesis will be aimed at evaluating experimentally the effectiveness and applicability of the two previously presented innovative blind riveting technologies, which are friction stir blind riveting and the robotized riveting system. The reason why they have been considered of higher interest with respect to the others, such as Resistance Spot Riveting, is that they allow the fastener installation without the need of a pre-hole. As already mentioned, this is not just an advantage from the cycle time reduction viewpoint, but it also improves the process management in the field of tolerance chain optimization. If the hole is machined directly along the assembly line (when the components are already overlapped in their final position) the following advantages can be achieved:

- Reduction of number of workstations, getting rid of those dedicated to the hole drilling operations.
- Being that the components overlap, one drilling operation can be performed instead of two and no holes concentricity issues arise during the component positioning.
- If the rivet itself is used as drilling bit, like in the case of FSBR, no coupling

tolerance issue between the fastener and the hole must be taken into account, so no hole over-dimensioning would be needed. Moreover, no hole finding function is required and the drilling bit wear would not be a concern

These advantages are connected to the process simplification, which is supposed to enhance the automation of the blind rivets installation operations. These, until now, have been mostly performed manually by several carmakers, as Audi with the A8 model.

This chapter is aimed at increasing the comprehension of FSBR process by presenting a set of experiment on this new riveting method. The testing activity has been performed on samples and rivet types different from those required by the FCA final application, but it highlights the most important process aspects of the FSBR process before focusing on the samples provided by supplier A.

4.1 First experimental campaign objectives

The first tests consisted in the joining in of CFRP and aluminum by means of the friction based riveting technology, which has been performed in the laboratory using a CNC machine. This initial experimental effort involved the CFRP-Al stacking sequence. The same samples types have been joined adopting also traditional blind riveting process, in order to get a reference case for the assessment of FSBR system performance.

One of the aspects of friction based riveting process, not yet investigated in the current literature, is the effect of samples thicknesses variation when the layers stack presents a brittle material on top, like carbon fiber. According to supplier A, which shared its experience in the field of frictional penetration of rivets, the presence of carbon fiber on top of the material stack can represent a critical aspect. Indeed, it is easier to penetrate carbon fiber by means of friction stir riveting when it is used as the bottom layer of the stack (like it has been done by [46] and [47]), providing the possibility to heat up more the composite and the fastener itself during the penetration of the top layer. Instead, dealing with the sequence CFRP-Al, it is necessary to increase the rivet rotational speed and decrease its feed rate, in order to comply with the low ductility of carbon fiber, especially when thick samples are riveted.

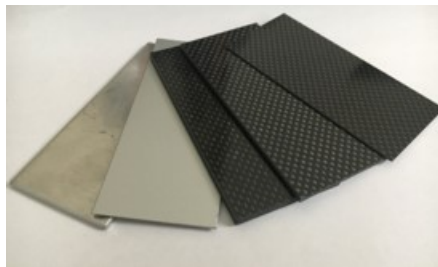


Figure 4.1: *Aluminum and carbon fiber samples*

Consequently, the feasibility and the effectiveness of FSBR method has to be assessed with respect to the thickness variation.

In this set of tests, three different thicknesses of carbon fiber composite were considered, namely 3.17, 1.6 and 0.8 mm, while two aluminum sample types were investigated, presenting thicknesses of 1 and 3.1 mm (figure4.1).

The tests have been designed in such a way to achieve the following targets:

- Joint feasibility verification for all possible combinations of the previously mentioned composite and aluminum samples
- Assessment of the joint strength with a comparison between FSBR and conventional blind riveting technology
- Analysis of the feed rate effect on the final joint strength
- Study of the stacking sequence effect on FSBR joining technology
- Friction based blind riveting process compatibility with the presence of adhesive
- FSBR application to CFRP to CFRP joints
- Identification of process failure mechanisms and quality issues

4.2 Experimental setup and dummy test

The first experimental campaign has been designed following well-defined experimental plan and setup, with the objective of getting reliable and statistically meaningful results. Three samples have been riveted for each material combination and for every joining technology (standard and FSBR), in order to deal with the intrinsic process variability.

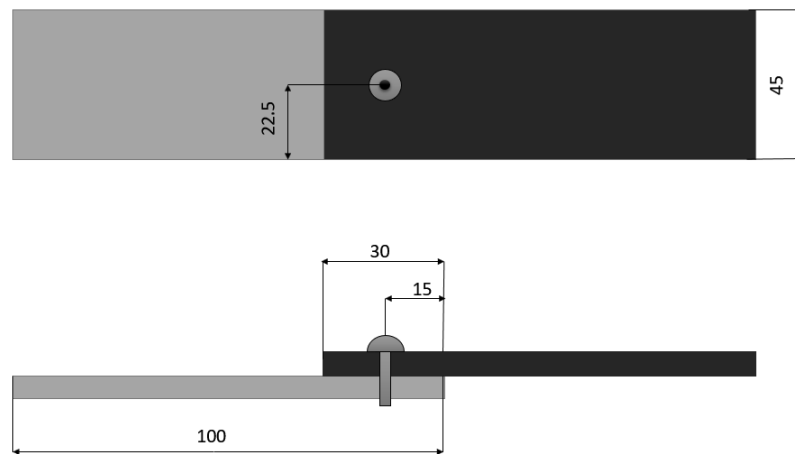


Figure 4.2: *Samples geometry*

The selected samples geometry is rectangular with 45 x 100 mm sides and variable thickness. The geometry is shown in figure 4.2.

Regarding the FSBR process, the working parameters have been selected so that to have a rivet rotational speed fixed at 6500 rpm and a variable feed rate. The aim of this parameter variation is to confirm the process robustness observed when riveting

Al-Al samples [29], and understand if the same applies when carbon fiber reinforced composites are involved. Consequently, the three tested samples for each combination have been riveted at a feed rate equal to 50, 150 and 250 mm/min. The feed rate value is expected to be slightly higher in the actual process carried out by the supplier, thanks to a rivet design specifically thought to enhance the fastener penetration through the material by means of friction.

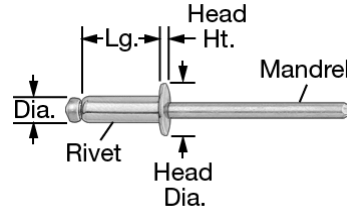


Figure 4.3: Zinc-Plated blind rivet geometry [48]

As just mentioned, the rivet choice has been that of a standard blind rivet, namely not the one optimized in its shape by supplier A. The reason of this choice is mainly related to the low availability of this kind of fastener in the early stages of the FSBR technology development. The selected fastener is a zinc-plated steel blind rivet manufactured by Avdel, whose geometrical and mechanical features are presented in table 4.1. They have been selected so that the same rivet is suitable to connect all the chosen samples, regardless of their thickness variation (ranging from 1.8 to 5.67 mm).

Table 4.1: Rivet characteristics

Rivet type	Blind
Material	Zinc-Plated Steel
Mandrel Material	Steel
Shank diameter	6.35 mm
For material thickness	1.6 mm - 6.35 mm
Length	12.7 mm
For hole size	6.53 mm - 6.62 mm
For drill size	F
Head type	Domed
Domed head profile	Standard
Head diameter	13.33 mm
Head height	2 mm
Shear strength	5.5 kN
Tensile strength	6.6 kN
Specifications Met	IFI 114 Standards

Concerning the material properties, the selected composite is a 250°F class epoxy resin reinforced by a 53-54% volume of carbon fibers. The number of reinforcement layers is dependent on the sample thickness and has been indicated by the supplier to be ranging between:

- 2 and 3 layers for 0.8 mm thick sheets
- 6 and 7 for 1.6 mm thick sheets

- 15 and 16 for 3.17 mm thick sheets

Their manufacturing process starts from conventional prepregs, namely fibers or fabrics pre-impregnated with resin.

Concerning aluminum, a commercial type has been used, namely a 6061 alloy which is typically employed for automotive manufacturing processes. The correspondent mechanical properties are reported in table 4.2. This aluminum is an aged alloy, meaning that potential its overaging could be possible considering the thermal effects of FSBR process, which have been discussed in chapter 3.

Table 4.2: 6061 Aluminum characteristics

Material	6061 Aluminum
Yield strength	241 MPa
Fabrication	Heat treated
Temper	T6
Temper rating	Hardened
Temperature range	-195°to 148°C
Specifications Met	AMS 4027, ASTM B209
Density	2.7 g/cm ³
Melting point	582°- 652 °C
Modulus of elasticity	68.9 GPa

The FSBR process, but also the standard drilling operation needed for conventional blind riveting, require the sample to be properly fixed and kept in position during the fastener installation. Consequently a specific fixture system has been designed, and it is schematically represented in figure 4.4.

The lower clamp is achieved by means of a solid flat base, while the samples alignment is achieved by means of movable spacers, in order to have a flexible setup for all sample thicknesses to be tested. The coupons are kept in the designed position by means of the upper clamps, which can be adjusted by means of threaded screws connected to the lower clamp.

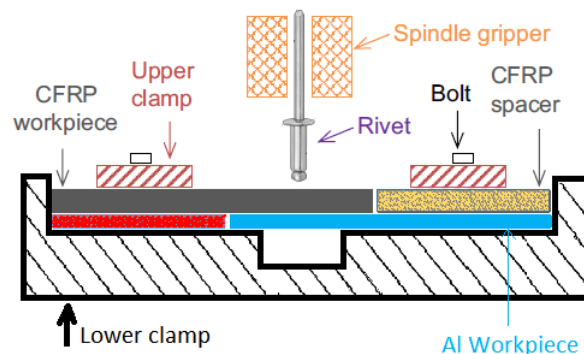


Figure 4.4: Schematic test layout

The riveting process has been carried out by means of a CNC machine, since it allowed achieving a sufficient rivet rotational speed and to vary the vertical feed rate according to the test targets, by simply setting the machine parameters by means of

the G code programming language. The employed machine was a Hartford LG-800, available at University of Windsor. As already mentioned, the FSBR technology has been developed by supplier A in such a way to make the installation process fully automated. This means that the system offered by the supplier is able to make the rivet rotate by means of an electric motor and to exploit an integrated pneumatic device to pull the rivet mandrel and set the fastener after its penetration is completed and the rotational motion is stopped. In the case of all the presented tests, the fastener has been set by a pneumatic riveting gun after the end of the CNC machine work program.

The adopted machine and fixture, with the first tested samples, are illustrated in figure 4.5.

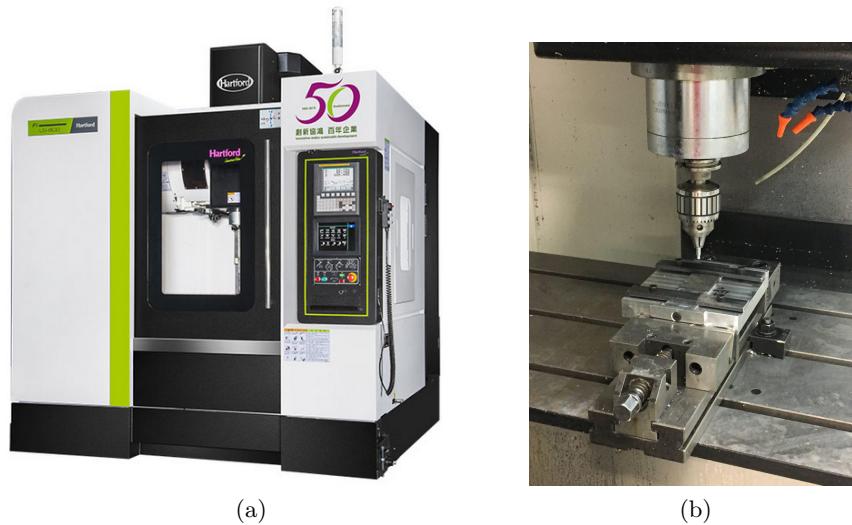


Figure 4.5: a) Hartford LG800 CNC Machine b) Experimental layout

The shown samples are those used for the machine and process setup, representing essentially scraps of the previous carbon fiber and aluminum cutting operations. They have been used in order to assess the process feasibility and effectiveness with the selected stacking sequence and to optimize the machine G-code. The joining parameters have been selected to be quite conservative, in order to avoid quality issues by generating enough frictional heat for the fastener penetration. Consequently, a quite low feed rate and high rotational speed have been chosen for the dummy test, that were 50 mm/min and 7000 rpm respectively.

The process provided satisfactory results, characterized by the easy and complete penetration of the rivet through the composite and aluminum samples. The obtained joint is shown in figure 4.6, representing the two sides of the samples before the rivet setting.

Some preliminary results were drawn from this dummy test. First, it demonstrated the process feasibility with the selected materials, stacking sequence and working parameters. The procedure was successful since none of the quality issues described by works [43] and [34] arose.

A second very interesting factor was the capability of the rivet to hold the samples in position despite the fact that mandrel was not yet pulled, namely the rivet was not

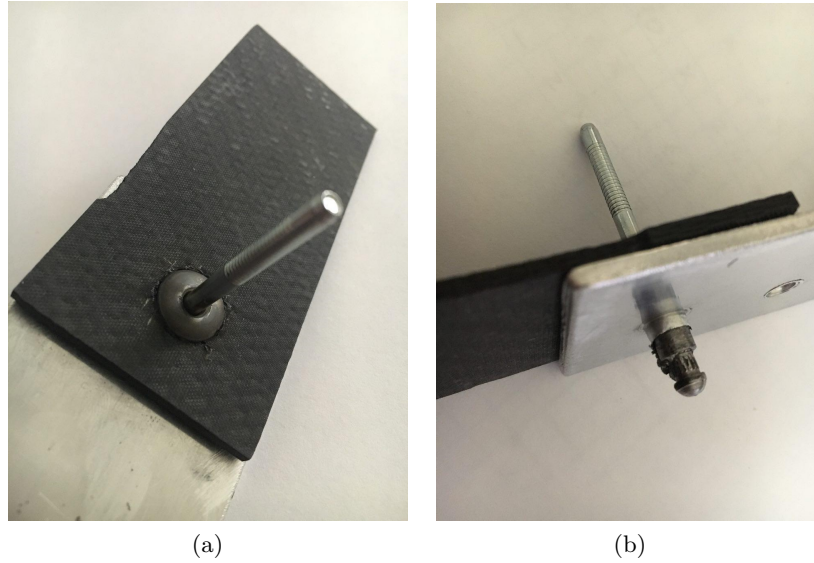


Figure 4.6: *Dummy sample a) inlet and b) outlet sides*

set. Moreover, it was not possible to easily move the rivet in the axial direction without applying a significant force. The reason is that the hole dimension is exactly that of the rivet since the fastener is used as a sort of drilling bit. Consequently, no clearance was present between the rivet and the hole and the samples were already kept in position after the fastener penetration. This is not the case for conventionally installed rivets, in which the fastener must be inserted through a pre-drilled hole. Indeed, in this case, there must be a minimum clearance between the hole and the rivet in order to allow the insertion. This difference was quite promising for the final performance comparison between the friction based and the standard riveting technology. Indeed, the absence of a rivet-hole clearance means that the hole is smaller and so less stress concentration can take place. Moreover, it implies a better and more homogeneous rivet loading can be achieved. These aspects suggest the possibility to use FSB method to get equal or higher joint mechanical performances with respect to the traditional technology.

The dummy test turned out to be useful in evidencing a further practical aspect of the joining process, namely the importance in the definition of the CNC machine vertical motion stopping point. Ideally, the fastener should stop as soon as the rivet head touches the carbon fiber sample. However, this aspect is not easy to be controlled with a simple CNC machine, since the contact between the rivet head and the material would initiate a stirring action, with the consequent damage of the composite layer beneath the fastener head. However, it was not convenient to stop the vertical motion before the contact between the sample and the rivet head because, due to the absence of rivet-hole clearance, it would have been difficult to push down the fastener after the end of the rotational motion. Consequently, a significant attention has been devoted to the definition of the CNC machine path stop point, so that the rivet cap could be in contact with the part without stirring or damaging it by rotating friction.

4.3 Test features and schedules

The following sections provide an overview of the main investigated aspects of the FSBR process during the first experimental campaign, providing also the testing schedule and process parameters.

4.3.1 Study of the thickness effect

Once the evaluation of the dummy test and the process setup were complete, the actual test schedule was defined. Table 4.3 provides the test program for the analysis of the thickness effect on FSBR and conventional blind riveting technology. It specifies, for each sample to be riveted, the constitutive materials, their thickness, stacking sequence and employed technology. As already mentioned, all available material and thicknesses combinations have been joined by means of both FSBR and conventional technology. In the former case, rivet feed rate and rotational speed are reported in the table. One of the reasons why different values of thicknesses have been tested is that of verifying the applicability of friction-based riveting in more and more demanding conditions, namely increasing the material thickness. Indeed, the larger is the thickness, the higher will be the material capability to dissipate heat, decreasing the localized softening of the aluminum and composite layers. This would finally result in a higher resistance to the fastener penetration. Furthermore, in the comparison between FSBR and conventional blind riveting, it is more significant to assess how potential differences vary by changing the involved material thicknesses.

Table 4.3: Test schedule for the study of riv-bonding process

Test number	CFRP layer thickness [mm]	Al layer thickness [mm]	Stacking order	Employed technology	Feed rate [mm/min]	Spindle speed [rpm]
1	0,8	1	CFRP-Al	Standard drilling	-	-
2	0,8	1	CFRP-Al	Standard drilling	-	-
3	0,8	1	CFRP-Al	Standard drilling	-	-
4	0,8	1	CFRP-Al	FSBR	50	6500
5	0,8	1	CFRP-Al	FSBR	150	6500
6	0,8	1	CFRP-Al	FSBR	250	6500
7	1,6	1	CFRP-Al	Standard drilling	-	-
8	1,6	1	CFRP-Al	Standard drilling	-	-
9	1,6	1	CFRP-Al	Standard drilling	-	-
10	1,6	1	CFRP-Al	FSBR	50	6500
11	1,6	1	CFRP-Al	FSBR	150	6500
12	1,6	1	CFRP-Al	FSBR	250	6500
13	3,17	1	CFRP-Al	Standard drilling	-	-

14	3,17	1	CFRP-Al	Standard drilling	-	-
15	3,17	1	CFRP-Al	Standard drilling	-	-
16	3,17	1	CFRP-Al	FSBR	50	6500
17	3,17	1	CFRP-Al	FSBR	150	6500
18	3,17	1	CFRP-Al	FSBR	250	6500
19	0,8	2,5	CFRP-Al	Standard drilling	-	-
20	0,8	2,5	CFRP-Al	Standard drilling	-	-
21	0,8	2,5	CFRP-Al	Standard drilling	-	-
22	0,8	2,5	CFRP-Al	FSBR	50	6500
23	0,8	2,5	CFRP-Al	FSBR	150	6500
24	0,8	2,5	CFRP-Al	FSBR	250	6500
25	1,6	2,5	CFRP-Al	Standard drilling	-	-
26	1,6	2,5	CFRP-Al	Standard drilling	-	-
27	1,6	2,5	CFRP-Al	Standard drilling	-	-
28	1,6	2,5	CFRP-Al	FSBR	50	6500
29	1,6	2,5	CFRP-Al	FSBR	150	6500
30	1,6	2,5	CFRP-Al	FSBR	250	6500

4.3.2 Study of the stacking sequence effect

Another interesting aspect that has been investigated in this experimental analysis is the effect of the samples stacking sequence. In other terms, despite the usual employment of carbon fiber as a reinforcement component implies to have the composite on top of the aluminum sheet, the opposite stacking order has been tested so that to get a more complete understanding of the friction based blind riveting method. As it has been discussed in the previous chapters of the thesis, the failure of a blind riveted sample generally tends to occur in the bottom material layer, where the rivet footprint on the material is smaller with respect to that of the fastener head, determining a higher stress concentration factor. Moreover, being the potential advantage of FSBR method based on the creation of a material sleeve on the blind side of the connection, it is useful to evaluate how this technology behaves when the bottom material layer is a brittle one, like the composite.

In these tests the three available thicknesses of carbon fiber layers have been riveted with just one aluminum sample thickness, namely that of 1 mm. Each combination has been joined by means of both friction based and conventional blind riveting technology (with a pre-hole). The correspondent test schedule for this set of tests is shown in table 4.4.

Table 4.4: Test schedule for the study of riv-bonding process

Test number	CFRP layer thickness [mm]	Al layer thickness [mm]	Stacking order	Employed technology	Feed rate [mm/min]	Spindle speed [rpm]
31	0,8	1	Al-CFRP	Standard drilling	-	-
32	0,8	1	Al-CFRP	Standard drilling	-	-
33	0,8	1	Al-CFRP	FSBR	50	6500
34	0,8	1	Al-CFRP	FSBR	150	6500
35	0,8	1	Al-CFRP	FSBR	250	6500
36	1,6	1	Al-CFRP	Standard drilling	-	-
37	1,6	1	Al-CFRP	Standard drilling	-	-
38	1,6	1	Al-CFRP	Standard drilling	-	-
39	1,6	1	Al-CFRP	FSBR	50	6500
40	1,6	1	Al-CFRP	FSBR	150	6500
41	1,6	1	Al-CFRP	FSBR	250	6500
42	3,17	1	Al-CFRP	Standard drilling	-	-
43	3,17	1	Al-CFRP	Standard drilling	-	-
44	3,17	1	Al-CFRP	Standard drilling	-	-
45	3,17	1	Al-CFRP	FSBR	50	6500
46	3,17	1	Al-CFRP	FSBR	150	6500
47	3,17	1	Al-CFRP	FSBR	250	6500

4.3.3 Study of FSBR compatibility with adhesive

The third kind of test, characterizing the first experimental campaign, consisted in analyzing the compatibility of the FSBR method with the presence of adhesive. This practice is quite often adopted by carmakers, as it has been presented in the case of Audi, Lotus, Jaguar (with the XJ) and BMW. Indeed, this is also the target of FCA process optimization, consisting in integrating an innovative and more effective riveting strategy with the application of structural adhesive. This technique is called riv-bonding, namely the combination of riveting and adhesive bonding. Riv-bonding has been successfully employed in several applications for aerospace and automotive sectors. The joining sequence consists in the adhesive application prior the assembly and the subsequent rivets installation. This allows adding the benefits of adhesive bonding to mechanical fastening methodologies, such as:

- Achieving a continuous and not localized joint
- The joint is made leak-tight
- The joint stiffness is increased

- The mechanical resistance of the joint is improved, since possible cracks nucleating close to the hole can be arrested by the adhesive bond

An advantage in riv-bonding stands in the possibility of significantly reduce the number of used fasteners, minimizing also the negative effect of stress concentration induced by holes and, consequently, improve the static and fatigue resistance of the joint. According to some carmakers, adhesives alone may have a poor peel strength, which can affect the vehicle crash performance. A better solution is to use them as the primary joining method of a hybrid methodology, reinforced by rivets. On one hand, adhesives provide the proper stiffness and NVH requirements, on the other hand the fastener, which in normal operating conditions represents a backup joining mechanism, becomes the primary one during a crash event when the adhesive would normally peel [49].

Table 4.5: Test schedule for the study of riv-bonding process

Test number	CFRP layer thickness [mm]	Al layer thickness [mm]	Stacking order	Employed technology	Feed rate [mm/min]	Spindle speed [rpm]
48	2.4	1	CFRP-Al	FSBR + adhesive	50	6500
49	2.4	1	CFRP-Al	FSBR + adhesive	50	6500
50	2.4	1	CFRP-Al	FSBR + adhesive	50	6500
51	2.4	1	CFRP-Al	FSBR + adhesive	100	6500
52	2.4	1	CFRP-Al	FSBR + adhesive	100	6500
53	2.4	1	CFRP-Al	FSBR + adhesive	100	6500
54	2.4	1	CFRP-Al	FSBR + adhesive	150	6500
55	2.4	1	CFRP-Al	FSBR + adhesive	150	6500
56	2.4	1	CFRP-Al	FSBR + adhesive	150	6500

Table 4.5 presents the test schedule for this kind of analysis consisting of the combination of adhesive and friction based blind riveting technology. Once more, the study is based on the comparison between FSBR process results when the joining is made at different feed rates. In order to improve the statistical reliability, three repetitions for each testing condition has been made. In this case, the 3M 468 MP High-Performance Acrylic Adhesive was used. It is quite commonly adopted in several industrial fields, such as the aerospace, appliance and automotive one, for bonding to metal and high surface energy plastics. As demonstrated in figure 4.7, the adhesion of this adhesive, in terms of minutes before failure and failure load for a given testing time, turns out to be among the best available on the market.

Furthermore, the 3M 468 MP High-Performance Acrylic Adhesive is the bonding solution suggested by the carbon fiber supplier for connecting their products to aluminum or other metallic materials. Concerning the carbon fiber supplier, a different provider has been selected for this kind of test, in order to try the friction based riveting technol-

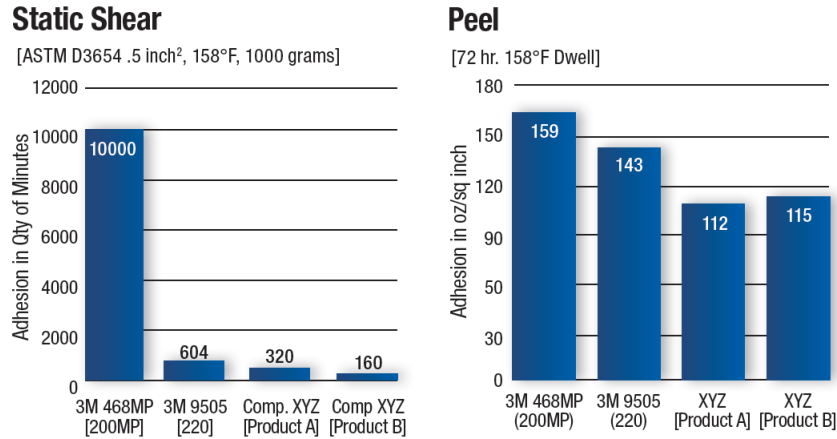


Figure 4.7: 3M 468 MP high performance acrylic adhesive adhesion performances with respect to other products (source 3M)

ogy with different types of composites fabrics. Indeed, in the tests presented so far, the plain wave woven fabric was adopted, while those involving adhesive have been carried out on 6K 2x2 twill carbon fiber composite.

The term 6K refers to the number of carbon filaments per tow, which in this case would be 6000. The tow is a bundle of specific diameter into which fibers are collected. From the tow, the plain or 2x2 twill fabric is obtained. It follows a vacuum infusion process during which the epoxy resin is injected through every filament of the reinforcement fabric

The difference with the composite used up to test number 47 consists in the way in which fibers are oriented in the carbon fiber sheet, namely plain or 2x2 twill. This difference is illustrated in figure 4.8. Moreover, a practical aspect driving the choice of a new composite type is the carbon fiber sheet thickness offered by the new supplier, which is closer to the one of interest for FCA application, being 2.4 mm.

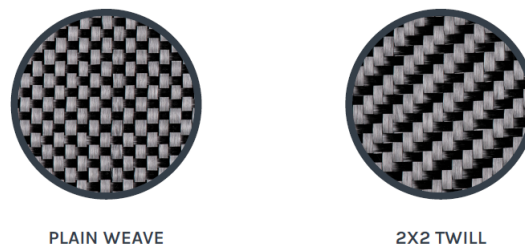


Figure 4.8: Fiber orientation comparison between the two used carbon fiber composites [50]

4.3.4 Study of FSBR application CFRP-CFRP samples

The first experimental campaign has been concluded by riveting two composite layers of 1.3 and 1.7 mm. The reason behind this test is that of applying the FSBR technology to a couple of brittle material sheets and to assess the process effectiveness in this particular condition. The selected carbon fiber was a 6K 2x2 twill composite, on which the 3M

468 MP High-Performance Acrylic Adhesive was applied prior to the riveting process. Once again, this was done trying to get similar joint features with respect to that of riv-bonding technique.

Table 4.6: Test schedule for the study of riv-bonding process for CFRP-CFRP samples

Test number	CFRP layer thickness [mm]	Al layer thickness [mm]	Employed technology	Feed rate [mm/min]	Spindle speed [rpm]
57	1.3	1.7	FSBR + adhesive	50	6500
58	1.3	1.7	FSBR + adhesive	50	6500

The test has been carried out on two samples, both of which presented the thicker composite layer (1.7 mm) at the bottom of the stack. This is what generally happens when a thinner reinforcement component is assembled on a thicker structural element. The riveting parameters choice is so that a lower feed rate, namely 100 mm/min, has been used in order to avoid failure issues in riveting brittle material sheets.

4.4 Process quality and visual inspection

Following the test schedule presented in the previous sections, most of the riveting processes provided sound joints. In some particular conditions, which will be discussed in the following sections, the FSBR method resulted in quality issues due to imperfections in the process setup or parameters. Nevertheless, they can be considered useful in the understanding of the FSBR process limits and critical aspects.

Concerning all the other cases, the installation processes, performed at the presented values of rotational speed and feed rate, resulted to be quite efficient and effective.

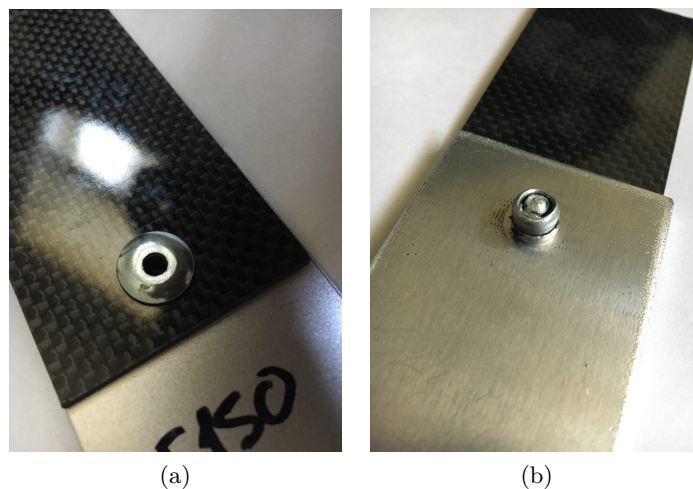


Figure 4.9: Example of sound joint between 0.8 mm CFRP and 3.1 mm Al samples ($f=150$ mm/s $rs=6500$ rpm: a) rivet inlet side b) outlet side

Figure 4.9 shows the inlet and outlet sides of a riveted coupon, which is representative

of the average quality level and features observed on the first batch of samples, namely those with the composite layer on top of the stack. Some particular features can be identified, starting from the proper rivet cap positioning with respect to the carbon fiber sample. Indeed, the feed stopping point was properly calibrated so that to avoid the friction stirring between the fastener head and the top material sheet.

The most interesting features can be noticed by observing the blind side of the connection, where the setting process is responsible for the rivet tail forming. Being FSBR a forming process, the rivet mandrel is not only surrounded by the deformed part of the shank, but also by the material sleeve, which is created during the fastener penetration process. The extension of this material sleeve depends on many factors, such as the material availability and ductility. For instance, figure 4.10 shows the comparison of said material protrusion depending on the bottom material thickness. It is quite easy to understand how the larger is the bottom material layer thickness, the more will be the material available to form the sleeve.



Figure 4.10: *Comparison of formed material sleeves on the connection blind side: a) 1.6 mm CFRP - 1 mm Al b) 0.8 mm CFRP - 3.1 mm Al*

Dealing with the study of the stacking sequence, positive results have been obtained by inverting the sheets order. The visual inspection of almost all the joined coupons provided the results illustrated in figure 4.11. The joint inlet side presents the same features already commented, while the outlet one allows assessing the material flow in the composite layer. The rivet penetration by friction is responsible for a local and unavoidable delamination phenomenon. However, despite its brittleness, the damage on the composite is quite restricted to the circumference around the rivet shank, where the reinforcement fibers have been broken.

In other terms, using friction based riveting method, the delamination does not propagate beyond the rivet surrounding zone, and the broken fibers are still capable to be arranged around the formed rivet tail. It has been noticed how the carbon fiber sleeve was more extended than the aluminum one regardless of the sample thickness and covering almost all the fastener deformed shank.

The second half of the available multi-material samples has been riveted by means a standard pre-drilling operation, in order to have a reference to be compared with the FSBR technology. An interesting evaluation turns out already from the visual analysis of this two different groups of riveted coupons, which are shown in figure 4.12. As already mentioned, FSBR is an almost chip-free process in which the joined material

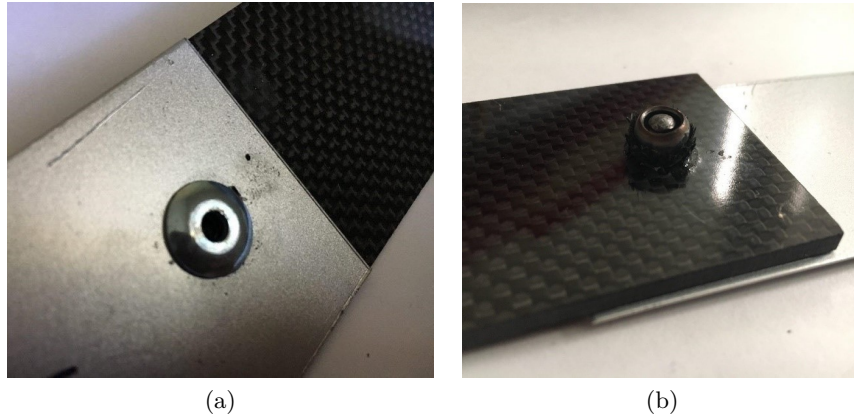


Figure 4.11: *Example of sound joint between 3.17 mm CFRP - 1 mm A6061 samples ($f=150$ mm/s $rs=6500$ rpm: a) inlet face b) outlet face*

is formed by the rivet penetration rather than being cut by the drill bit. This concept is very evident when the blind side of the samples joined with the friction-based and the standard riveting operations are observed. What in the second case gives life to the machining chip, constitutes a material collar in the case of friction riveted coupons, especially when carbon fiber was placed on the bottom of the layers stack. One of the key points of the present analysis will be that of assessing if this material collar around the rivet tail plays a role in the mechanical resistance of the joint.

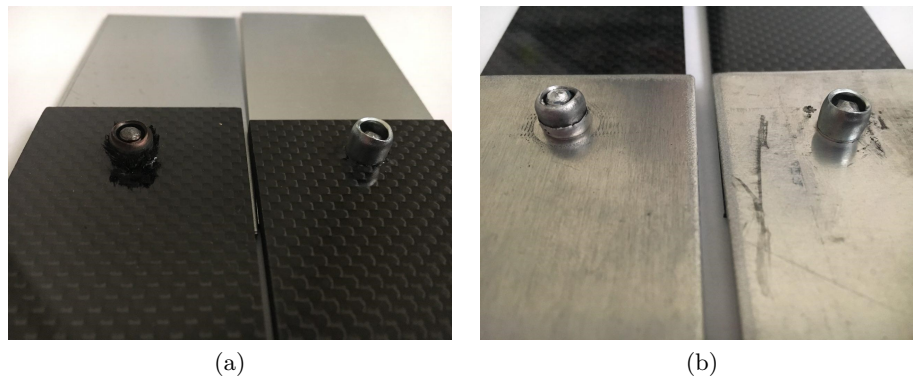


Figure 4.12: *Rivet outlet sections with FSBR technology (left) standard pre-drilling (right): a) 1 mm A6061-3.17 mm CFRP b) 0.8 mm CFRP-3.1 mm A6061*

Concerning the samples joined by means of the riv-bonding technology, no particular differences have been detected during the joining process of the pre-bonded coupons, neither during their visual inspection, meaning that the FSBR technology is fully compatible with the presence of adhesive (as it has been confirmed also by supplier A).

The other category of coupons which has been tested is the composite-to-composite sample, namely the 1.3 mm CFRP - 1.7 mm CFRP. The obtained joint is illustrated in figure 4.13. Once more, when using the FSBR technology, most of reinforcement fibers are fractured just in correspondence of the fastener axis formed a collar surrounding the rivet deformed tail.

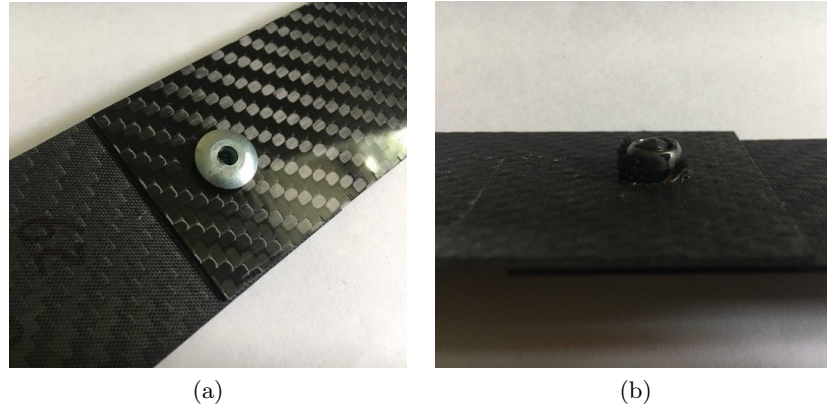


Figure 4.13: *1.3 mm CFRP - 1.7 mm CFRP sample joined by fsbr technology: a) top view b) bottom view*

4.4.1 Process quality issues and criticalities

It is worth to introduce this section concerning quality issues with an important premise. The friction based blind riveting process, despite conceptually simple, involves complex thermomechanical aspects which depend not only on the process parameters, but also on the used materials and setting equipment. In other terms, even if most of the riveted samples provided good results, these tests were not aimed at achieving the same quality level obtained by supplier A, which is offering this riveting technology on a large market scale. Nevertheless, the first campaign of testing activity provided the opportunity to assess potential weak points, limitations and criticalities of the process, being aware that some of them can be or have already been solved by the process optimization carried out by the supplier.

The first observed failure mode was similar to one of those encountered in work [34], in which the rivet mandrel is broken during the rivet frictional penetration. The results of this process failure are illustrated in figure 4.14.

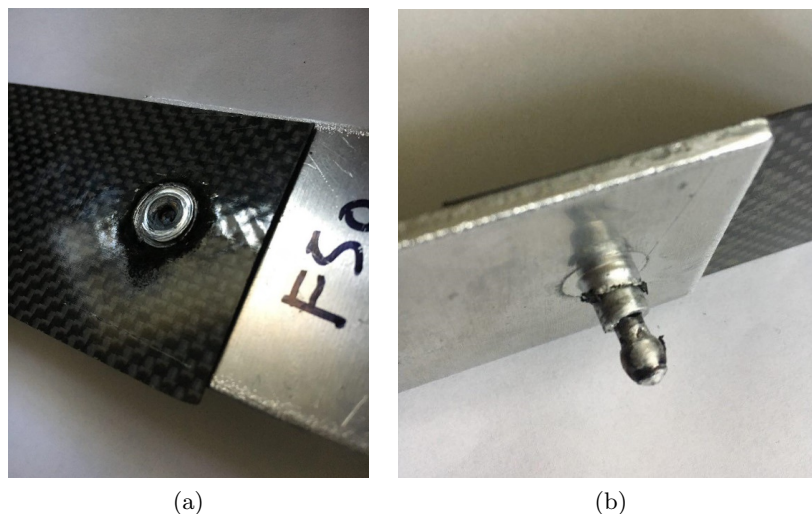


Figure 4.14: *0.8 mm CFRP - 3.1 mm A6061 riveted sample characterized by a quality problem ($f=50$ mm/s, rs 6500 rpm: a) top view b) bottom view*

As it has been mentioned in the description of the process layout, the fastener is connected to the spindle gripper by means of its mandrel. If the resisting torque resulting from the process is too high, the mandrel will unavoidably break in the designed weakened section. Observing the two sides of the failed fastener, it was possible to recognize the cause of the quality problem. Indeed, since the rivet fully penetrated both the composite and aluminum layers, the excess in resisting torque was not due to the penetration of the rivet shank. On the other hand, the damage on the carbon fiber sample testifies a too deep feed motion of the fastener, due to a wrong calibration of the vertical motion stopping point. Consequently, the reaction torque resulting from the rivet head contact with the sample was the cause of the mandrel breakage before the end of the spindle motion. Figure 4.14.b shows also how the mandrel has been pushed down by the CNC machine, while the rivet body was stopped in this motion due to the resistance exerted by the fastener head. This kind of criticality can be addressed to the testing equipment which is not strictly specific for FSBR process application. Indeed, it has been overcome by supplier A which, as it will be discussed, uses an on-line monitoring system which measures the torque and force acting on the fastener. Using these data as a negative feedback, it is possible to control the feed motion and stop it when the rivets get in the proper position, avoiding exceeding the upper thresholds of resistance force or torque.

Another process failure was observed by increasing the thickness of the samples. In particular, joining the 1.6 mm CFRP with the 3.1 mm A6061, the effect of feed rate on the reacting force was evidenced by a rupture of the rivet mandrel and by the fastener overheating. Using a 50 mm/min feed rate, no quality issues have been observed and the samples have been properly riveted. By increasing the linear motion of the fastener up to 100 mm/min, the rivet has been highly damaged, as it can be seen in figure 4.15.

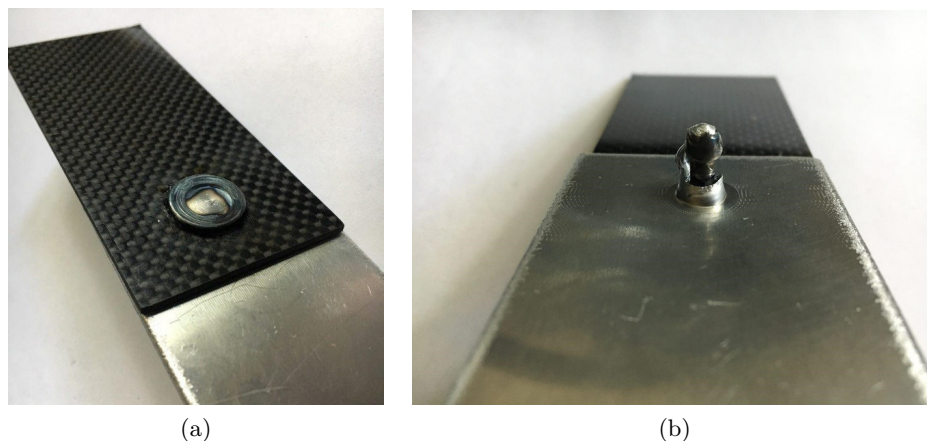


Figure 4.15: 1.6 mm CFRP - 3.1 mm A6061 riveted sample characterized by a quality problem ($f=150$ mm/s, rs 6500 rpm: a) top view b) bottom view

As it can be seen, the rivet mandrel broke during the installation process. Moreover, the rivet head appeared to be significantly flattened by the machine spindle. This phenomenon can be explained by the high resistance that the two thick samples exerted during the penetration. Indeed, comparing the bottom views of figure 4.14 and figure

4.15, it can be noticed how in the first case the rivet shank already penetrated the two layers before the failure occurred (being it caused by the rivet head contact with the sample), while in the second case just the mandrel was pushed through the material whereas the penetration of the shank caused an excessive feed force acting on the rivet. According to what has been evidenced also by work [34], when the feed rate is too high, the reaction force on the rivet exceeds a given threshold above which the spindle gripper (figure 4.4) slides over the mandrel, causing a double effect. First, a reduction of the actual rivet rotational speed which leads to a lower softening effect and increase of the resisting torque. Second, the relative motion between the spindle gripper and the rivet mandrel determines a contact between the rivet head and the spindle itself. Once this contact occurs the gripper-rivet relative rotation causes the frictional heating of the fastener head which, combined with the downforce, flattens the rivet domed hat. Furthermore, the resulting heat, combined with the aforementioned increase of the resisting torque, causes the mandrel breaking. If the process is not stopped immediately, the prolonged friction between the spindle gripper and the rivet head can cause the melting of the rivet mandrel with the fastener hat, as it can be seen in figure 4.15.a. This shows how the typical hole of the blind rivet head has been filled with the melted metal of the mandrel.



Figure 4.16: *1.6 mm CFRP - 3.1 mm A6061 inlet section of the sample after the rivet removal ($f=150$ mm/s, rs 6500 rpm)*

The analysis of the same failed sample has been carried out also by removing the fastener from the material layers. As it can be seen in figure 4.16, once the rivet mandrel started to slide with the fixture, the fastener head touched the spindle and has been deformed and pushed against the carbon fiber layer causing a severe delamination phenomenon, beside a further increase of the reaction torque exerted on the rivet itself.

This quality issue explanation has been confirmed by the failure occurred in the same sample type when riveted at 250 mm/min as feed rate. In this case, the spindle rotation was immediately stopped after the mandrel fracture. It can be noticed how the rivet penetration is even smaller than in the case with 150 mm/min feed rate. In this case the overheating of the rivet caused a partial melting of the fastener itself with the spindle, which was made of mild steel.

A further attempt has been made on the same type of samples (1.6 mm CFRP and 3.1 mm A6061) by increasing the fastener rotational speed up to 8500 rpm and maintaining a feed rate of 150 mm/min. Nevertheless, once more the resistance to the

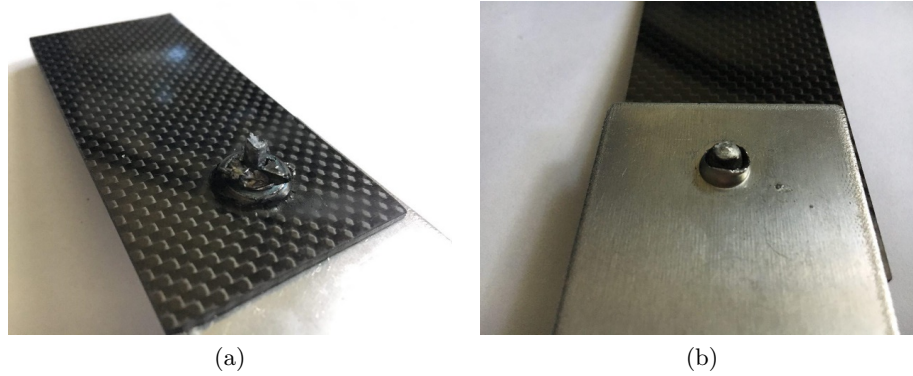


Figure 4.17: 1.6 mm CFRP - 3.1 mm A6061 riveted sample characterized by a quality problem ($f=250$ mm/s, rs 6500 rpm: a) top view b) bottom view

fastener penetration resulted to be too high in relation to the capability of the gripping system to hold the rivet without causing a relative motion. Figure 4.18 shows the side view of the mentioned attempt, in which the CNC machine has been stopped as soon as the axial sliding of the machine spindle with respect to the mandrel has been observed. It can be noticed how this sliding phenomenon occurs when the rivet starts the penetration of the thick aluminum layer, causing a significant increase of the resisting force and moment.

As a consequence of the just described joining issues, the 1.6 mm CFRP - 3.1 A6061 has been considered as the limit case in terms of riveting process feasibility according to the discussed testing conditions. Indeed, just one sample of this type has been correctly joined without causing any quality problem. On the base of this joining effort, some considerations for process improvement can be made:

- The spindle gripper should present a collar capable to increase the grip between the machine and the rivet also when dealing with higher resisting loads.
- The rivet mandrel should present a high friction surface finishing, so that to avoid the axial sliding with the spindle when the vertical resistance force increases.
- The spindle fixture material should be chosen in such a way to present higher hardness and melting point. In this specific case, the spindle was made of mild steel which caused an incipient of melting with the carbon steel rivet when the fastener overheated.
- The rivet should present a mandrel head shape more suitable to the penetration process. For instance, rivets can be featured by a conical shaped mandrel, recalling that of a flow drilling screw, which is basically exploiting the same principle of FSBR.

However, the discussed thickness limitation is not that restrictive if considered in the automotive field of application. Indeed, thick aluminum sheets generally do not exceed 2 mm in thickness for body in white applications. This is confirmed by the choice of

FCA to provide suppliers A and B with aluminum samples of 1 and 2 mm for testing their riveting technology (as it will be discussed in the next chapter).

Moreover, the obtained result in terms of CFRP-Aluminum joinable thickness is still above the results found in literature and in particular by reference [28], in which 3 mm composite layer has been riveted with 0.9 mm aluminum.



Figure 4.18: *Maximum achieved penetration depth for a 1.6 mm CFRP - 3.1 mm A6061 riveted sample characterized by a quality problem ($f=150$ mm/s, rs 8500 rpm)*

In conclusion of this section, it is worth to underline how the advantage of carrying out this experimental activity, replicating the process developed by supplier A, is to have a more complete view of the process itself rather than just analyze the coupons obtained from the supplier. This allows pointing out some potential criticalities not explicitly declared by the technology provider. One of these is the potential hazard and uncomfortable working condition due to the forming of carbon fiber composite. Indeed, if on one hand the friction-based penetration of aluminum does not cause any chip formation or fume release, that of carbon fiber cause the local melting of the epoxy resin, which is related to the generation of fumes and a potential safety hazard when implementing this technology in an intensive industrial production process. Fumes resulting from assembly operations (for instance welding) are quite common in the automotive production context, and are generally tolerated since the vehicle BIW assembly is a machine intensive activity (few operators are close to the automated machines). However, proper ventilation systems and safety countermeasures must be considered for the potential application of FSBR method. For instance, during the testing activity performed at University of Windsor, a vacuum system has been used to get rid of these epoxy fumes, ensuring a safe work environment. In this regard an extract of the material safety data sheet for liquid epoxy is present in the appendix B, in which it is reported the safety hazard of vapors and fumes generated by the heated resin.

Another process aspect which is in contradiction with what declared by supplier A, is concerning the formation of composite chip on the inlet side of the sample (with respect to the riveting direction). Indeed, it is true that FSBR process does not form machining chip like in the case of standard drilling, but this applies just in the case

of ductile materials, such as aluminum. Conversely, when dealing with brittle carbon fiber a visible amount of composite chip is produced, even if less with respect to what observed during standard drilling operation.

4.5 Lap shear methodology

Lap shear (tensile) testing is a method for assessing the strength of lap joints by pulling the layers apart along the plane of adhesion. Shear testing is different from other mechanical material characterization tests, such as tensile and compression ones, since the applied forces are parallel to the upper and lower faces of the tested sample. The mechanical response of materials to shear testing is different with respect to tensile one, particularly in terms of strength and stiffness. Shear testing applies a lateral shear force to the specimen until failure results.

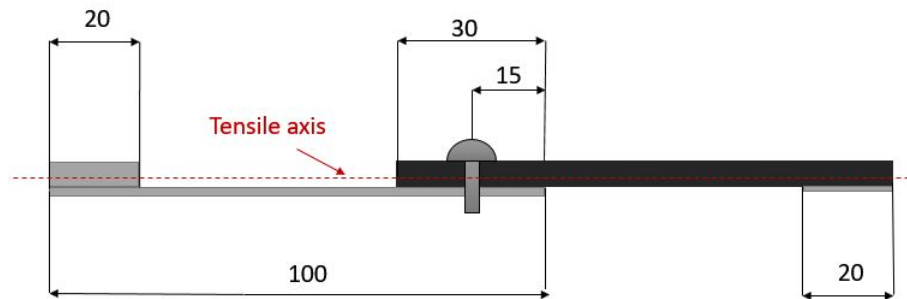


Figure 4.19: *Lap shear test schematic layout*

A crucial aspect of this test is to identify the failure mode and initiation point when pure shear acts on the material layers, namely when the fastener is not subjected to any bending moment. Indeed, by fixing the machine grippers directly on the samples, the pulling action would generate a couple of forces acting on the midplane of each layer and at a certain distance (d) between them. This means that the fastener will be undergoing not only a pure shear load, but also a bending moment equal to $F \cdot d$, being F the tensile force. In other terms, the larger the thicknesses of the involved layers are, the more severe would be the rivet loading condition, making results not really comparable. Moreover, by applying tensile force accurately along the plane gives rise to a configuration minimizing distortion away from the plane. In order to achieve this loading configuration, the tensile forces have to act on the same line. From a practical view point, a couple of spacers with the same thickness of the two samples can be used, so that the forces lie on the same plane and are parallel to the coupons surfaces, as schematized in figure 4.19. Consequently, the tensile axis will be passing through the middle of the layers stack.

In order to avoid the relative sliding between the sample and the spacer, they have been bonded together by means of the 3M 468 MP High-Performance Acrylic Adhesive.

The shear test has been carried out with the MTS Criterion model 43 tensile testing machine, characterized by a fixed lower gripper and an upper moving crosshead equipped

with a load cell. The data acquisition system allowed visualizing and collecting the instantaneous values of applied load and crosshead displacement. In order to catch as many process details as possible, it has been selected a quite low deformation rate corresponding to 1 mm/min. The recorded signal was discretized and acquired using a sampling frequency equal to 10 Hz.



Figure 4.20: *MTS Criterion model 43 tensile testing machine*

4.6 Shear tests results

The shear test results discussion will be provided in the following sections by distinguishing among the multiple investigation targets. An important premise is concerning the overall observed failure modes. Indeed, regardless of the specific typology of samples failure, all of them occurred in a gradual way. This aspect can be considered positive if thinking to the implementation of this joint in the automotive BIW, in which a sudden fracture or joint failure can have catastrophic effects. Before entering into details about the tests results, it is worth to recall the most common failure modes which occur in riveted lap joints.

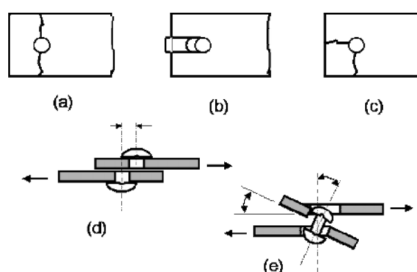


Figure 4.21: *Most common failure modes in riveted lap joints. (a) tensile failure in the riveted material, (b) fastener shear out, (c) cleavage, (d) rivet-shear, (e) pull-out (bearing) [51]*

It can be anticipated that the dominant failure mechanisms for this set of tests have been the rivet shear out and pull out, which are represented in figure 4.21.b and figure

4.21.e respectively. In some cases, also a combination of these two failure modes has been detected.

Rivet pull-out is accompanied by secondary bending phenomena. It is strongly suggested for the reader to go through the description of regular and nonregular secondary bending phenomena, which are described in appendix C.

The occurrence of these different failure modes was observed to be in relation with the breakage nucleation site, material type and thickness.

4.6.1 Thickness factor

This kind of factor has been studied by comparing the force-displacement curves resulting from the lap shear testing of different sample thickness combinations. All the samples discussed in this section have been joined by means of friction-based riveting technology. First, the samples with composite on top of the stack have been considered in figure 4.22.

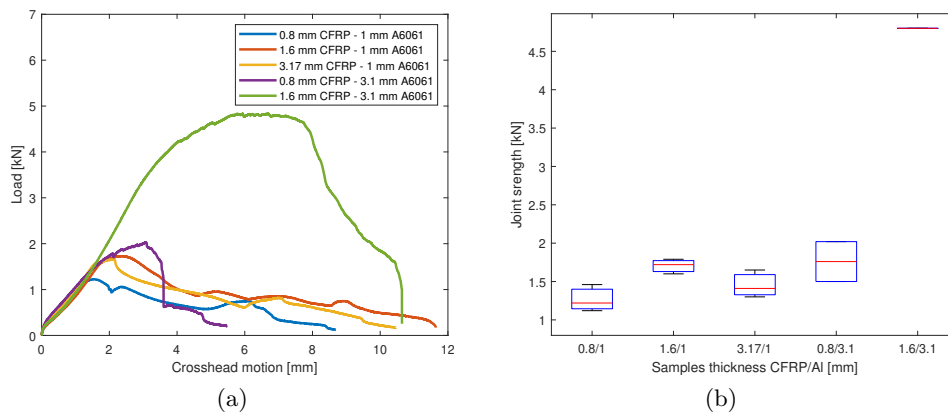


Figure 4.22: a) load-displacement curves b) box plot of the samples joint strength according to different thicknesses (CFRP-A6061)

It can be noticed how the increase of the samples thickness generally leads to higher peak values of loads, namely of joint strength. However, the thickness variation is not just responsible of the joint resistance but also of the observed failure mode. For instance, all the samples with the 1 mm A6061 and represented in the force-displacement diagram presented a failure due to secondary bending and subsequent rivet pull-out (bearing mechanism), while the samples with 3.1 mm A6061 failed because of rivet shear out in the upper CFRP layer. This is reflected in a different trend of the force-displacement curve which, in the case of fastener pull-out, presents a more gradual decrease load during the fastener progressive rotation. Conversely, in the case of rivet shear out in the upper composite layer, the joint resistance has a sharp decrease due to the nucleation and propagation of two cracks in the brittle carbon fiber layer.

Increasing the composite layer thickness leads to a general increase of strength in the samples with 1 mm A6061, since the upper layer becomes stiffer and less prone to rotate, opposing the rivet pull-out phenomenon. In other terms, the increase of the composite

thickness determines a transition from regular to nonregular secondary bending, with a consequent increase of the measured joint strength.

Similarly, in the coupons with 3.1 mm A6061 the increase of the composite thickness (where the failure starts) directly opposes the crack formation and shear out process. Figure 4.23 shows the failure modes observed in the CFRP-Al samples riveted by means of FSBR technique.

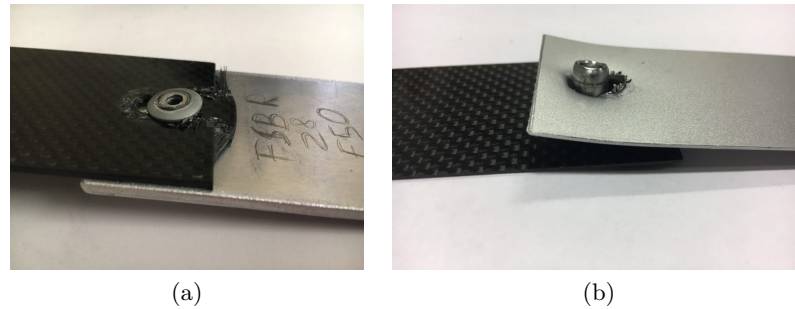


Figure 4.23: Observed failure modes: a) rivet shear out in the top composite layer (1.6 mm CFRP - 3.1 mm A6061) b) secondary bending and fastener pull-out (0.8 mm CFRP - 1 mm A6061)

The second reported diagram (figure 4.22.b) is a box plot in which the peak joint strength of each sample type has been included for each test repetition. The upper and lower sides of the box represent the first and third quartile respectively, while the band inside the box indicates the second quartile, namely the median. Finally, the lines outside the box are called whiskers and provides the maximum and minimum measured values.

With reference to the obtained data, the average joint strength of the 3.17 mm CFRP - 1 mm A6061 resulted to be 14% lower than the 1.6 mm CFRP - 1 mm A6061. The reason is related to the transition from rivet pull-out to aluminum shear-out failure mode which has been observed in the first sample group. Indeed, two of the three 3.17 mm CFRP - 1 mm A6061 samples failed by shear out in the aluminum layer, which occurred at a lower load with respect to the sample failed by rivet pull-out. Finally, concerning the 3.17 mm CFRP - 3.1 mm A6061 sample, just the median is present since only one sample was available to be tested, namely the one riveted at 50 mm/min as feed rate.

The same type of analysis has been carried out on the samples presenting aluminum and composite respectively at the top and at the bottom of the layers stack. With reference to figure 4.24, it appears quite evident how the increase of the composite thickness results in the improvement of the joint mechanical resistance.

Once more, the thickness factor is responsible of a variation in the failure mode of the discussed samples and, consequently, of their load-displacement curves. Indeed, in the 1 mm A6061 - 0.8 mm CFRP the failure occurred in the composite layer through a shear out mechanism. Conversely, with thicker carbon fiber layers, the failure occurred in the aluminum, still by means of a shear out process. In this set of tests, when the rivet shear out took place in the composite layer, the crack propagation close to the fastener

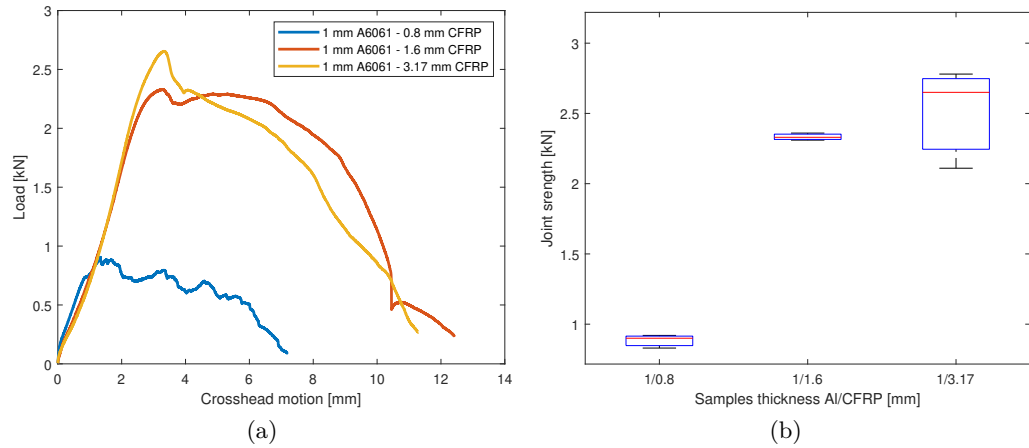


Figure 4.24: a) load-displacement curves b) box plot of the samples joint strength according to different thicknesses (A6061-CFRP)

head was slow and progressive. This is proven by the trend of the force-displacement curves, which presented waviness due to the progressive breakage of the reinforcement fibers. Considering the box plot, quite consistent measurements have been obtained for the joints strength, especially in the case of samples with 0.8 mm and 1.6 mm CFRP layers. A larger variability has been observed in the case of the thickest samples of this set, which presented a variation of about 0.6 kN between the maximum and the minimum recorded strength. However, the median value resulted to be the highest of the discussed samples set. The two failure modes observed during the testing of Al-CFRP samples are represented in figure 4.25.

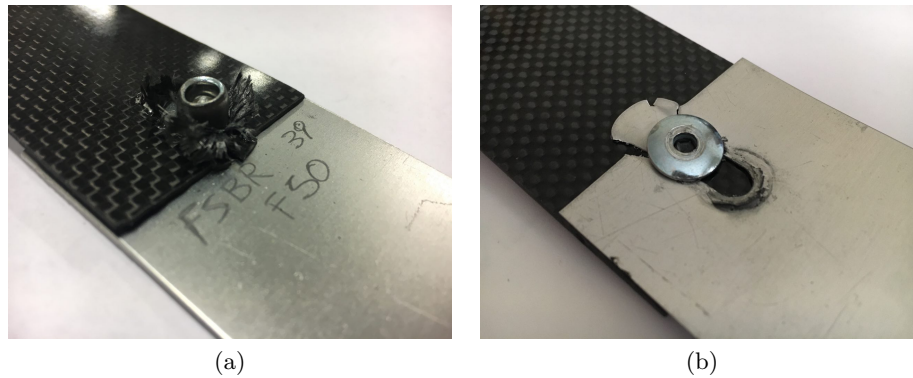


Figure 4.25: a) Rivet shear out in the bottom CFRP layer (1 mm a6061 - 0.8 mm CFRP) b) Rivet shear out in the top aluminum layer (1 mm A6061 - 1.6 mm CFRP)

4.6.2 Riveting technology factor: comparison between FSBR and hole pre-drilling methods

One of the main targets of the first experimental investigation consists in assessing if the FSBR method provides, besides a more efficient process, a joint mechanical performance improvement with respect to the standard methodology. This analysis has been carried out by distinguishing the cases with different stacking orders, namely CFRP-A6061

and A6061-CRFP. Starting from the former, the force-displacement curves comparing the two technologies are represented in figure 4.26. For sake of clarity, two graphs are shown separating the samples with 1 mm and 3.1 mm aluminum, which presented quite different values of involved forces. As it will be discussed in the following, this distinction involves also the effects of friction-based riveting method, failure mode and location in the sample.

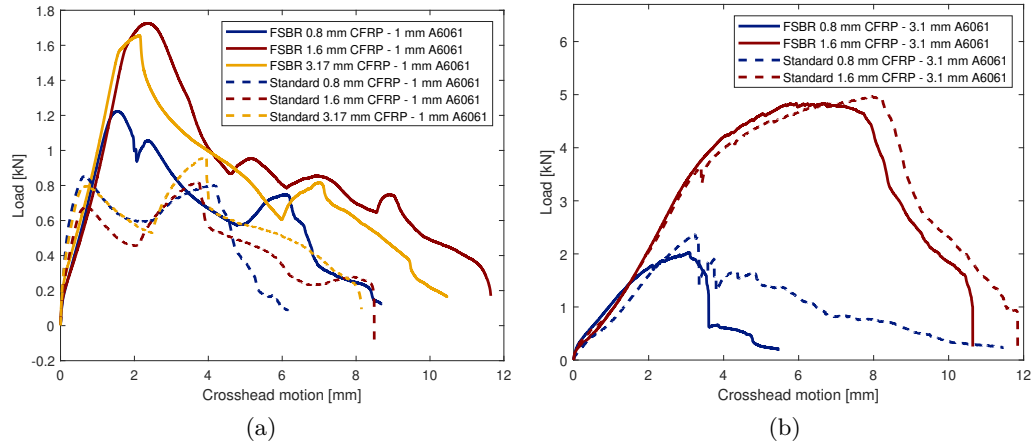


Figure 4.26: Force-displacement diagrams comparing FSBR and conventional riveting technology for the CFRP/Al stacking sequence: a) samples with 1 mm A6061 b) samples with 3.1 mm A6061

With reference to the tests illustrated in figure 4.26.a, the dominant failure mode has been the initial rivet shear out followed by the fastener pull-out. Only the 3.17 mm CFRP - 1 mm A6061 presented the pure fastener shear out as the main failure mechanism. However, both failure types have been observed in the aluminum layer.

It is interesting to notice how all these samples riveted by means of FSBR technology presented a higher value of joint strength with respect to the reference case (rivet inserted in the pre-drilled hole). The main explanation for this effect is related to the formation of an aluminum sleeve around the rivet tail. This element helps to better distribute the load when the riveted layers are pulled apart, and also plays a role in the amount of shear out that is observed before the rivet pull out. This concept is well described in figure 4.27 in which it can be seen how the two samples joined through friction-based riveting experienced a more significant fastener shear out with respect to the reference case. Indeed, the rivets of samples number 4 and 5 are closer to the edge when the final pull-out occurs. This means that the material sleeve helps the rivet to resist the pull out up to when the aluminum around the hole is deformed enough (through a shear out mechanism) to let the fastener being pulled out. This confirms that when the failure takes place in the aluminum layer, the FSBR technique provides a beneficial effect on the resulting joint strength.

Concerning the second group of tested samples, namely those presenting a 3.1 mm aluminum layer on the bottom of the stack, a different result has been obtained, as it can be seen in figure 4.26.b. Indeed, comparing the FSBR technology with the standard one, the mechanical properties evidenced by the shear test are quite close for the two



Figure 4.27: Comparison between failed samples joined by means of FSBR (4 and 5) and reference samples (1 and 2)

techniques. The reason is that all the samples belonging to this group presented a failure on the composite layer (whether it was the 0.8 or the 1.6 mm thick one), which resulted to be weaker than the 3.1 mm aluminum sample. The failure is illustrated in figure 4.28.a. Being this mechanism not related to the aluminum or, more in general, to the lower layer, no improvements are provided by the friction-based technology. Conversely, slightly higher joint strength has been observed by employing the conventional riveting procedure. A possible explanation can be formulated by analyzing the failed coupons in figure 4.28.b. By looking at the surface of the composite in the region beneath the rivet head, the material resulted to be damaged by the contact with the rotating rivet during the installation process. This damage is instead not present in the pre-drilled sample and can be considered as the discriminant factor determining the small difference in strength between the samples riveted with the two technologies. Indeed, the damaged area of the composite can represent an easier nucleation site for the cracks developing from the hole.



Figure 4.28: a) Composite layer shear out failure in samples joined with standard drilling (left) and FSBR (right) (0.8 mm CFRP-3.1 mm A6061) b) Composite surface damage under the rivet cap due to the fastener stir action (1.6 mm CFRP - 3.1 mm A6061)

The problem of upper layer damage when the rivet touches the sample is due to the riveting process setup. With a more advanced installation system, equipped with reaction force, torque sensors and specifically designed for the friction-based installation

of rivets, this problem can be easily avoided. This is the reason why no evidence of composite damage has been found on the samples provided by supplier A.

All the results concerning the effect of the FSBR technology for CFRP - Al samples are summed up in the bar chart in figure 4.29.

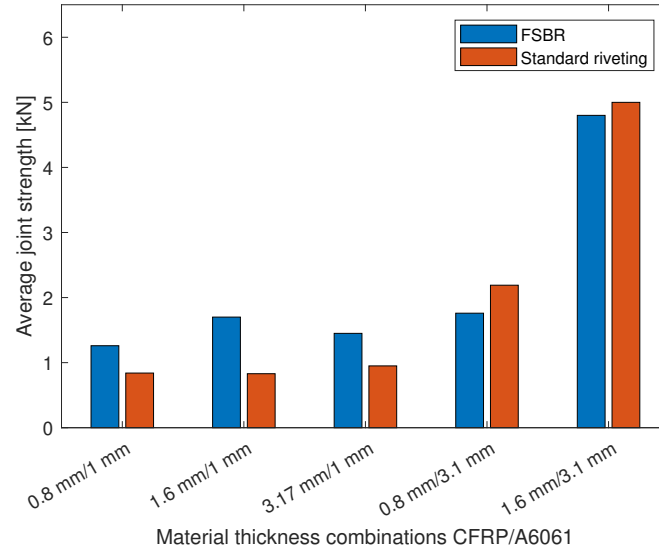


Figure 4.29: Bar chart comparing FSBR and conventional riveting technology

The chart reports, for each sample type and employed technology, the mean of the measured joint strength. In conclusion FSBR technology provided a 50%, 105% and 53% gain for the 0.8 mm CFRP - 1 mm A6061, 1.6 mm CFRP - 1 mm A6061 and the 3.17 mm CFRP - 1 mm A6061 samples respectively. On the other hand, the friction-based riveting method determined a loss of joint resistance equal to 25% and 4% with respect to the reference case for the 0.8 mm CFRP - 3.1 mm A6061 and the 1.6 mm CFRP - 3.1 mm A6061 samples respectively.

The same kind of analysis and tests have been performed on the samples resulting from the inversion of composite and aluminum in the coupons stacking sequence.

Once more, the comparison between the FSBR standard riveting performance is depending on the materials thickness combinations. The dominant failure mode was the rivet shear out which occurred in the upper or lower level depending on the involved thicknesses and employed joining technology. Figure 4.30 shows the force-displacement diagrams resulting from the shear tests and the bar chart with the joint strength comparison.

The first interesting consideration is related the failure modes observed in the 1 mm A6061 - 0.8 mm CFRP, which resulted to be dependent on the employed technology. Indeed, using the friction based riveting method, the shear out failure has been observed in the composite layer on the bottom. On the contrary, the conventionally riveted samples still presented a shear out failure, but in the upper layer, namely the aluminum one. This failure mode variation is also reflected in the difference between the two technologies in terms of obtained joint strength. The peak value of joint resistance for friction-riveted samples has been found to be 29 % lower with respect to those employing

a conventional riveting technology. The explanation for this difference in strength and failure mode is related to the composite layer damage induced by the rivet penetration. Indeed, it has been mentioned how a material protrusion is formed also on the composite layer when it is placed at the bottom of the stack and FSBR is used (figure 4.10.b). Many sources available in literature support the hypothesis that this collar made of fibers is increasing the riveted joint strength, like it happens in the just discussed case with aluminum on the bottom of the stack. Nevertheless, the tests carried out on the 1 mm A6061 - 0.8 mm CFRP provided a different result. Rather than showing a failure in the upper aluminum layer, like it happened in the reference coupons, the rivet shear out took place in the composite, which is supposed to be more resistant than the metallic layer, given the similar thicknesses.

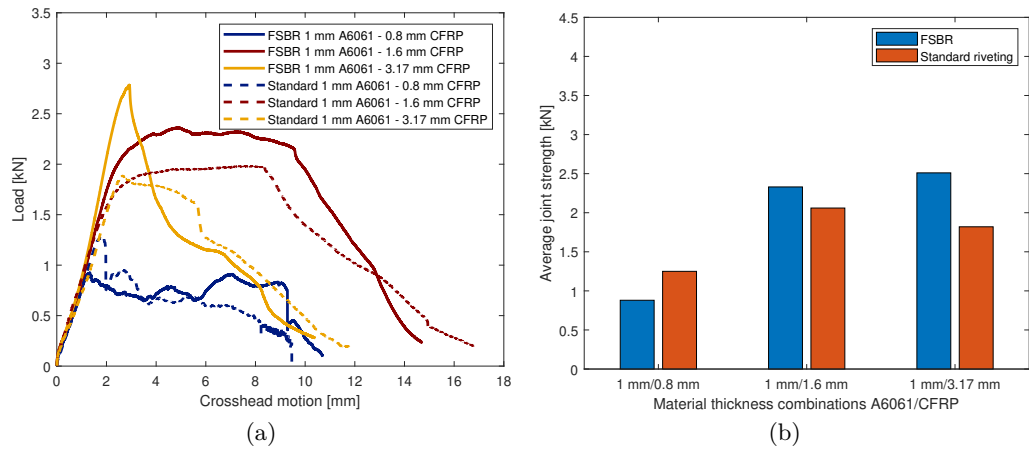


Figure 4.30: Comparison between FSBR and conventional riveting for the Al/CFRP stacking sequence: a) Force-displacement diagram b) bar chart

The reason is that the small delamination of fibers close to the rivet hole weakened the composite and encouraged the initiation of a slow and gradual shear out of the carbon fiber, as it has already been shown in figure 4.25.a.

Concerning instead the other two types of samples, namely the 1 mm A6061 - 1.6 mm CFRP and 1 mm A6061 - 3.17 mm CFRP, the composite thickness was so that the failure was always localized in the aluminum layer. In these cases, in comparison with the standard riveting technology, the friction-based technique provided an average joint strength gain of 13% and 38% for the samples with 1.6 mm and 3.17 mm CFRP respectively. The explanation for that can be reconducted to the interaction between the rivet and the aluminum layer, where the failure occurred. As mentioned in the literature review of previous experiments with FSBR, it has been proven the occurrence of a grain refinement phenomenon in the aluminum layer and close to the rivet hole. This is responsible of the hardness increase as well, which contributes to rise the material resistance to the fastener shear out. Moreover, work [29] hypotized the possible presence of a rivet/workpiece bonding interaction due to the heat generated during the penetration process. Indeed, figure 4.31.a shows how the sample on the left (riveted by frictional penetration) presented an interaction between the aluminum layer and the

fastener which, when reaching high temperatures, create a sort of weak welding between them. It results a stronger joint when the failure tends to occur in the aluminum layer.

Another consideration is related to the force displacement curve of the 1 mm A6061 - 3.17 mm CFRP coupons shear test, which presented a much sharper force decrease after the load peak. The reason is due to the observed failure mode, which turned out to be different with respect to the shear out observed in the other samples. This failure mode is still illustrated in figure 4.31.b, in which it can be seen how, after a partial shear out, two cracks propagated from the rivet hole up to almost reaching the aluminum layer edge. The nucleation of these cracks was followed by their propagation at 45° with respect to the shear direction, which led to a sharp decrease of the recorded load.

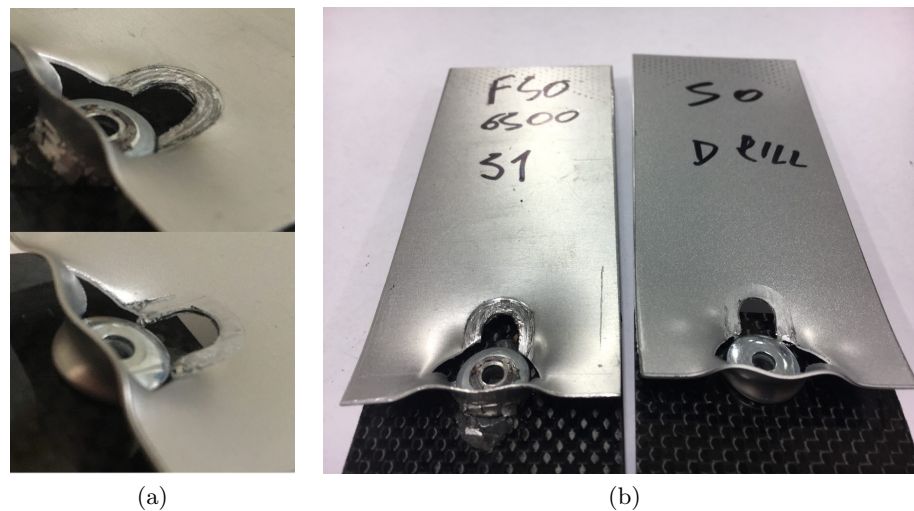


Figure 4.31: a) Detail of the rivet-aluminum interface in the sample joined with FSBR (up) and with conventional riveting (down) b) Failure by cracks propagation at 45° with respect to the sample edge for samples riveted with FSBR (left) and conventional methods (right)

Concluding this section on the analysis of the riveting technology effect on the joint mechanical properties, it is worth to provide few remarks. Considering the stacking sequence with composite on top, which represents the one with the highest applicability in the automotive industry, the FSBR technology provided an overall similar or better result with respect to the reference technique. Possible improvement concerns the avoidance of the contact between the upper composite layer and the rotating rivet. When the stacking sequence was reverted, friction-based riveting still provided better mechanical properties, but in the case with very thin composite layer, which tended to be weakened by the frictional penetration close to the rivet hole.

4.6.3 Analysis of feed rate effect

Another target of the present analysis is that of evaluating the potential effect of the rivet feed rate during its penetration through the material layers. Three values of feed rate have been tested for each type of riveted coupon, namely 50, 150 and 250 mm/min. The overall result was essentially in agreement with what presented in work [29], that is no significant variation of the joint mechanical properties has been observed as a result

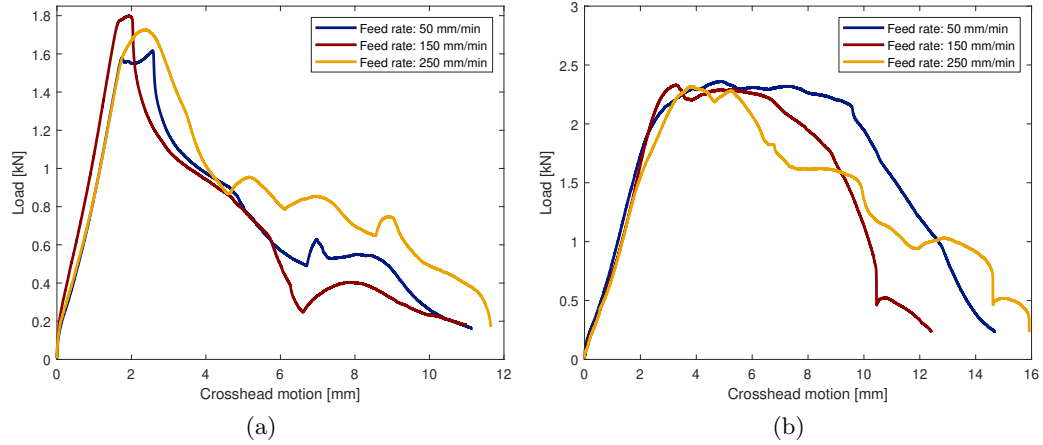


Figure 4.32: Feed rate effect on 1.6 mm composite - 0.8 mm aluminum: a) CFRP-A6061 b) A6061-CFRP

of the feed rate modification. This aspect can be confirmed by the force displacement diagrams in figure 4.32, comparing the mechanical behavior, at the three employed fastener penetration speeds, of 1.6 CFRP - 1 mm A6061. Both the two possible stacking sequences have been considered.

Moreover, when a more evident difference has been noticed between samples riveted at different feed rates, this effect has been found to be not systematic, but due to the intrinsic process variability. However, this variability resulted to be more significant for the samples joined by means of friction-based riveting than in the reference ones. Moreover, this variability, measured in terms of standard deviation, resulted to be generally increasing with the increase of the samples thickness.

4.6.4 Study of the stacking sequence effect

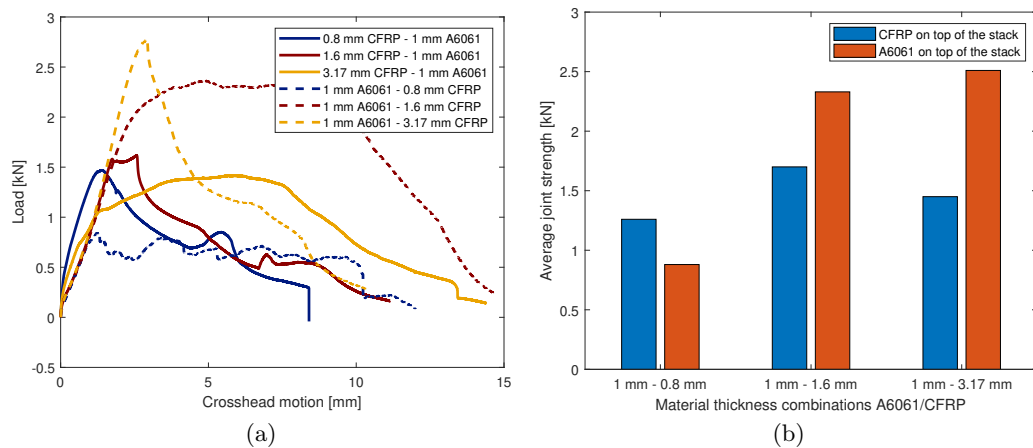


Figure 4.33: Joint strength comparison in relation to the stacking sequence: a) Force-displacement diagram b) Bar chart

The stacking sequence effect has been analyzed in this section considering 1 mm A6061 and three different thicknesses of carbon fiber layers. Figure 4.33 presents the

comparison between couples of samples constituted by the same material layers but arranged in two different stacking orders.

With reference to the given data, a common trend can be detected consisting in the increase of joint strength when the composite is positioned on the bottom of the stack. The only exception to this phenomenon is represented by the thinnest sample, namely the 0.8 mm CFRP - 1 mm A6061, for which the highest joint strength is obtained when the aluminum layer is placed below the composite (with respect to the riveting direction). The reason is that, as already mentioned, when a thin composite layer is placed at the bottom, the frictional penetration of the rivet weakens this layer providing an incipient to the shear out of the fastener when loaded. Conversely, when the same composite layer is on top of the stack, the sample failure occurs by means of a rivet pull out mechanism, which is mainly due to the bending of aluminum (the composite did not present any damage).

Considering all the other samples, characterized by a thicker and less delicate composite layer, the failure has been always localized in the aluminum layer. Those with carbon fiber on top failed because of rivet pull-out, while those with aluminum on top failed because of rivet shear out in the upper layer. The second group of samples provided higher values of strength since the composite, and so the more resistant layer, was placed in the weakest position for a riveted joint. Indeed, as mentioned in the previous sections, the lower layer is the one presenting the highest stress concentration during the joint loading, while the upper one exploits the wide rivet head to better distribute the load. Consequently, moving the carbon layer to the stack bottom moves also the failure site from the bottom to the upper layer, where a higher force is required to cause the final breakage. Figure 4.34 provides a similar information of the bar chart but including also the observed variability range for each measurement.

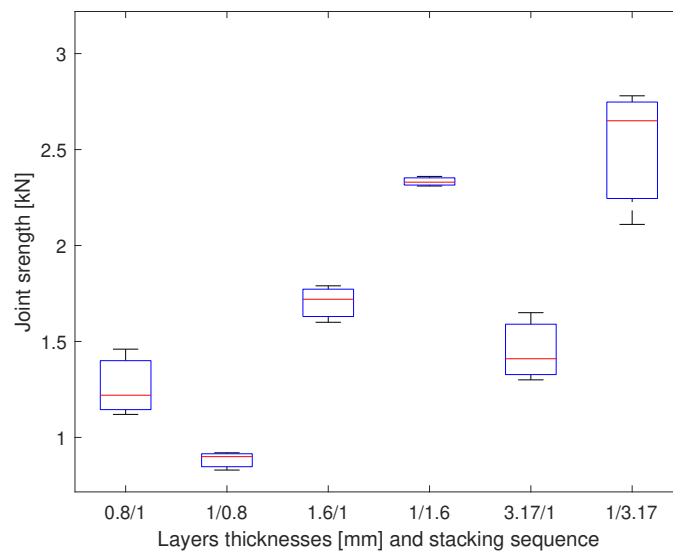


Figure 4.34: *Box plot representing the samples joint strength according to thickness and stacking order (0.8 mm, 1.6 mm and 3.17 mm refer to CFRP samples thicknesses. 1 mm refers to A6061 samples thickness)*

4.6.5 Shear tests on riv-bonded samples

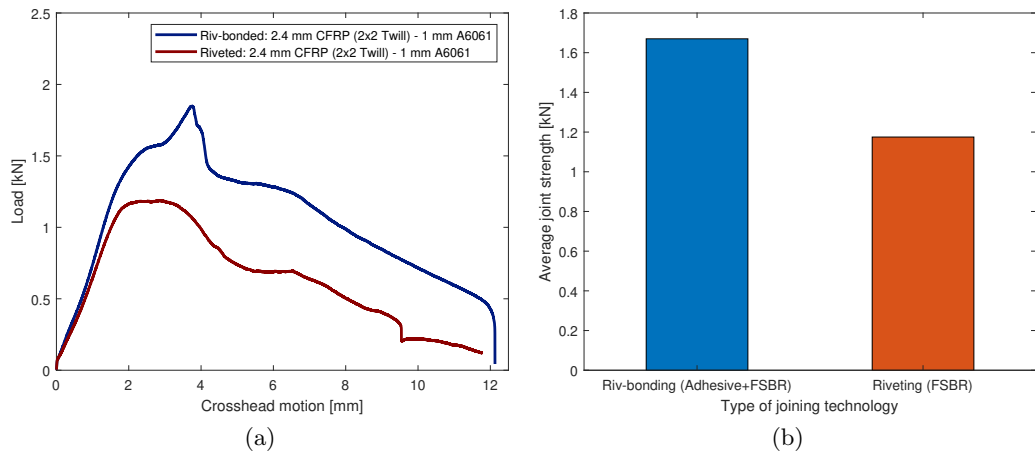


Figure 4.35: Comparison between riv-bonding and riveting techniques: a) Force-displacement curves b) Bar chart

The second part of this sets of tests is concerning the evaluation of the FSBR method compatibility with the presence of adhesive, constituting the hybrid joint referred as riv-bonding. As mentioned in the sections related to the process feasibility, the friction-based riveting resulted to give good process and visual results. From the mechanical viewpoint, the advantage of riv-bonding with respect to simple riveting has been confirmed by the resulting joint strength. The data presented in figure 4.35 confirm how the hybrid joining technology allows achieving a joint strength gain of about 42% with respect to the simple riveting (still performed using the FSBR method).

All the investigated samples failed because of the fastener shear out in the aluminum layer. The adhesive always resisted the shear load together with the rivet and, after the final failure of the riveted connection, the aluminum and composite layers resulted to be still partially bonded. The observed failure mode is shown in figure 4.36.a.

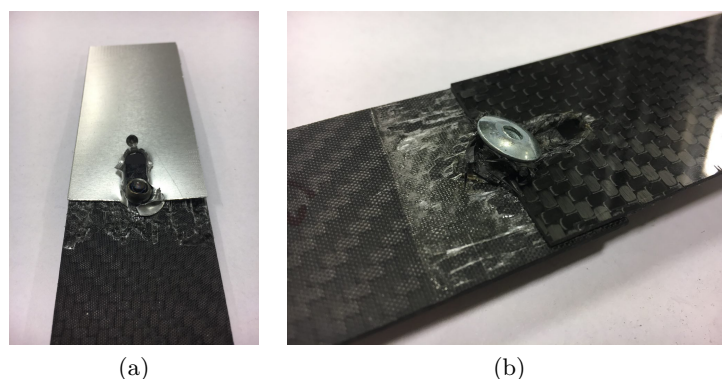


Figure 4.36: Riv-bonded sample shear out failure: a) 2.4 mm CFRP-1 mm A6061 b) 1.3 mm CFRP-1.7 mm CFRP

Finally, the shear testing activity has been focused on the CFRP-CFRP samples riveted by means of the FSBR method. Also in this case, the riv-bonding hybrid joining

technology has been used. The two composite samples have been joined in such a way to have the thicker layer (1.7 mm) below the thinner one (1.3 mm), so that to achieve a higher joint resistance. This resulted to be equal to 1.5 kN. The failure, which is illustrated in figure 4.36.b, turned out to be a mix between rivet pull-out and shear out, since the fastener rotated before breaking the composite layer up to the sample edge. It occurred in the upper layer, namely the thinner one. Indeed, despite the difference in thickness was quite moderated, a small fraction of millimeter can determine a significant strength variation when dealing with carbon fiber composites.

4.7 Conclusions on the first experimental campaign

Concluding this chapter on the first set of tests, it is worth to recap the main concepts and aspects that have been assessed. Concerning the multi-material connection between aluminum and carbon fiber, the friction based riveting technology provided significantly better results with respect to the standard methodology. Nevertheless, two important exceptions to this general trend have to be pointed out.

When a really thin composite layer is placed on the bottom of the stack and below a thicker aluminum sheet, the risk of damaging it during the rivet frictional penetration is higher. This phenomenon can lead to a serious worsening of the friction-riveted joint strength with respect to what achievable with the reference and standard method. This reduction reached a maximum of 29% with respect to conventional riveting

The second remark is concerning the possible damage that can be caused by the rotating rivet head when it enters in contact with the composite layer (when this is placed on top of the stack). In this case the joint strength reduction was much less significant, being in average around 15%.

However, both the two mentioned process criticalities can be easily overcome if thinking that carbon fiber is not placed below aluminum in automotive applications, since the vehicle BIW is generally made of aluminum while the composite sheet or component represents a reinforcement located on top of the main body. Moreover, the problem of the rivet head-upper layer contact can be easily avoided with the design of a specific equipment for the FSBR process, which works according to a force and torque feedback system. This means that the system (developed by supplier A) is capable to detect when the rivet penetration has been completed and to slow down the rotation to avoid the damage of the upper metal or composite layer when it touches the fastener head.

On the bases of what was said, being that the FSBR technology is already better than the conventional one from a process viewpoint, its application in automotive and other production industries can be potentially really successful. Indeed, it is not only capable to reduce the process cycle time, get rid of the hole location function (necessary for standard riveting automated equipment) and solve many tolerance chain aspects, but it also provides an increase of strength per joined spot. This means that, in order to get the same overall stiffness of the connected structures, a lower number of rivets is

necessary, saving installation time and also weight.

Still, the discussed technology needs to go through the FCA validation process, with particular focus on the technology and fastener type provided by supplier A. The following chapters will be devoted to the supplier product validation aspects and to compare the friction-based technology with the robotized one (developed by supplier B). Indeed, it is true that using the same rivet, the FSBR technique provides a mechanical strength improvement, but the two different suppliers involved in this research employ also different kind of fasteners, according to the process features and specific application. Consequently, the final validation process will take into account also this and other aspects.

Chapter 5

Test methodology and experimental evaluation of supplier A process feasibility and joint quality

5.1 Suppliers validation process

Chapters 5 and 6 describe the suppliers quality evaluation process. This is aimed at analyzing the potential implementation of their technology in the FCA production process. The main company target is that of assessing whether friction-based and robotized riveting (the actual commercial names are not disclosed in this thesis) can be successfully adopted with the combinations of material requested by the carmaker and if the two processes are compliant with FCA requirements in terms of automation level and flexibility.

It is worth to remark how most of the experimental work reported in this thesis is concerning mainly with the characterization of the obtained joints. Nevertheless, this study is based on an investigation of industrial interest with commercial and process validation aspects that went beyond the final joint quality validation. Indeed, the supplier development and qualification activities, carried out in the automotive industry, are quite complex and require long periods of information exchanges and parallel processes development before the definition of a nondisclosure agreement between the carmaker and the supplier itself. In other terms, the experimental activity which will be presented in the following, is just the result of a long cooperation with suppliers A and B, concerning technical aspects (rivet choice, type of coating, process parameters definition) and logistics-managerial considerations (sub-suppliers choices, definition of nondisclosure agreements and material flow issues) which are not explicitly matter of the present work, despite being the core of the actual work done when dealing with suppliers technologies validation.

From a strictly experimental viewpoint, the carmaker policy is that of carrying out

a set of mechanical characterization tests which allow developing a database of all the studied joining solutions for dissimilar materials. In this case, the study of the two investigated technologies has been carried out on three material types and two different combinations. All of them have been selected in relation to the technical requirements of the company and to their application needs. The involved materials are:

- Carbon fiber reinforced composite
- 6016 Aluminum alloy
- 6160 Aluminum alloy

The composite material is representative of the actual carbon fiber which will be used in FCA production process as a reinforcement in the aluminum BIW of the group premium brands vehicles. Similarly, the choice of these specific aluminum alloys is strictly related to the design choice of FCA engineers and aimed at ensuring the proper structural stiffness to the vehicles body. Both carbon fiber and aluminum samples for these tests have been provided by the FCA group.

The presented experimental analysis of the technology developed by the two suppliers consists of three types of test, which are:

- Shear tests
- Corrosion tests
- Macrographic analyses

The standards followed for these tests will be discussed in the methodology section.

5.2 Methodology

5.2.1 Samples geometry and materials

Tensile, corrosion tests and macrographic analyses have been carried out on the same sample geometry, shown in figure 5.1.

It can be noticed how, differently from the first experimental campaign, this sample geometry presents two closely spaced fasteners. This allows verifying the interaction between multiple rivets and to assess if the minimum spacing achievable with the examined technology is compliant with FCA requirements. The sample geometry has been provided to both supplier A and B, together with the material to be riveted. The following material sheets have been made available for each supplier:

- 40 layers of carbon fiber composite (2.7 mm thick)
- 20 layers of A6060-T4 (1.0 mm thick)
- 20 layers of A6061-T4 (2.0 mm thick)

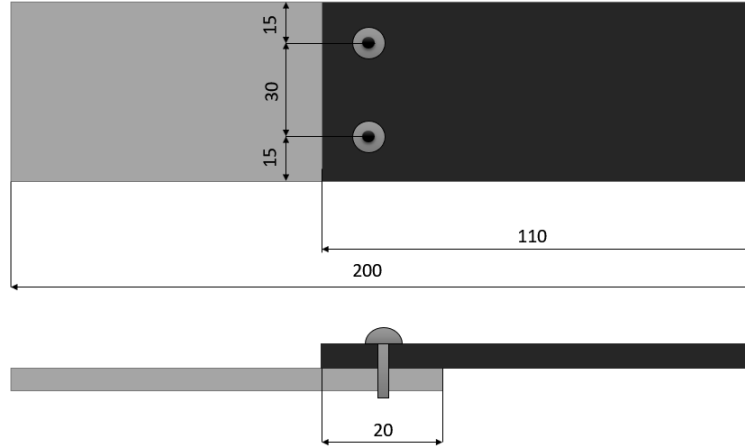


Figure 5.1: *Geometry of the samples provided by the OEM*

In such a way to receive the following riveted coupons:

- 20 CFRP - A6060-T4 samples
- 20 CFRP - A6061-T4 samples

Concerning the involved material, the carbon fiber provided by FCA is a new composite design, whose features will not be disclosed in this thesis because of confidentiality reasons. Concerning the aluminum samples, commercial alloys have been employed, which are quite common in the automotive production field.

Table 5.1: A6061 and A6060 mechanical properties

Aluminum alloys comparison	6016	6060
Young Modulus [Gpa]	69	68
Elongation percentage	27	16
Fatigue strength [MPa]	68	37
Ultimate tensile strength (UTS)	200	140
Yield Strength	110	71
Resilience (unit rupture work) [MJ/m ³]	47	19
Strength to Axial	29	22

What distinguishes the two alloys from the percentage composition viewpoint is the silicon content, which ranges between 1 to 1.5 and 0.3 to 0.6 in A6016 and A6060 respectively. A summary and comparison between the two alloys mechanical properties can be seen in table 5.1. Both the alloys underwent a T4 heat treatment, that means a strengthening mechanism of solution heat treatment, followed by natural aging in stable conditions. Unlike artificial aging, performed at elevated temperatures, natural aging takes place at room temperature.

The mechanical properties of A6016 alloy are clearly better than the A6060 ones and that is why its use in structural applications generally allows employing thinner sheets with respect to the A6060 alloy. This is why A6016 samples are thinner than the A6060 ones.

5.2.2 Lap shear tests

The first validation test is the tensile one, which has been carried out by following a modified version of the UNI EN ISO6892-1 [52] norm. The reasons for the modification are mainly related to the coupon geometry. In order to strictly follow said norm, the sample should present a reduced width section where the extensometer should be placed. Consequently, the displacement has been measured simply as the travel of the machine moving crosshead. In order to have a quite high statistic reliability, five coupons have been tested for each material combination.

A 400 kN Galdabini axial load cell has been employed as well as a Galdabini dynamometer (model SUN40).

5.2.3 Corrosion test

Corrosion is probably the main concern when dealing with multi-material connections, due to the galvanic reactions of dissimilar materials.

In the investigated joint type, three different materials are in contact in the joint, namely carbon fiber, aluminum and the rivet made of steel. Concerning aluminum alloys, they are extremely vulnerable when in contact with carbon fiber reinforced composites, especially in presence of salted vapors. The result of galvanic corrosion is the formation of a white and jelly product on the aluminum surface.

Similar considerations can be done for the steel contact with carbon fiber and aluminum. This is the reason why galvanic insulators are generally inserted in between these dissimilar materials. As already mentioned, the final purpose of the blind riveting evaluation process is to identify the best and more efficient installation technique between FSBR and the robotized system before integrating it with the structural adhesive, getting the so-called riv-bonding technique. The presence of the adhesive will allow a significant mitigation of the galvanic corrosion effect, exploiting the bond as an insulating factor for most of the composite and aluminum overlapping surfaces. Consequently, the real focus of this corrosion test is to understand the oxidation phenomenon which develops from the steel rivet to the samples, while galvanic corrosion is expected to be solved with the future adhesive application.

This is the reason why the corrosion test can reveal potential differences between the set of samples coming from supplier A and B, particularly for what concerns fastener resistance to the oxidation process. In other terms, it will be evaluated the effect of the zinc coating choice made by the two suppliers and its effectiveness during the test.

However, it is worth to remember how the study of multi-material joining technology is a quite recent field of investigation. Indeed, most of the evaluation methodologies do not present a well-known standard, as in the case of corrosion testing and the correspondent result evaluation. The corrosion test performed in the present study is based on an internal standard of FCA originally used to determine the resistance of organic coatings to the propagation of bubble under skin corrosion. This test is called SCAB20 or SCAB60 depending on the exposure time of the samples to the corroding agent,

namely the salt vapor. The test is based on a cycle which is repeated several times up to reaching the designated time duration. Two samples per material combination have been used for this kind of test.

Table 5.2: Corrosion test cycle

Cycle parameters	Cycle stages	
	Humid stage	Drying stage
Sodium chloride concentration	0.5%	-
Spray pressure of the saline solution	0.6 - 1 bar	-
Ph value of the saline solution	6.0 - 6.5	-
Stage duration	60 min	40 min
Temperature inside the test chamber	55 ± 2 °C	
Relative humidity of the test chamber	90 - 95%	55 - 60%

Table 5.2 shows the features of the test unit cycle, characterized by a humid and drying stage. The latter is furtherly consisting of the following two stages:

- 20 min necessary for the equipment to reach the relative humidity percentage required
- 20 min in the required relative humidity conditions.

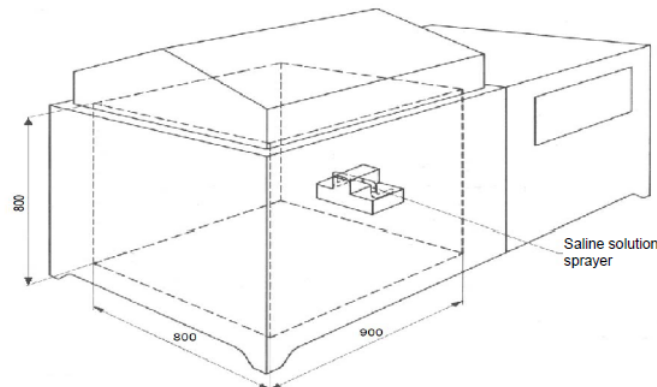


Figure 5.2: Schematic representation of the corrosion test chamber

The procedure consists in placing the samples in the test chamber (sketched in figure 5.2) and start the test cycle with the humid stage by using a nozzle to diffuse the saline solution in the chamber. The drying stage is obtained by hot air diffusion in the testing environment.

5.2.4 Macrographic examination

Macrographic analysis of the joint has been carried out following another internal standard of the manufacturer. The aim of this examination is to define the quality/acceptability of the mechanical joint and to determine the presence of internal faults.

The procedure consists of sectioning the sample on the axis passing through the center of the rivet. The sectioned surface is then polished, taking care to completely

remove tool marks and scoring. It follows the sample observation under a magnification higher or equal to 5X and in lighting conditions higher than 100 lux. The section observation should lead to the definition of key parameters and dimensions of the rivet-material interface, which can be compared with the requirements and limits of the fastener provider. Concerning the involved samples, one coupon per type has been sectioned and observed. Being each sample characterized by two rivets, it has been possible to perform two observations per joint type.

5.3 Supplier A process features and coupons visual inspection

Table 5.3: Supplier A joining process features

Standard process parameters for hybrid joining (CFRP-Al)	Friction stir blind riveting (Supplier A)
Accessibility	One side
Operation required before assembly	None
Cycle time to spot	4.0 s
Nail presence	Yes
Gun process velocity [m/min]	0,3 m/min
Possible combination with adhesive	Yes
Max numbers of layers	No limitation
Minimum thickness [mm]	0.8 mm (backside)
Maximum thickness [mm]	Al 6 mm CFRP (no knowledge for Epoxy based beyond 2.7 mm)
Aesthetical joining	No
Required soundproofed station	No
Power supply system	Electric/Pneumatic
On-line checking	Nail force/Torque Setting Way/Setting Force
Off-line inspection	Non destructive

The carbon fiber and aluminum samples have been delivered to supplier A, in order to let the supplier performing the riveting process, based on the FSBR principle, at the best of their possibility.

It means that all the process parameter and the final choice of the fastener has been made by the supplier after an exchange of information concerning the final application. The process data and system information have been then collected after the riveting process. They are summarized and shown in table 5.3.

The process is fully automated and equipped with on-line checking systems monitoring the setting parameters. As it will be discussed later on, the minimum thickness requirement can be critical for the process quality, particularly for the backside of the material stack and it depends on the material type as well as the top material thickness.

The feed rate employed for the joining process was chosen to be 300 mm/min, that is higher to that used during the first experimental campaign. This is possible thanks to an optimized shape of the rivet head, specifically designed for this kind of application. Indeed, supplier A evidenced how a significant effort has been made in order to equip the rivet mandrel with a special head shape for the punching process, allowing the fastener penetrating the material under the proper rotation speed and pressure values. These are crucial for minimizing the reinforcement phase damage in continuous fiber composites.

Considering the whole riveting process, including rivet penetration and setting, an average cycle time of 4 seconds has been indicated. The visual inspection of the received samples leads to some considerations.

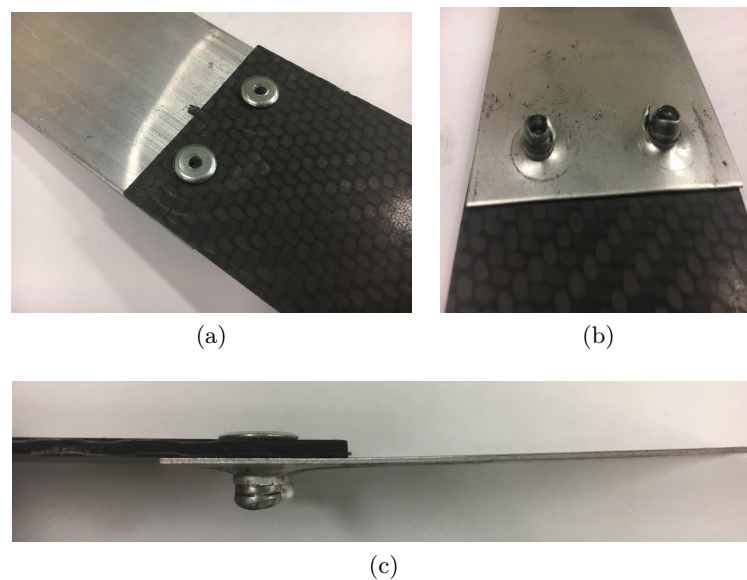


Figure 5.3: 2.7 mm CFRP - 1 mm A6016 FSBR joint details: a) top view b) bottom view c) sideview

With reference to figure 5.3, it can be seen how the material has been formed downward during the fastener penetration. However, a negative aspect resulted from the first visual inspection, that is the slight bending of the aluminum layer due to the force exerted by the rivet during the penetration process. This is caused by a poor support of the lower sample during riveting but it must be taken into consideration when thinner panels are placed at the bottom of the material stack. This is basically the reason why a lower thickness threshold has been indicated by the supplier. This factor is not an issue when the aluminum thickness is increased to 2 mm (figure 5.4), providing a better balancing of forces during the rivet penetration.

The aesthetic appearance of the sample backside is not optimal, mainly due to the formation of an aluminum cup, which has been often observed also during the FSBR process application at the University of Windsor laboratories. However, this is the unavoidable result of the aluminum forming process in which the created cup, together with the metal collar around the fastener shank, takes the place of the chip formed during a standard drilling operation. Furthermore, dealing with blind rivets, the backside of

the connection is not visible so the aesthetic appearance is not really an issue as long as the joint is effective.

Finally, concerning the inlet side of the fastener, a good quality rivet head-carbon fiber interface can be observed, with no composite damage due to the fastener rotation.

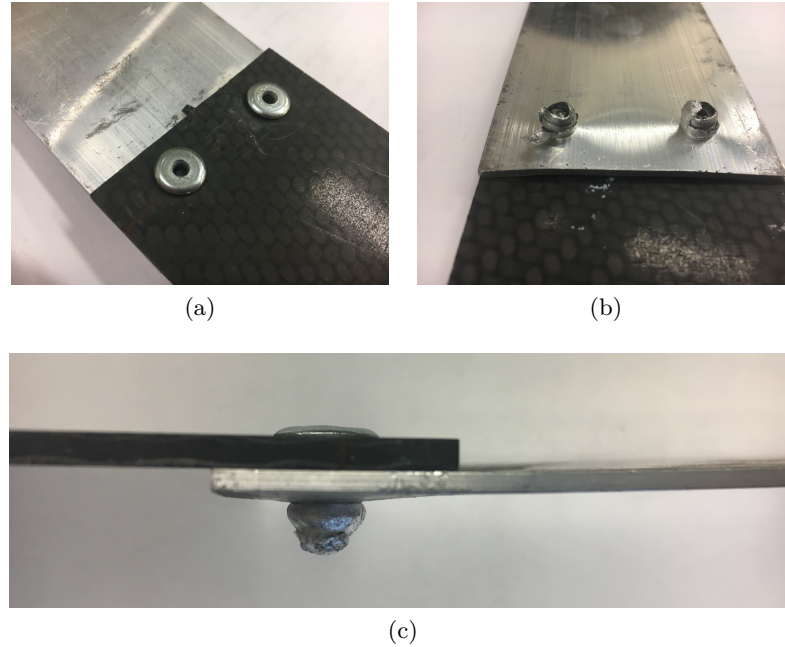


Figure 5.4: 2.7 mm CFRP - 2 mm A6060 FSBR joint details: a) top view b) bottom view c) sideview

5.4 Lap shear test results

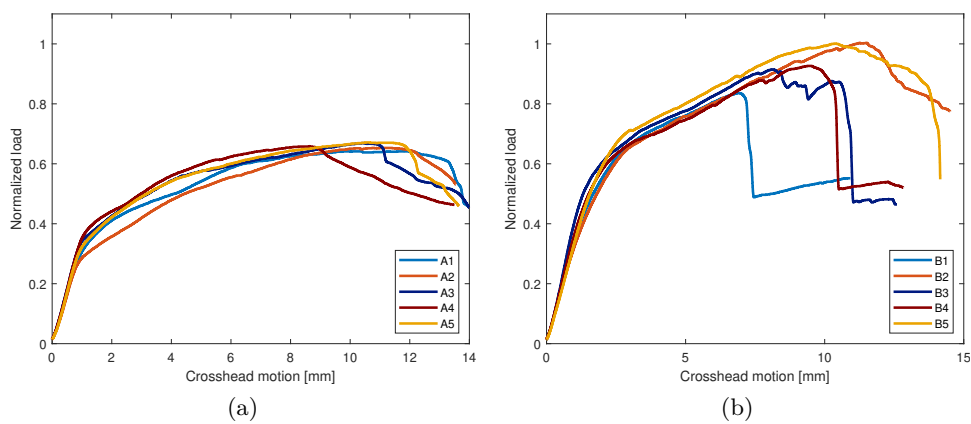


Figure 5.5: Shear test curves referring to supplier A samples testing: a) 2.7 mm CFRP - 1 mm A6016 b) 2.7 mm CFRP - 2 mm A6060

Figure 5.5.a and 5.5.b show the curves resulting from the tests performed on the 2.7 mm CFRP - 1 mm A6016 and 2.7 mm CFRP - 2 mm A6060 samples respectively. Because of confidentiality reasons, the load has been normalized with respect to the

maximum recorded value (sample B2). As it can be noticed, five samples have been tested to achieve a good measurement reliability and to verify the joint strength range.

The shear test repeatability resulted to be quite satisfactory especially in the case of samples containing the thinner A6016 layer. A couple of samples among those containing the thicker A6060, presented instead a higher variability, due to changes in the failure mode.

Both the two samples types failed because of fastener rotation and pull-out. However, in two of the samples with the A6060, one of the fasteners has been literally pulled out from the hole (figure 5.6), meaning that the two rivets have not always worked in parallel during the test. This can be due to a wrong fasteners alignment during the joining process. For instance, this phenomenon can be observed in the sample number three (B3), in which after the first rivet pull-out a load decrease is detected. The resisting action of the other fastener is responsible of a second and lower peak, before the final joint failure. Conversely, in samples B4 and B5 the two fasteners always worked in parallel and failed at the same time, providing a more regular curve shape. This aspect contributed to a much higher test variability observed for the 2.7 mm CFRP - 2 mm A6060 coupons with respect to those with the A6016.

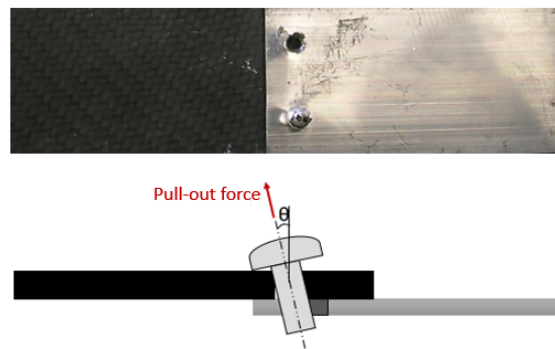


Figure 5.6: *Sample picture after failure and schematic representation of fastener rotation*

The fastener rotation is responsible of a gradual and progressive deformation process involving the aluminum layer, whereas the thick composite sample remained undamaged. This is the reason why the curves shape recalls the one of a ductile metal.

In terms of pure joint strength, the 2.7 mm CFRP - 1 mm A6016 samples presented an average maximum load of 5.73 kN, with a standard deviation of 103 N. Clearly, the increase of the lower layer thickness resulted in the increase of the joint resistance of about 42%. Indeed, the 2.7 mm CFRP - 2 mm A6060 coupons provided an average joint strength of 8.15 kN, but with a larger standard deviation which corresponded to 604 N.

5.5 Corrosion test results

Figure 5.7 shows the corrosion test results on the friction-riveted samples. At the end of the scab20 indoor test, three rivets out of four presented an incipient of ferric corro-

sion. Further considerations on this corrosion test result will be presented in chapter 7, comparing the samples batches coming from supplier A and B.

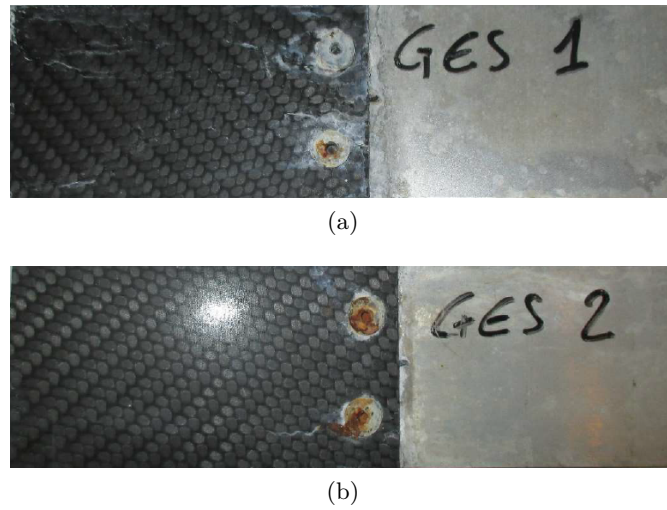


Figure 5.7: Supplier A samples after the scab20 corrosion test

5.6 Macrographic analysis results

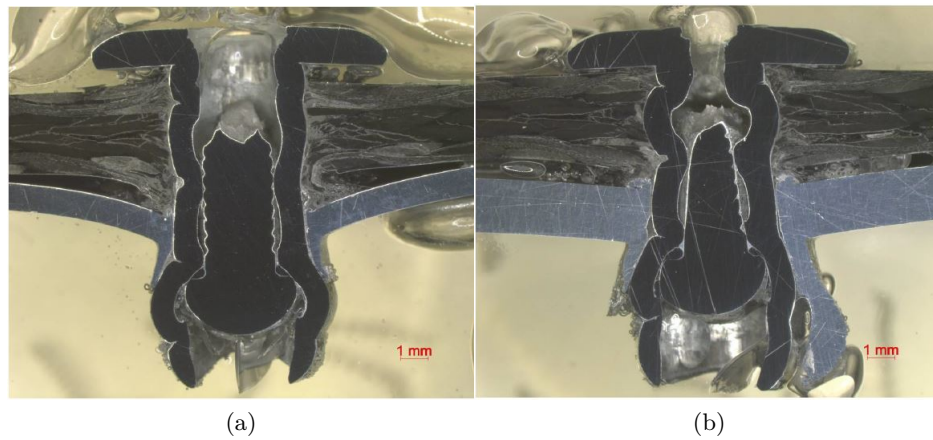


Figure 5.8: Macrography images of supplier A samples: a) 2.7 CFRP - 1 mm A6016 b) 2.7 CFRP - 2 mm A6060

The macrographic examination provided the most significant results in terms of joints quality evaluation. Despite of what declared by the supplier, the most relevant aspect is the significant damage of the composite layer due to stir action of the rotating rivet, which caused an unacceptable delamination of carbon fibers. Moreover, especially in the samples containing the 1 mm A6016, a not negligible bending of the metallic layer has been observed, with a consequent separation between the two connected materials. This is clearly not acceptable from the functional viewpoint since it strongly affects the final joint mechanical properties. The aluminum bending, as well as the composite delamination, is related to the wrong choice of the riveting parameter, particularly the

feed rate which caused an excessive reaction force on the samples with the consequent bending.

Another negative aspect, pointed out by the macrography, is the lack of contact between the rivet head and the composite layer in the 2.7 CFRP - 1 mm A6016. This is clearly a process error which severely affects the mechanical resistance of the connection. Indeed, the fastener head is aimed at distributing the fastening load on a wider surface, trying to minimize stress concentrations on the upper material layer and improving the mechanical interlock quality. If the rivet head does not touch the rivet, not only stress would be more localized, but the rivet tendency to rotate around an axis perpendicular to the fastener one (during shear loading) will increase.

Another very important consideration to be underlined is a negative comment on the supplier rivet choice. As underlined many times, the friction based riveting method is based on the utilization of a rivet with a conical mandrel head, similar to that of flow drilling screws, in order to minimize the penetration resistance. This aspect has been largely promoted and pointed out by the supplier itself when this rivet technology has been launched on the market. Nevertheless, the macrographic examination revealed the usage of a different rivet design, with an almost spherical mandrel head, which is not obviously the best choice to enhance the rivet penetration by friction and to minimize the composite damage. This lack of coherency between the product description and what actually obtained from supplier A, has to be necessarily taken into account for the final technology evaluation.

Chapter 6

Experimental evaluation of supplier B process feasibility and joint quality

Following the same joint validation plan, the second investigated blind riveting technology will be described in this chapter. The robotized riveting solution has been presented by supplier B as an innovative drilling-riveting coupled automated system already adopted for the industrial production of agricultural vehicles, heavy trucks and cars. Despite the supplier stated that the joint mechanical properties are entirely dependent on the choice of the rivet model, and not on the installation system, it has been explicitly requested to rivet the provided coupons with the fully automated system. In this way, the process feasibility with carbon fiber and aluminum layers has been tested in a way consistent with the final and potential system application in FCA production process.

6.1 Supplier B process features and coupons visual inspection

Analogously to what done working with supplier A, a process description has been formulated and reported in table 6.1.

Supplier B provided several feedbacks concerning the performed riveting operation and potential process improvements. First of all, the process has not been carried out with the specific target of cycle time minimization, since several variables must be analyzed and understood first. For instance, when drilling mixed materials some considerations must be done, evaluating the tradeoff between bit cost, bit life, cycle time, cooling complexity and hole quality. Indeed, the optimization work will require a specific research effort on the base of the OEM application and priorities.

The joining of the discussed samples has been made following a relatively conservative choice in terms of drill bit according to the company pre-existing know how.

During the samples assembling process, supplier B pointed out how holes in carbon

Table 6.1: Supplier B joining process features

Standard process parameters for hybrid joining (CFRP-Al)	Robotized blind riveting (Supplier B)
Accessibility	One side
Drill speed	2400 rpm
Feed constant force	25 N
Drill type	-6.75 mm diameter -Solid carbide -Mapal (company code) -140 degree (point angle 1st step) -custom. 10094682
Lubricant	None
Drill time	About 3.5 s
Operation required before assembly	None
Cycle time to spot	6.5 s
Nail presence	Yes
Gun process velocity [m/min]	Variable (force feed control)
Possible combination with adhesive	Yes
Max numbers of layers	No limitation
Minimum thickness [mm]	limited by fastener
Maximum thickness [mm]	limited by fastener
Aesthetical joining	No
Required soundproofed station	No
Power supply system	230/480V 3phase + air
On-line checking	Force feedback
Off-line inspection	Vision inspection system option

fiber were mostly clean with little splintering and minimal backside delamination. The carbide drill started to show signs of wear after approximately 60 holes and some small degree of carbon splintering was noted. Delamination did not seem to be too much of an issue but, according to the supplier, it will vary with drill force and backside support.

Holes in Aluminum can have backside extrudes which is affected by drill geometry and by the dry, lubricant-free drilling process. Chips tended to build up on the cutting edges and adhere to the drilling flutes. This may require periodic drill bit cleaning which, however, was not performed by the supplier in this effort.

The drilling dry operation has been reported by the supplier as a potential criticality. Indeed, it presents some challenges with managing heat buildup, tool life and a generally finer process. Chip adhesion to the drill bit can be an issue when dry drilling through the aluminum. However various polishing techniques or coatings can be utilized to decrease adhesion and increase chip ejection by adding a lubricity agent/coating.

Concerning the second process step, namely the fastener insertion and setting, no issues or criticalities reports have been provided by supplier B. Nevertheless, the quality of this process can be improved by exploiting the modular design of the robotized riveting system by adding features and additional subsystems. They may include the pintail

presence detection and depth measurement systems (acting after the rivet placement) as well as to log information on the pull/set pressure curve from the hydraulic supply.

One of the most interesting aspect of the robotized riveting system is its capability to work with basically all rivet geometries and types. Most of the actual joint properties depend on the fastener type. For instance, the maximum and minimum joinable thickness depend on the rivet choice. In this specific case, it has been carried out an information exchange with a third supplier. This is one of the biggest blind riveting technologies providers, working in collaboration with several OEMs. After a detailed description of the FCA desired application, the experts of this company suggested the use of their Huck Auto-Bulb product line. This particular fastener type has been specifically designed for applications involving thin materials and delicate composites. It meant to form a broad blind side bulb, capable to spread the clamping load over a larger area. Figure 6.1 demonstrates how differently the rivet shank is deformed in Auto-Bulb rivets with respect to competitors products. It can be anticipated a comparison with what observed in samples riveted by supplier A, where the bulb formed above the sheet line.

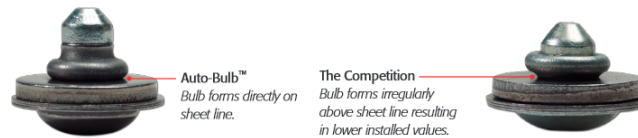


Figure 6.1: Rivet shank deformation in Huck auto bulb fasteners with respect to competitors

This potentially allows achieving higher joint strength, being the blind side of the rivet the higher stress concentration point where failures are generally observed.

According to the supplier company specialists, the sheet materials chosen for the discussed application, namely aluminum and composite, cannot provide enough strength around the hole to resist effectively when loaded in tension or peel. Consequently, thanks to the creation of a large footprint, Auto-Bulb rivets are the best choice to deal with this specific application. According to the thickness requirements for the riveted samples, the ABP-R8-M3 rivet has been selected, whose features are shown in table 6.2.

Table 6.2: ABP-R8-M3 rivet specifications

Product part number	ABP-R8-M3
Material	Steel
Surface finish	Zinc clear trivalent
Shank diameter [mm]	6.4
For material thickness [mm]	2.8 - 4.8
Head diameter [mm]	13
Hole diameter [mm]	6.7-6.9
Tensile strength [kN]	7.12
Shear strength [kN]	11.57

The rivet bulb formation claimed by the supplier, has been confirmed by the visual inspection of the obtained samples. The bottom and side views of the riveted samples illustrate the formation of a wide rivet footprint on the aluminum layer. Moreover,

unlike the samples riveted by supplier A, the process has not caused any bending of the samples close to the riveted area. This is due to a better fixing system but also to the lower forces resulting from the drilling operation with respect to the friction-caused rivet penetration. Furthermore, from the visual inspection, no visible aluminum protrusions resulted from the drilling process and the aesthetic quality of the joint is pretty good with no evidence of defects. The same considerations apply for the 2.7 mm CFRP - 2 mm A6060 coupons, which presented the same visual and qualitative features.

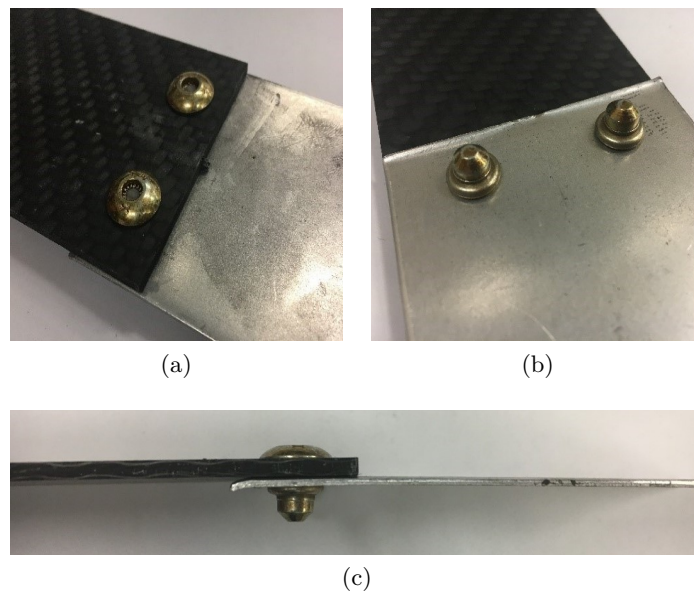


Figure 6.2: 2.7 mm CFRP - 1 mm A6016 joined with robotized system: a) top view b) bottom view c) sideview

6.2 Lap shear test results

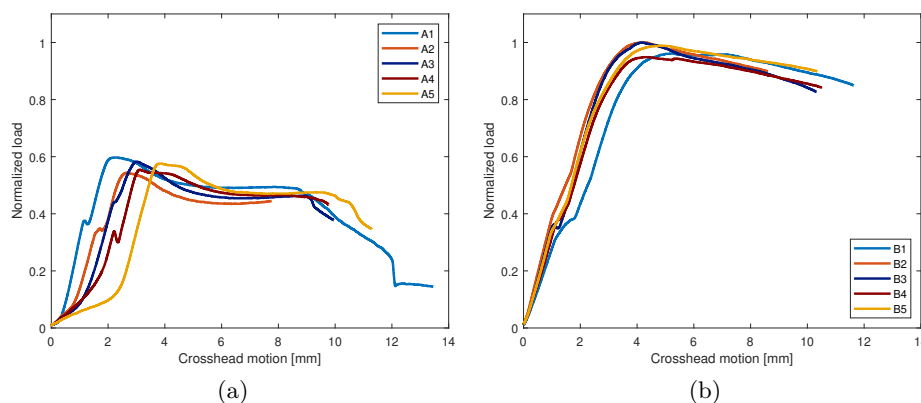


Figure 6.3: Shear test curves referring to supplier B samples testing: a) 2.7 mm CFRP - 1 mm A6016 b) 2.7 mm CFRP - 2 mm A6060

The lap shear tests of the two coupons type provided quite robust results, both in terms of joint strength measurement and of failure modes. This resulted in quite

overlapping force-displacement curves. Once again, because of confidentiality reasons, the force-displacement curves have been normalized with respect of the peak load recorded on the B3 sample.

As it can be seen looking at the two set of curves shape, the observed failure modes resulted to be different for the two coupon types. The 2.7 mm CFRP - 1 mm A6016 samples failed because of nonregular secondary bending followed by fastener pull-out. On the other hand, the lower layer thickness increase in the 2.7 mm CFRP - 2 mm A6060 coupons constrained the material bending and made the aluminum bearing the only observed failure mode. The failed samples are illustrated and schematized in figure 6.4. Concerning the samples with A6016, almost all the force-displacement curves revealed a small wrinkle, indicating the moment in which both rivets provided their resisting action against the shear loading. After the force peak, a progressive shear out took place. The subsequent curve slope decrease is representative of the lower layer bending and shear out. The wrinkle presence demonstrated that the two fasteners were not working at the same time at the beginning of load application. Just sample A5 has not shown this phenomenon before the joint strength limit was reached.

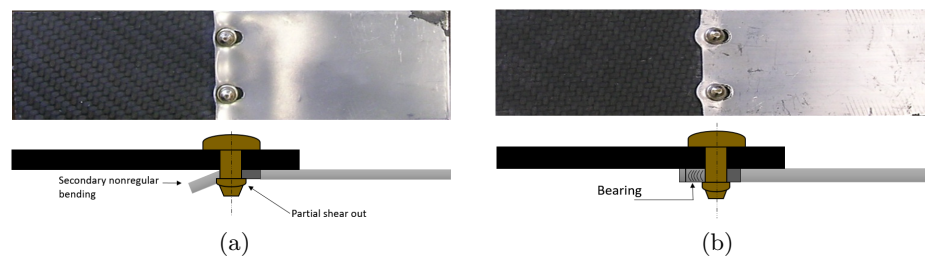


Figure 6.4: Failure in samples riveted by supplier B: A) 2.7 mm CFRP - 1 mm A6016 b) 2.7 mm CFRP - 2 mm A6060

Similarly, the curve wrinkle has been detected in all the 2.7 mm CFRP - 2 mm A6060 samples. However, this set of coupons provided very high values of force peaks and a slow resistance decrease during the bearing process.

Concerning quantitative measurements, the 2.7 mm CFRP - 1 mm A6016 samples presented an average value of joint strength equal to 5.88 kN, with a standard deviation of 224 N. The presence of the thicker A6060 increased the joint strength of about 72%, reaching an average value of 10.11 kN with a pretty constant standard deviation of 228 N.

6.3 Corrosion test results

Figure 6.5 presents the samples riveted by supplier B. The 20 hours testing, according to the indoor scab standard, resulted in the corrosion development in 3 of the four total tested fasteners. These results will be better commented in chapter 7, where a comparison with supplier A samples is provided



(a)

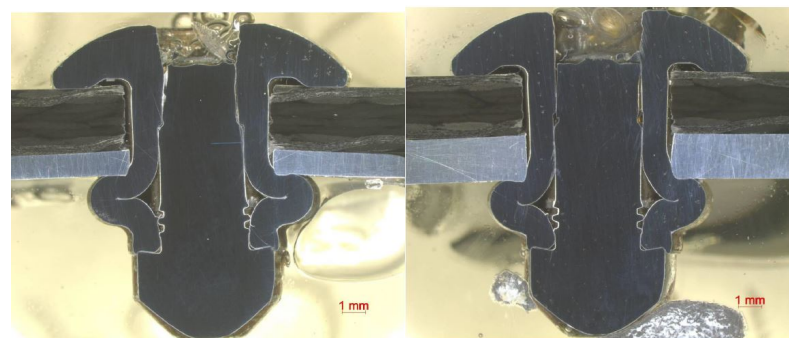


(b)

Figure 6.5: Supplier B samples after the scab20 corrosion test

6.4 Macrographic analysis results

Supplier B macrographic examination provided quite positive results. In both samples type, the magnified sections show an optimal joint quality concerning the interlock formation and the integrity of the assembled components. All the examined samples presented an optimal shank deformation, characterized by a wide rivet footprint formation which increases the extension of rivet surface in contact with the material, improving the load distribution. The rivet head is perfectly in contact with the composite layer, contributing to the joining load distribution. The composite and aluminum components do not present any clearance between each other and no bending due to the riveting process. Another important aspect is the rivet mandrel rupture point, which is not only above the joint line, but also above the upper carbon fiber sample, providing a very high resistance to possible shear loading, as demonstrated by the previous tests.



(a)

(b)

Figure 6.6: Macrography images of supplier A samples: a) 2.7 CFRP - 1 mm A6016 b) 2.7 CFRP - 2 mm A6060

Chapter 7

Technologies comparison

Once completed the analysis of the robotic and friction-based riveting technologies, some comparison and conclusions can be made. The final considerations will be formulated taking into account process features, supplies know how and involvement in this research, system implementation potential in the automotive sector and resulting joint properties.

7.1 Shear test comparison discussion

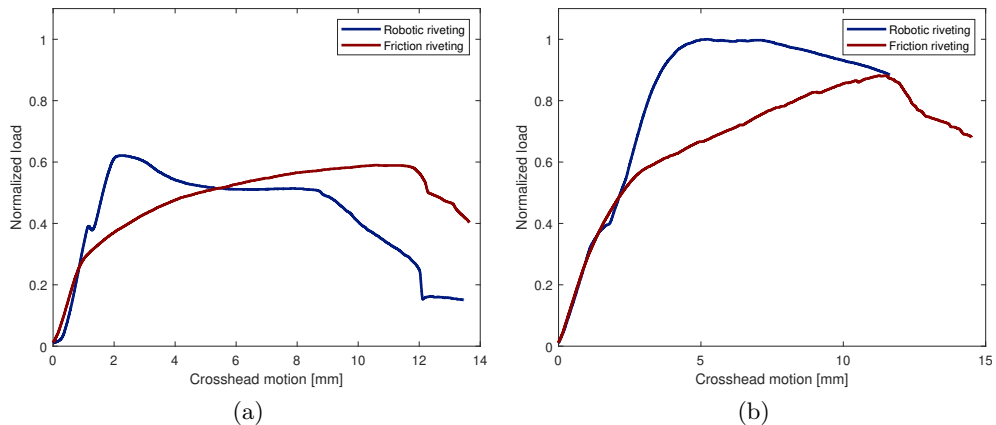


Figure 7.1: *Shear test curves comparison for a) 2.7 CFRP - 1 mm A6016 and b) 2.7 mm CFRP - 2 mm A6060*

Figure 7.1 presents the comparison between the robotic and the friction based riveting technologies. Some quantitative and qualitative considerations can be made. Data are normalized with respect to the maximum recorded load.

Starting with the samples containing the thin A6016 (figure 7.1.a), it can be seen how the final value of joint strength resulted to be only slightly different for the two technologies. In terms of average maximum recorded load, the samples riveted by supplier A (friction stir blind riveting) provided a value just 2.5% lower than what observed in supplier B samples (robotic riveting). This small difference cannot be a discriminant factor in the joint evaluation process. A more significant aspect is the difference in terms of joint stiffness in the linear region of the two curves, which is 50% higher in the case

of supplier B samples. In these coupons a gain of 3.75 kN/mm has been observed with respect to the 1.88 kN/mm of the friction riveted samples. This results in a much faster force increase in the case of supplier B samples which eventually reached the maximum joint strength at the elongation of 2.2 mm and right after the occurrence of yielding in the aluminum. After that, the lower layer is progressively sheared out and bent without being able to properly resist the load increase.

Conversely, FSBR samples from supplier A presented a lower rate of joint resistance force increase which, however, continued after yielding. Indeed, the red curve follows the typical strain hardening process of aluminum material, since the rivet rotates inside the hole deforming the metallic layer. Consequently, the peak load is reached just before the rivet pull out, at an elongation around 11.4 mm, so more than five times the one observed for Robotic riveting.

Concerning the samples containing the thicker A6060 aluminum layer, quite evident differences can be observed by comparing the two technologies, both in terms of joint strength and failure modes. The increase of the aluminum thickness (and change in the alloy type) determined a substantial improvement of the joint mechanical properties, which has been more significant in the coupons riveted with the robotic module. Indeed, the resulting value of joint strength turned out to be 24% higher in the case of supplier B samples. Conversely, supplier A coupons resulted to fail at a lower force value. In this case, the slope of the two curves in the first linear elastic stage of the test proves that the joint stiffness was equal for the two sample types.

Dealing with the analysis of the failure modes, once again the two set of samples presented quite evident differences. Supplier A coupons maintained the same failure mode of those with the thinner A6016, namely that of rivet pull-out. Consequently, the qualitative trend of the curve resulted to be still similar to that of the aluminum tensile test, characterized by a first linear region, yielding and strain hardening phenomena before rivet pull-out and subsequent failure. Conversely, samples riveted with the robotic module better exploited the increase of the lower layer thickness by changing their failure mechanism and presenting the bearing phenomenon.

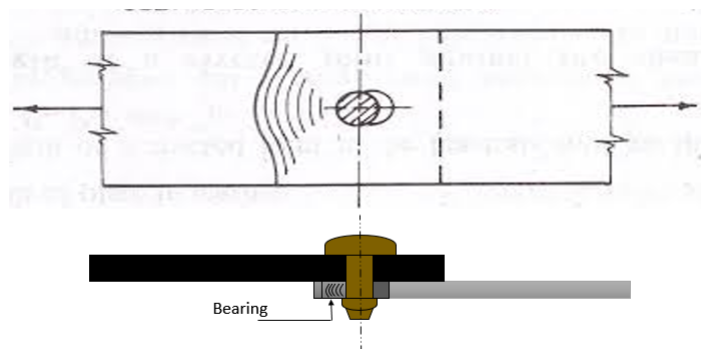


Figure 7.2: Schematization of the bearing failure mode observed on the samples riveted by supplier B

As shown in figure 7.2, the bearing failure mechanism causes a compression of the material (in this case aluminum) in the region between the fastener and the sample edge. This failure mode prevents large deformation to take place but uses efficiently the ductile material ahead of the rivet to resist the shear loading. This is the main reason why such high value of joint strength has been observed for this coupon type. The advantage of this failure mode is not just related to the peak value of resistance but also in the fact that it starts after the linear part of the force-displacement curve and it then takes place slowly, with a gradual decrease of load. This progressive strength decrease allowed having higher value of force with respect to supplier A samples, even at high values of elongation. This shift from secondary bending to bearing failure is explaining the higher gain of joint strength which has been observed for the robotized riveting technology with respect to the friction based one. Moreover, as for the previous material combination, also the 2.7 mm CFRP - 2 mm A6060 showed a value of elongation at maximum load higher in the case of friction-riveted samples. In particular, the maximum joint strength has been reached at 11.4 mm and 5 mm for supplier A and B respectively.

Another interesting way to evaluate and compare the force-displacement curves is the energetic approach. This implies to integrate said curves, in order to get the overall work needed to deform the samples up to the failure occurrence. This can be obtained as the area beneath the force-displacement curve:

$$W = \int_0^d F(x) dx$$

Note that d is the maximum elongation at fracture. With reference to the curves compared in figure 7.1, supplier A samples provided 14% and 4% higher values of absorbed energy before failure for the samples with the A6016 and A6060 respectively. However, even if the deformation energies resulted to be pretty similar, they differ for the elastic-plastic energy share. Indeed, most of the supplier A samples work represents plastic deformation energy, while supplier B total work is mainly consisting of elastic energy. However, the difference between the two curves energy is not relevant to draw conclusions about the two systems.

Considering the application of these technologies to the automotive industry, particularly as joining methods for the vehicle body in white, it is important to ensure the proper structural stiffness to the multi-material assembly. Consequently, the higher deformation of FSBR samples would not be so good for the specific application even if, with the 2.7 mm CFRP - 1 mm A6016 the final joint strength resulted to be the same for the two technologies. Moreover, the samples resulting from the robotic riveting process provide their peak of resistance immediately after the joint yielding, meaning that if the (significantly high) joint strength value is not reached by the external load, the structure is just elastically deformed and remains undamaged after the load application. Conversely, the friction-riveted samples presented their maximum strength well after the yielding occurrence. This means that, even if the joint does not reach the complete failure, it is significantly deformed at relatively low load. In particular, the plastic deformation resulted to start already at a force value 53% and 48% lower than the final joint

strength of 2.7 mm CFRP - 1 mm A6016 and 2.7 mm CFRP - 2 mm A6060 samples respectively. Therefore, it can be concluded that supplier B technology provided the best performance during the mechanical properties evaluation.

This result may appear to be in contrast with what observed and discussed during the first experimental campaign. However, as mentioned previously, a notable factor is represented by the use of two different fasteners. The rivet adopted by supplier B, according to the experience of a further and different fastener provider, resulted to be much more specific and suitable for the discussed application. Figure 7.3 shows the key features of the two fasteners employed by the suppliers.

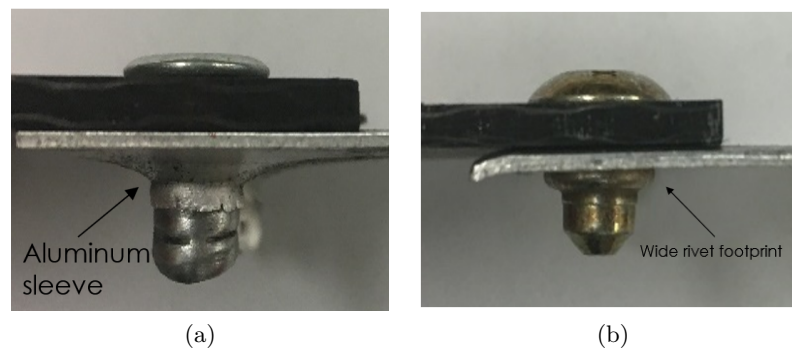


Figure 7.3: *Installed rivets: a) friction-based technology b) robotic installation method*

Figure 7.3.a illustrates the typical material sleeve formation on the blind side of the connection, which is one of the main element responsible of the joint load bearing capability with respect to conventional riveting. However, this is true as long as the comparison is done between samples riveted with the same fastener. Indeed, it can be stated that, on the base of what observed during the first experimental campaign on FSBR method, this material sleeve widens the load exchange area between the rivet and the lower material layer, opposing also the fastener rotation-pull out and providing a benefit with respect to conventional riveting. Nevertheless, the riveter provider for the robotic riveting technology application has been able to integrate a similar feature directly in the rivet, which during the setting process creates a wide footprint on the lower metal sheet. This fastener feature, evidenced in figure 7.3.b, is able to achieve an optimal distribution of force on the layer on the bottom of the stack, which is normally where stress is concentrated. The wide footprint has been specifically developed by the supplier to work with applications involving composites and thin metal sheets. Indeed, this feature represents almost a second rivet head which not only increases the joint load bearing capability, but it also successfully prevented the rivet from rotating and being pulled out from the hole. This is proven by the fact that the rivet always remained perpendicular with respect to the shear load application direction. In so doing, the material around the rivet hole is better exploited resisting the shear loading.

7.2 Measured joint strength statistic reliability

Another interesting aspect to be included in this comparison is the statistical reliability of the obtained results. Concerning the 2.7 mm CFRP - 1 mm A6016 samples, a quite low measurement variability has been observed, especially if the interval between first and third quartile are considered (represented by the box height). Conversely, when the 2.7 mm CFRP - 2 mm A6060 samples have been examined, quite different results variability has been detected.

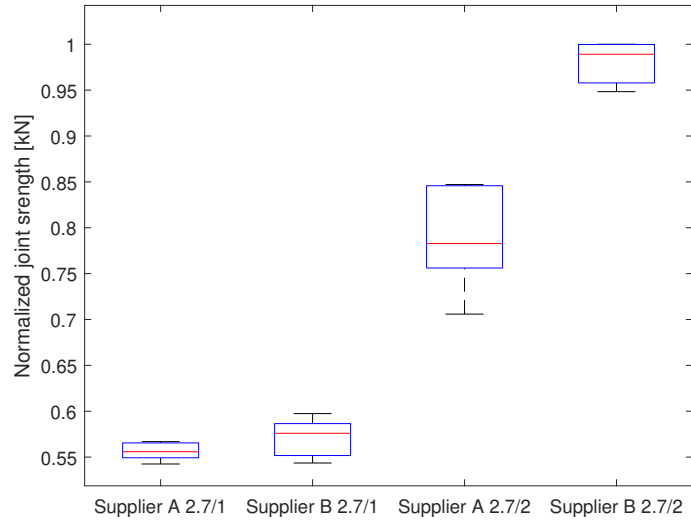


Figure 7.4: Box plot representing the median and the statistic reliability interval of the joint strength measurements

On one hand, the robotic riveting process of supplier B presented a constant result spread, characterized by a standard deviation slightly above 200 N. On the other hand, the distribution of joint strength for friction-based riveting method has shown a significant increase of variability when thicker samples have been tested. The standard deviation for the 2.7 mm CFRP - 2 mm A6060 samples has been found to be above 600 N, and almost six times greater than in the case of 2.7 mm CFRP - 1 mm A6016 samples. This result was not unexpected if looking at the joint strength variability of the samples tested during the first experimental campaign. Indeed, also in that case the result spread has shown an increasing tendency when thicker material layers have been involved. The reason is still uncertain and the study of this phenomenon would require further research efforts. However, some considerations can already be done. It has been said that the FSBR technologies can provide an increase of joint strength based on four main factors which are summarized in the following:

- A material sleeve is formed around the rivet tail during fastener penetration and hole forming process.
- Incipient of welding or formation of intermetallic compounds (IMC) generate a weak bonding effect between the rivet and the metallic layer.
- The rivet stirring action is the cause of a recrystallization phenomenon, grain

refinement and consequent hardness increase in the aluminum layer and close to the rivet hole.

- Stress concentration due to the hole presence is minimized thanks to the size reduction of the hole itself, whose diameter is corresponding exactly to that of the rivet body diameter.

All these factors have been assessed or proposed in literature. However, the first three introduce a significant number of variables affecting the process. For instance, not always the formed sleeve of material resulted to be symmetric around the rivet tail, being this process depending on the material flow around the fastener during its penetration and setting stage (figure 7.5.a and 7.5.b respectively). Both are strictly related to the mandrel tip (which in this case was conical) but it can also be affected by slight misalignment of the tip with respect to the material or by the clamping system.

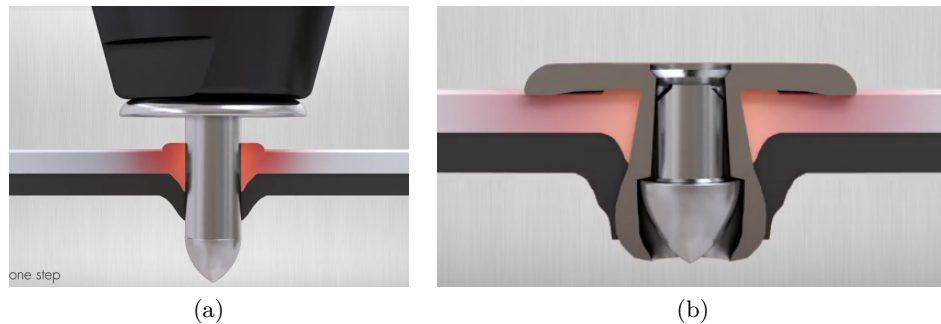


Figure 7.5: *FSBR process and material forming: a) penetration phase b) qualitative thermal field representation around the rivet hole (source: supplier A)*

The formation of a weak welding between the steel rivet and the aluminum layer is even more uncertain. Dalong Gao et al. [29] had discussed already the possibility of an extra bonding creation due to IMC formation, even if the conditions in which this occurs have not been investigated. Junying Min et al. [33] has instead analyzed the recrystallization phenomenon due to FSBR technique adoption. It successfully demonstrated the increase of material hardness close to the rivet hole thanks to the grain refinement process. Nevertheless, no studies have been carried out on the temperature field around the rivet, which is qualitatively illustrated in figure 7.5. Indeed, the effectiveness of this phenomenon, which can be regarded as a heat treatment process, depends not only on the temperature level that is reached in the aluminum (which influences also the IMC formation) but also the time evolution of this thermal field. For instance, how fast the heat is dissipated by conduction in the base metal and so how much time is available for the recrystallized grains to grow before the aluminum gets cold.

These explanations are aimed at underlining how many unknown factors have an influence on the final joint strength and quality of a friction-riveted connection with respect to a conventional one. These can be an explanation for the higher results standard deviation observed in samples coming from supplier A. Indeed, this spread of obtained results increases with the increase of aluminum thickness, which in turns increases the

effect that inter-metallic compound formation can have (increased rivet-material contact surface) on the final joint quality. The same applies to the material sleeve formation (more aluminum is available to the forming process) and to the recrystallization process (larger thickness influences the thermal field and heat dissipation rate).

However, regardless from the sources of the results variability, the higher uncertainty on the final strength of the joint is a negative aspect of FSBR technology, especially if considering its application in a high volume production process. Even if visual and nondestructive in-line quality checks can be integrated in the supplier A installation system, the higher robustness and consistency of the robotic riveting module is by sure preferred for this kind of application.

7.3 Corrosion test results comparison

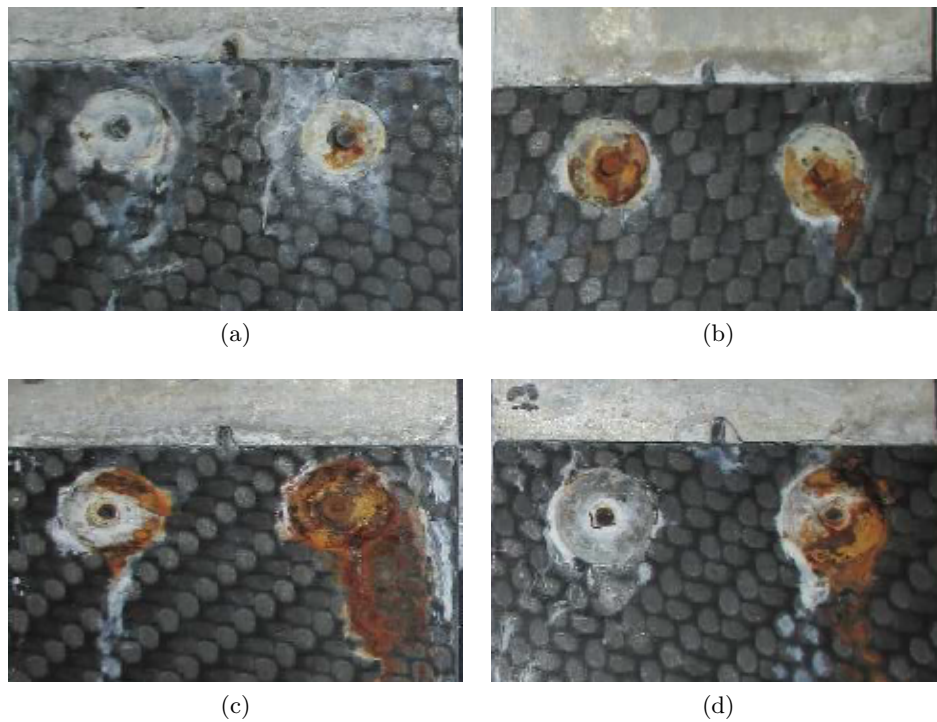


Figure 7.6: Rivet corrosion after scab20 testing: a-b) supplier A samples c-d) supplier B samples

The 20-hours corrosion test resulted substantial rust formation for all the tested samples. In both cases, three rivets out of four have been affected by a significant corrosion phenomenon. This process is not really dependent on the selected riveting method, but mainly on the fastener type, including material and external coating.

Both supplier A and B samples have been riveted with carbon steel fasteners, while the technology providers have been left free to choose the best coating for the specified FCA application.

The choice of carbon steel for the rivet material is a direct consequence of some economic and process considerations. Indeed, the utilization of stainless steel rivets would be highly beneficial against corrosion phenomena, but the cost increase per rivet

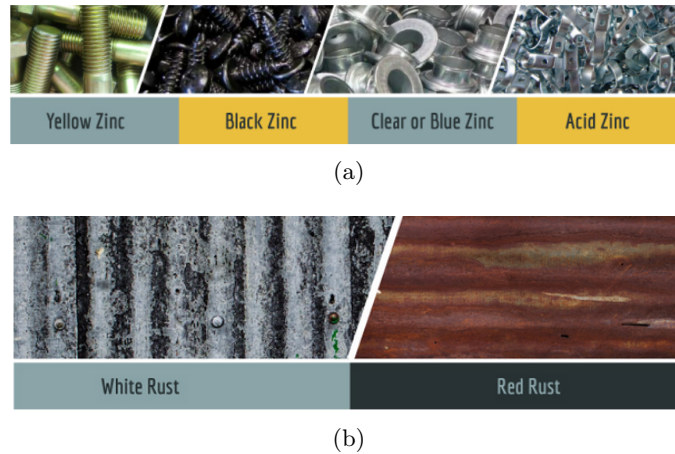


Figure 7.7: a) Zinc plating typologies b) Rust stages for zinc coated steel [53]

would be significant as well. This is one of the reason why carbon steel fasteners are generally used for automotive applications. A second reason is that the vehicle body in white, after the assembling process, undergoes the cataphoresis operations. This is a process of metal electro coating which allows getting a high resistance to atmospheric agents. Consequently, cataphoresis improves also the rivets resistance to corrosion, so that the fasteners can be made of cheaper carbon steel. Indeed, stainless steel fasteners are used just when they are installed after the cataphoresis process.

The presented corrosion test allows to evaluate the starting point in terms of rivet resistance to corrosion prior the cataphoresis operations. This means that the corrosion test result will be worse that the actual one, but still indicative of the quality of the initial rivet coating selected by the supplier.

In this case, the two suppliers applied two different types of zinc coating, as can be understood from the difference in the fasteners color (figure 7.3). Supplier A and B selected the clear and yellow zinc plating respectively.

Clear (or blue zinc) coating is generally obtained through tri-valent-based processes, which are considered the most ecofriendly ones. This coating type can be used in conjunction with various topcoats and waxes to meet a wide variety of performance requirements. However, clear zinc plating tends to offer lower corrosion resistance with respect to other zinc coating methodologies [53].

Yellow zinc coating (also called gold zinc) is quite commonly used in the automotive field and it is obtained by means of a hexavalent post treatment, allowing the formation of a thicker zinc layer with respect to the clear coating. This is done to provide better corrosion resistance [53].

Both supplier A and B samples present two types of rust, namely the white and red ones, which are typical of zinc plated materials (figure 7.7.b). White corrosion is the first observed phenomenon during the tests and is due to the reaction of the zinc passivation layer. Conversely, red rust is a corrosion phenomenon occurring in the parent material. This represents the real failure for a corrosion test since it is related to the damage of the structural component, namely the rivet.

Observing the investigated samples in figure 7.6, some considerations can be made. First of all, since no standards have been formulated to specify the acceptance limits for this test, it is not straightforward to assess whether the results are satisfactory or not. There are some references in literature which supports the idea that red rust is acceptable after 140 hours of testing and that having just white rust after 300 testing hours is a benchmark result. These considerations make the obtained results quite positive if considering the overall test duration of 480 hours. However, the most important aspect is the acquisition of the corrosion test results, which will allow the carmaker to compare these riveting technologies with other currently investigated joining methodologies.

Concerning just the comparison between supplier A and B samples, the latter provided slightly worse result, despite the difference in the adopted coating would have suggested the opposite test outcome. Indeed, samples riveted with the robotic system present a red corrosion phenomenon affecting not only a wider rivet area, but also a higher amount of material. Indeed, the darker red rust on supplier B samples indicates how the red corrosion gradually affected a higher amount of steel. Conversely, the results in supplier A samples appear to be less critical, despite the clear coating utilization. In particular one of the two samples showed only a small red corrosion spot on one of the two rivets.

A possible explanation to this corrosion performance difference is related to the quality of the zinc coating application on the rivet. Observing figure 7.8, representing supplier B samples prior the discussed test, it can be noticed a set of silver spots, where the yellow hexavalent zinc coating was not properly applied. This would justify the more severe corrosion results detected in these samples.



Figure 7.8: *Yellow zinc coating non-homogeneity for supplier B samples*

However, it is worth to remark that these corrosion resistance qualities of the investigated riveted joints are not much related to the riveting technology, but mainly to the rivet type. Consequently, the corrosion test does not allow to express judgement defining the best technology between FSBR and robotic riveting but helps to have a more complete description of these joints quality, suggesting potential developments. For instance, one of them could be the improvement of the rivet post treatment for the zinc coating application. This clearly applies to the production process of the rivets provider, which in this case does not correspond to supplier B and so to the technology

provider.

7.4 Installation equipment comparison

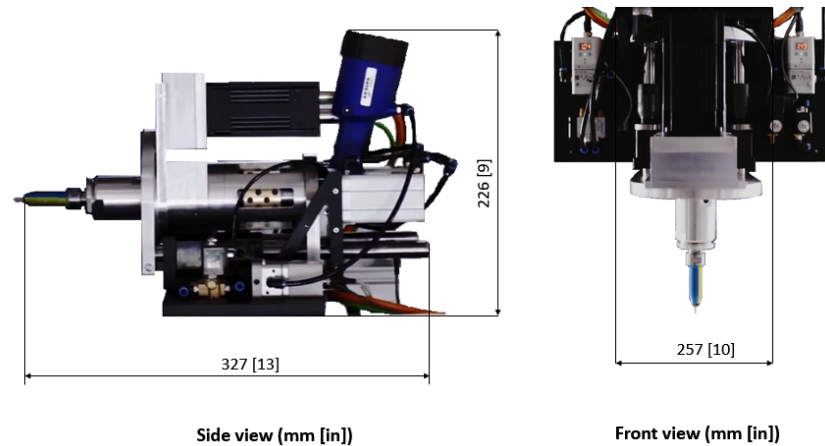


Figure 7.9: *Supplier A installation module*

One of the most important aspects of the present study is that of considering the implementation of either supplier A or B riveting systems in the automotive production process. This requires also a comparison in terms of compactness, level of automation, efficiency and options available for the two suppliers installation systems. Figure 7.9 presents the equipment used by supplier A to prepare the tested coupons. This module can be mounted on a six-axis robot in order to make the process fully automated and suitable to be implemented along the body shop assembly line. According to supplier A, this riveting equipment can offer:

- Compatibility to robots and automated devices
- Adjustment of the device head to the system (geometric connection)
- Adaptation of the device head to the application (e.g., limited accessibility)

Some functions are available as options:

- Feeder rivet (pick & place or direct)
- Downholder (pneumatic)
- process monitoring

An important consideration that has to be made concerns the development state of the two technologies. The FSBR technology (supplier A) is much more recent and still in a development stage. This means that the fully automated version of this technology is, despite already available, still to be better assessed by FCA. Indeed, no visual evidences demonstrated the utilization of the riveting module in figure 7.9 on a fully automated

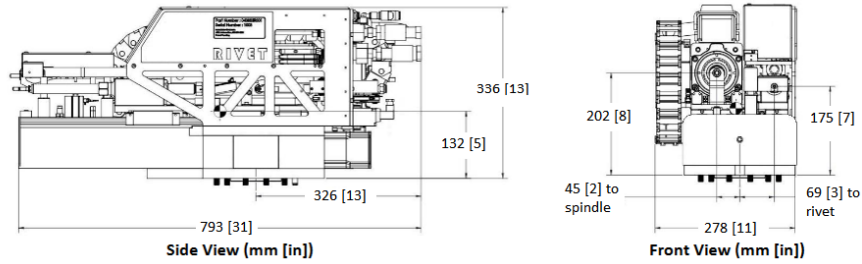


Figure 7.10: *Supplier B installation module*

robot. Indeed, the figure illustrates the module used in the stationary workstation which, however, should be easily mountable on a six-axis robot.

Figure 7.10 illustrates the robotic riveting installation module with the main dimensions. The following features can be provided for this system:

- Fully automated drill and/or rivet tools integrated into a compact assembly
- Servo control of the drill and/or rivet axes, providing force feedback and fault detection
- Adaptable spindle axis and/or rivet axis to support specific production requirements of the manufacturing line
- Automatic fastener feed and pintail collection system via the robotic module Supply Cabinet
- Fastener vision inspection system option to prevent incorrect or damaged fasteners from reaching the tool
- Drill and rivet commands operated via inputs at the system control interface
- Chip collection option for extracting debris away from the drilling area, helping to maintain a clean work area
- Multiple robotic modules can operate from a single Supply Cabinet (factory option) reduces equipment footprint
- Full featured, on-board HMI unit with direct access to system functions and technical documentation
- Mountable to any robot via a robot-specific mounting adapter plate or configurable for mounting on a stanchion/gantry
- Integrated vision system hardware options for part inspection and/or robot guidance via the facility control system
- Process specific drill and/or rivet tool versions available for added flexibility to the manufacturing operation



Figure 7.11: *M-900iB/700 six-axis robot used to implement the robotic riveting module along the production lines*

As declared by supplier B, the riveting module can be mounted on any robot system. Video and documentation from the supplier company demonstrated how this module has been integrated with the M-900iB/700 (figure 7.11), characterized by a strong wrist, wide motion envelope and a 700kg payload. It is produced by a renowned brand actually working with the FCA group in the NAFTA region plants.

7.5 Macrography results comparison



Figure 7.12: Macrography results comparison (2.7 CFRP - 1 mm A6016): a) supplier A sample b) supplier B sample

Figure 7.12 shows the final macrographic results comparison for the samples riveted with supplier A and B technologies. As mentioned in the previous chapters, several features observed in samples riveted with the friction-based technology make the obtained result definitely not acceptable. For instance, the sample bending, the clearance between layers and the composite damage could not be tolerated for structural connections in a vehicle body in white.

Conversely, the combination of the robotic riveting method with the adopted Auto-Bulb rivet provided optimal results from several viewpoints already commented in the previous chapter.

The next chapter of the thesis will take into account all these considerations in order to define the final conclusions.

Chapter 8

Conclusions

The most important aspects which influenced this final evaluation of the two riveting solutions are summarized and reported.

The bending of the 1 mm A6016 sample after the riveting process performed by supplier A (described in section 5.3) must be carefully taken into account when thinking about a potential FSBR application to the automotive industrial field. Indeed, the friction-based riveting requires a certain supporting action of the lower material layer during the fastener penetration. If this is not the case, the rivet installation is likely to cause the metal sheet deflection. This can be an issue especially when thin aluminum layers are placed below thicker composite sheets, like it the case of 2.7 mm CFRP - 1 mm A6016 sample.

Concerning the joint mechanical performance, supplier B samples demonstrated to provide higher values of strength and stiffness when loaded in shear mode. Moreover, the transition from elastic to plastic behavior resulted to be occurring at higher force values with respect to supplier A coupons. This means that the plastic joint deformation, severely affecting the assembly integrity, occurs at higher force values in supplier B samples. From an energetic viewpoint, no significant differences have been observed between the two samples batches.

Dealing with the joining process repeatability and robustness, the first experimental campaign and the supplier validation process provided sufficient data to assess the lower predictability of FSBR with respect to robotic or standard riveting. From the process viewpoint, this gives an important advantage to supplier B technology, whose quality management would be consequently much easier.

Corrosion tests provided more positive results in the case of supplier A coupons, where the quality of the zinc layer distribution allowed to achieve a more effective protection of the rivet. However, the impact of this aspect on the final technology choice is limited by the attenuation of the corrosion phenomenon which can be achieved with the cathoporesis process. Moreover, the adoption of supplier B system, does not preclude the possibility of changing the rivet model, coating type or even the fastener provider.

The previously mentioned decoupling between system supplier and rivets provider applies just in the case of supplier B, while these two figures are coincident in the case of supplier A technology. Indeed, in the latter case, a specific rivet design must be provided

for friction-based riveting. This is actually offered only by supplier A itself, which can supply a limited range of fasteners designs, since the technology commercialization has been found to be not mature yet. It must be said that supplier A offers its availability to work with carmakers in the development of customized solutions, but this will require additional waiting times for each specific application, which are not coherent with the time to market minimization tendency. Conversely, one of the most interesting advantages of supplier B solution is the system capability to work basically with any type of blind rivet. This allows exploiting the initial equipment investment for any type of blind rivet installation necessary during the body in white assembly process. In other terms, a wide range of suppliers can provide their fastener solution, among which the carmaker can select the most suitable to the needed application, without the obligation to deal with the specific supplier of the riveting equipment. For instance, this is what has been done in order to prepare the coupons for the previously discussed experimental activity during which, apart from the two technologies providers, a third supplier has been involved in order to provide the rivets compatible with the robotic riveting method.

According to the performed researches, the supplier B system seems to guarantee, from the automation viewpoint, a readier implementation in the manufacturing process. Indeed, the robotic-riveting technology has been already used for several industrial applications including agricultural machines and trucks production, whereas supplier A system is still in a technology development phase. This explains the higher information availability in the case of supplier B equipment features.

Concerning the macrographic examination results, the overall quality of the joining process performed by supplier A turned out no be not compliant with FCA requirements. Possible further investigations of the friction-based technology would require the supplier to review its process features and quality level with the selected material combination.

In conclusion, based on the performed experimental activity, the FCA group preference is oriented toward supplier B system for potential future applications in which carbon fiber and aluminum structural elements need to be joined.

8.1 Future research directions

Despite the conclusions that have been provided, some aspects related to the two riveting processes require further investigation. The joint validation process will still require additional tests, such as peel and cross tension. These kinds of analyses require specifically designed samples with non-regular shapes. Dealing with carbon fiber, characterized by complex and expensive shaping and production processes, a specific planning effort should be done in order to achieve a full characterization of the joint properties.

Once the riveting technologies undergo the full FCA standard procedure for joint validation, it will be possible to focus only on the selected riveting method. This will be combined with the structural adhesive used by the carmaker. The results of new shear, corrosion, macrograph, peel and cross tension testing on the riv-bonded connection will finally provide the definitive joint properties characterization.

Even if supplier B technology has been preferred, FSBR method can still be considered an interesting alternative for blind riveting technique. However, this technology requires further investigations capable to quantify the effect of each involved process (sleeve formation, grain refinement, IMC formation) on the final joint properties. This should allow increasing the joint quality predictability. The same target can be achieved by further development of the study presented by work [39], in which the final joint strength can be predicted by exploiting the process data of resistance torque and force during the rivet installation.

It is worth to underline once more that the result of the first experimental campaign (when friction-based and conventionally riveting technologies have been compared using the same fastener model) demonstrated the improved mechanical performance of FSBR. This suggests that the utilization of a rivet like the Auto-Bulb one (used by supplier B) can highly improve the mechanical capabilities of FSBR system, even if specific fastener modification would be required. In conclusion, the FSBR system should undergo additional investigations with more advanced rivet designs in order to assess its full potential. However, this technology does not seem to be mature enough for an immediate industrial application.

Bibliography

- [1] “Aluminum Content in Cars (Public Summary)”. In: *Ducker Worldwide* (2016).
- [2] S. Hu K. Martinsen and B. Carlson. “Joining of dissimilar materials”. In: *CIRP Annals - Manufacturing Technology* 64.2 (2015), pp. 679–699.
- [3] Kurt M. Marshek Robert C. Juvinall. *Fundamentals of Machine Component Design*. John Wiley and Sons, Inc., 2011, p. 430.
- [4] S. Black. “Structural adhesives, Part I:Industrial”. In: *Composite world* (2016).
- [5] T. Tripp. “High-strength lightweight joints using Flow Drill Screw Technology”. In: *Lightweighting World* (2017).
- [6] T. Bingelis. “Flush riveting Tips”. In: *EAA Sport aviation* (1987).
- [7] Walt Disney Industrial Training Film. *Four methods of flush riveting*. 1942.
- [8] The Welding Institute. *What is self-piercing riveting and how does it work? (Available online)*. URL: http://www.marshallsales.com/pr_rivets.php..
- [9] Tatsuya Sakiyama et al. “Dissimilar metal joining technologies for steel sheet and aluminum alloy sheet in auto body”. In: *Nippon Steel & Sumitomo Metal Corp., Tokyo, Nippon Steel Technical Report* 103 (2013), pp. 91–98.
- [10] Marshall Sales. *Rivets and Installation Tools (Available online)*. URL: http://www.marshallsales.com/pr_rivets.php..
- [11] G. Gardiner. “Is the BMW 7 Series the future of autocomposites?” In: *Composites World* (2016).
- [12] S. Birch. “Audi reveals new A8 technologies, tightens links with Porsche”. In: *SAE international* (2017).
- [13] J. Huetter. “Upcoming Audi A8 uses UHSS, aluminum, carbon-fiber, magnesium; joins body 14 ways”. In: *Repairer Driven News* (2017).
- [14] S. Collie. “Audi mixes-and-matches materials in lightweight A8 chassis”. In: *New Atlas* (2017).
- [15] M. Simms. “Joining Aluminum”. In: *Automotive Manufacturing Solutions* (2014).
- [16] Haris Ali Khan, Jingjing Li, and Chenhui Shao. “Analyses of Friction Stir Riveting Processes: A Review”. In: *Journal of Manufacturing Science and Engineering* 139.9 (2017), p. 090801.
- [17] J. Sprovieri. “Resistance spot riveting”. In: *Assembly Magazine* (2017).

- [18] J. D. Samuel. “Friction-Stir Riveting: An Innovative Process for Joining Difficult-to-Weld Materials”. M.Sc. thesis. University of Toledo, 2012.
- [19] W. Zixi. “Characterization of Friction-stir Riveting AA5754”. M.Sc. thesis. University of Toledo, 2014.
- [20] Sergio De Traglia Amancio Filho, Matthias Beyer, and Jorge F Dos Santos. *Method of connecting a metallic bolt to a plastic workpiece*. US Patent 7,575,149. 2009.
- [21] J Altmeyer, JF Dos Santos, and ST Amancio-Filho. “Effect of the friction riveting process parameters on the joint formation and performance of Ti alloy/short-fibre reinforced polyether ether ketone joints”. In: *Materials & Design* 60 (2014), pp. 164–176.
- [22] Vijay K Stokes. “Joining methods for plastics and plastic composites: an overview”. In: *Polymer Engineering & Science* 29.19 (1989), pp. 1310–1324.
- [23] MF Borges et al. “Development of computational models to predict the mechanical behavior of Friction Riveting joints”. In: *Computational Materials Science* 54 (2012), pp. 7–15.
- [24] AB Abibe et al. “Development and analysis of a new joining method for polymer-metal hybrid structures”. In: *Journal of thermoplastic composite materials* 24.2 (2011), pp. 233–249.
- [25] YongBing Li et al. “Friction self-piercing riveting of aluminum alloy AA6061-T6 to magnesium alloy AZ31B”. In: *Journal of Manufacturing Science and Engineering* 135.6 (2013), p. 061007.
- [26] Yunwu Ma et al. “Effect of rivet hardness and geometrical features on friction self-piercing riveted joint quality”. In: *Journal of manufacturing science and engineering* 137.5 (2015), p. 054501.
- [27] Mario Klein et al. “Advanced Joining Technologies for Load and Fibre Adjusted FRP-Metal Hybrid Structures”. In: *Journal of Materials Science Research* 4.4 (2015), p. 26.
- [28] Junying Min et al. “Friction stir blind riveting of carbon fiber-reinforced polymer composite and aluminum alloy sheets”. In: *The International Journal of Advanced Manufacturing Technology* 76.5-8 (2015), pp. 1403–1410.
- [29] Dalong Gao et al. “A new one-sided joining process for aluminum alloys: friction stir blind riveting”. In: *Journal of Manufacturing Science and Engineering* 131.6 (2009), p. 061002.
- [30] Junying Min et al. “Mechanical property of Al alloy joints by friction stir blind riveting”. In: *Procedia engineering* 81 (2014), pp. 2036–2041.
- [31] Sri Lathabai et al. “Friction stir blind riveting: a novel joining process for automotive light alloys”. In: *SAE International Journal of Materials and Manufacturing* 4.2011-01-0477 (2011), pp. 589–601.

- [32] A Zachary Trimble, Brennan Yammamoto, and Jingjing Li. “An Inexpensive, Portable Machine to Facilitate Testing and Characterization of the Friction Stir Blind Riveting Process”. In: *Journal of Manufacturing Science and Engineering* 138.9 (2016), p. 095001.
- [33] Junying Min et al. “Affected Zones in an Aluminum Alloy Frictionally Penetrated by a Blind Rivet”. In: *Journal of Manufacturing Science and Engineering* 138.5 (2016), p. 054501.
- [34] Junying Min et al. “Friction stir blind riveting for aluminum alloy sheets”. In: *Journal of Materials Processing Technology* 215 (2015), pp. 20–29.
- [35] R. L. McCullough T.-W. Chou and R. B. Pipes. *Composites*. Scientific American, 1986, pp. 193–203.
- [36] Cédric Bonnet et al. “CFRP drilling: Fundamental study of local feed force and consequences on hole exit damage.” In: *International Journal of Machine Tools and Manufacture* 94 (2015), pp. 57–64.
- [37] Vijayan Krishnaraj et al. “Optimization of machining parameters at high speed drilling of carbon fiber reinforced plastic (CFRP) laminates”. In: *Composites Part B: Engineering* 43.4 (2012), pp. 1791–1799.
- [38] R Piquet et al. “Experimental analysis of drilling damage in thin carbon/epoxy plate using special drills”. In: *Composites Part A: Applied Science and Manufacturing* 31.10 (2000), pp. 1107–1115.
- [39] Jingyu Chen, Shenghan Guo, Jingjing Li, et al. “Process Monitoring of Friction Stir Blind Riveting for Lightweight Materials”. In: *IIE Annual Conference. Proceedings*. Institute of Industrial and Systems Engineers (IISE). 2017, pp. 2165–2170.
- [40] Mustafa Kemal Kulekci. “Magnesium and its alloys applications in automotive industry”. In: *The International Journal of Advanced Manufacturing Technology* 39.9-10 (2008), pp. 851–865.
- [41] Chao-Chi Jain and Chun-Hao Koo. “Creep and corrosion properties of the extruded magnesium alloy containing rare earth”. In: *Materials transactions* 48.2 (2007), pp. 265–272.
- [42] Dale L Atwell and Matthew R Barnett. “Extrusion limits of magnesium alloys”. In: *Metallurgical and Materials Transactions A* 38.12 (2007), pp. 3032–3041.
- [43] Junying Min et al. “Friction Stir Blind Riveting for Joining Dissimilar Cast Mg AM60 and Al Alloy Sheets”. In: *Journal of Manufacturing Science and Engineering* 137.5 (2015), p. 051022.
- [44] Frank Podlesak. “Entwicklung und Verifizierung eines vorlochfreien mechanischen Fügeverfahrens zum Verbinden von Leichtmetallen und Faser-Kunststoff-Verbunden”. In: (2016).
- [45] J. Harker. “IN-DEPTH: Gesipa on its Flow Drilling Rivet process”. In: *Torque* (2017).

- [46] F Podlesak et al. “Spin-blind-riveting: secure joining of plastic with metal”. In: *Welding in the World* 59.6 (2015), pp. 927–932.
- [47] Frank Podlesak, André Hälsig, and Peter Mayr. “Spin-Blind-Riveting-A new joining technology for hybrid components.” In: *Materials Science Forum*. 2015.
- [48] McMaster-Carr. *Zinc-Plated Steel Blind Rivets (Available online)*. URL: <https://www.mcmaster.com/#97519a652/=1ckxq36>.
- [49] Assembly. “Hybrid Riveting: The Best of both Worlds”. In: (August 16th 2005).
- [50] Protech composites. *Carbon fiber 101*.
- [51] Robert S Birch et al. “Modelling the dynamic failure of riveted joints in aerospace fuselages”. In: *WIT Transactions on Engineering Sciences* 49 (2005), pp. 121–134.
- [52] European Standard. *Metallic Materials - Tensile Testing EN ISO 6892-1*. 2009.
- [53] SPC-Surface Treatment Experts. *Corrosion resistance of zinc plating (Available online)*. URL: <https://www.sharrettsplating.com/blog/corrosion-resistance-of-zinc-plating/>.

Appendix A

Structural adhesive chemical aspects overview

The intrinsic complexity of adhesive utilization is related to the variety of their base chemical composition. The latter is the key to achieve an effective adhesion which, in turns, is the consequence of adhesive molecules diffusion in the adherend surface, resulting in covalent chemical bonds formation, locking the parts together. There are three main typologies of thermosetting resins for industrial applications, which are epoxy, polyurethane and acrylic. The former is that characterized by the highest adhesion power, chemical and thermal resistance. These features make epoxy quite common especially in aerospace and marine construction fields. Acrylics, which include methyl methacrylate or MMA, provide better performances than epoxies in bonding oily and low temperature surfaces. Finally, urethanes are characterized by high performances flexibility in several working environments, but lower strength with respect to the previous categories of resins [3]. Concerning the composite industry, it is possible to identify at least 40 different adhesives suppliers, whose target is to find the proper chemical formula to match the specific industrial application in terms of composite features, stress and chemical working environment. In order to achieve this demanding target, numerous additives can be employed like rubbers, plasticizers, curatives or viscosity agents. Nowadays it is also common to employ microspheres in order to set a proper bond-line thickness. As often it happens, the different blends of these additives are resulting from a tradeoff amongst different adhesive features. The main conflicting aspects and phenomena to be considered are listed below:

- Tougheners added to improve the adhesive impact resistance can reduce the glass transition temperature.
- Especially when using epoxies, it is advisable to perform a heating action during fixturing and cure in order to achieve high adhesion, but this practice is more likely to cause the read-through phenomenon. The latter is a visible distortion of the substrate over a cured adhesive bond-line. It is mainly caused by a difference in the thermal expansion coefficients between the substrate and the adhesive. The

incidence and severity of the phenomenon is strictly related to the substrate and adhesive thermo-mechanical properties.

- Bonding of different types of material must be performed in such a way to consider the different surfaces properties and differences in thermal expansion.

Given the specific application, a key property for the employed structural adhesives is the compliance and elongation. This requirement comes from the fact that, since adhesives are entitled to bond together different materials components, they have also to deal with different thermal behavior, namely different coefficient of thermal expansion (CTE). Moreover, since a vehicle is a dynamic system, adhesives must be compliant in order to accommodate relative movements of the bonded parts under fatigue and dynamic loads. Furthermore, as every industrial activity, vehicle production process must be oriented toward cycle time reduction and throughput optimization, so high performing adhesives should present rapid curing times and, possibly, no or little surface preparation. It is presented, in the following sections, the main adhesive suppliers working in automotive field, and the main properties of their products.

Appendix B

Extract of the epoxy resin chemical family hazard identification

EMERGENCY OVERVIEW

May cause skin irritation, eye irritation and allergic reactions

POTENTIAL HEALTH EFFECTS

ACUTE INHALATION

If product is heated, vapors generated can cause headache, nausea, dizziness and possible respiratory irritation if inhaled in high concentrations.

CHRONIC INHALATION

Repeated exposure to high vapor concentrations may cause irritation of pre-existing lung allergies and increase the chance of developing allergy symptoms to this product.

ACUTE SKIN CONTACT

May cause allergic skin response in certain individuals. May cause moderate irritation to the skin such as redness and itching.

CHRONIC SKIN CONTACT

May cause sensitization in susceptible individuals. May cause moderate irritation to the skin.

EYE CONTACT

May cause irritation.

INGESTION

Low acute oral toxicity.

SYMPTOMS OF OVEREXPOSURE

Possible sensitization and subsequent allergic reactions usually seen as redness and rashes.

MEDICAL CONDITIONS AGGRAVATED BY EXPOSURE

Pre-existing skin and respiratory disorders may be aggravated by exposure to this product.

Source: Material safety data sheet West System inc.

Appendix C

Description of secondary bending in riveted samples

Secondary bending is a rivet failure mode observed during the first experimental campaign, particularly in the case of samples constituted by thin material layers. Secondary bending phenomena are divided into two groups, namely regular and nonregular ones.

A regular secondary bending consists in the bending of both top and bottom layers (figure C.1.a). Conversely, when one of the layers presents a much higher bending stiffness with respect to the other one, just one of the riveted workpiece bends. This phenomenon is referred as nonregular secondary bending and it is represented in figure C.1.b. The angle between the fastener axis and the unbent layer, due to the rivet rotation during samples pulling, is a key factor for the resulting joint strength.

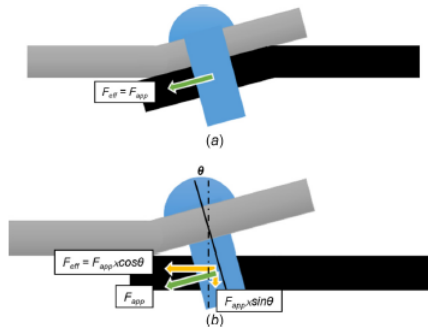


Figure C.1: *Schematic representation of: a) regular secondary and b) nonregular secondary bending*

When a regular secondary bending takes place, the force acting on the two material layers (F_{eff}) is equal to that applied by the machine (F_{app}). On the other hand, when a nonregular secondary bending occurs, the force acting on the unbent layer decreases by the factor $\cos \theta$, being θ the angle between the fastener axis and the unbent material layer.

$$F_{eff} = F_{app} \cos \theta$$

Moreover, a vertical load arises from this failure mode, which tends to push out the

rivet and contributes to the less stiff layer bending. This force is the larger the wider the θ angle is.

Consequently, when the unbent layer (which in the present discussion is the composite one) reaches the failure load the actual F_{app} value in nonregular secondary bending is higher than in regular one, which implies a larger joint strength is actually recorded. Clearly, the larger the angle θ is, the more significant this effect will be.

Vita Auctoris

NAME: Alessandro Limentato

PLACE OF BIRTH: San Cataldo

YEAR OF BIRTH: 1994

EDUCATION: Liceo Scientifico "A. Volta", Caltanissetta, CL, Italy, 2008 - 2013
Politecnico di Torino, B.Sc., Torino, TO, Italy, 2013 - 2016
Politecnico di Torino, MAsc., Torino, TO, Italy, 2016 - 2018
University of Windsor, MAsc., Windsor, ON, Canada, 2017 - 2018